



1 **Description and evaluation of the UKCA stratosphere-troposphere chemistry scheme**
2 **(StratTrop vn 1.0) implemented in UKESM1.**

3
4 Archibald, Alexander T. ^{1,2,*}, O'Connor, Fiona M. ³, Abraham, N. Luke ^{1,2}, Archer-Nicholls,
5 Scott¹, Chipperfield, Martyn P. ^{4,5}, Dalvi, Mohit ³, Folberth, Gerd A. ³, Dennison, Fraser ⁴,
6 Dhomse, Sandip S. ^{4,5}, Griffiths, Paul T. ^{1,2}, Hardacre, Catherine³, Hewitt, Alan J. ³, Hill,
7 Richard³, Johnson, Colin E. ³, Keeble, James^{1,2}, Köhler, Marcus O. ^{1,7,†}, Morgenstern, Olaf⁶,
8 Mulcahy, Jane P. ³, Ordóñez, Carlos^{3,‡}, Pope, Richard J. ^{4,5}, Rumbold, Steven^{3,8}, Russo,
9 Maria R. ^{1,2}, Savage, Nicholas³, Sellar, Alistair³, Stringer, Marc³, Tumock, Steven³, Wild,
10 Oliver⁹ and Zeng, Guang⁶.

- 11
12 1) Department of Chemistry, University of Cambridge, Cambridge, UK, CB2 1EW
13 2) NCAS-Climate, University of Cambridge, UK, CB2 1EW
14 3) Met Office Hadley Centre, FitzRoy Road, Exeter, UK, EX1 3PB
15 4) School of Earth and Environment, University of Leeds, Leeds, UK, LS2 9JT.
16 5) National Centre for Earth Observation (NCEO), University of Leeds, Leeds, U.K.
17 6) National Institute of Water & Atmospheric Research Ltd (NIWA), 301 Evans Bay
18 Parade, Greta Point, Wellington, New Zealand.
19 7) Centre for Ocean and Atmospheric Sciences, School of Environmental Sciences,
20 University of East Anglia, Norwich, U.K.
21 8) NCAS-Climate, Department of Meteorology, University of Reading, Reading, UK,
22 RG6 6BB.
23 9) Lancaster Environment Centre, Lancaster University, Lancaster, UK, LA1 4YQ

24
25 (†) Now at ECMWF, Reading, UK.

26 (‡) Now at Departamento de Física de la Tierra y Astrofísica, Facultad de Ciencias
27 Físicas, Universidad Complutense de Madrid, Madrid 28040, Spain

28
29 *Email: ata27@cam.ac.uk

30
31
32 **Abstract**

33 Here we present a description of the UKCA StratTrop chemical mechanism which is used in
34 the UKESM1 Earth System Model for CMIP6. The StratTrop chemical mechanism is a merger
35 of previously well evaluated tropospheric and stratospheric mechanisms and we provide
36 results from a series of bespoke integrations to assess the overall performance of the model.

37
38 We find that the StratTrop scheme performs well when compared to a wide array of
39 observations. The analysis we present here focuses on key components of atmospheric
40 composition, namely the performance of the model to simulate ozone in the stratosphere and
41 troposphere and constituents that are important for ozone in these regions. We find that the
42 results obtained from the use of the StratTrop mechanism are sensitive to the host model;
43 simulations with the same chemical mechanism run in an earlier version of the MetUM host
44 model show a range of sensitivity to emissions that the current model does not fall within.

45
46 Whilst the general model performance is suitable for use in the UKESM1 CMIP6 integrations,
47 we note some shortcomings in the scheme that future targeted studies will address.

48



1
2
3
4
5
6
7
8
9
10
11
12
13
14
15
16
17
18
19
20
21
22
23
24
25
26
27
28
29
30
31
32
33
34
35
36
37
38
39
40
41
42
43
44

1.0 Introduction

The ability to model the composition of the atmosphere is vital for a wide range of applications relevant to society at large. Atmospheric composition modelling can broadly be subdivided into two sub disciplines: (1) aerosol processes and microphysics and (2) atmospheric chemistry. Coupling these processes in climate models is paramount for being able to simulate atmospheric composition at the global scale. The most societally important questions revolve around understanding how the composition of the atmosphere has changed over the past, attributing this change, understanding how this system is likely to change into the future and what the impacts of these changes are on the Earth system and on human health. It is these pressing issues that have led to the development of the new UK Earth System Model, UKESM1 (Sellar et al., 2019a), which uses the UK Chemistry and Aerosol model (UKCA) (O'Connor et al., 2014; Morgenstern et al., 2009; Mulcahy et al., 2018) as its key component to simulate atmospheric composition in the Earth system. The key challenge UKCA is applied to is understanding and predicting how the concentrations of a range of trace gases, especially the greenhouse gases methane (CH₄) ozone (O₃) and nitrous oxide (N₂O), and aerosol species will evolve in the Earth system under a range of different forcings. UKCA simulates the processes that control the formation and destruction of these species. Here we describe and document the performance of the version of UKCA used in UKESM1, which includes a representation of combined stratospheric and tropospheric chemistry that enhances the capability of UKCA beyond that used in the Atmospheric Chemistry and Climate Model Intercomparison Project (ACCMIP; Young et al., 2013; O'Connor et al., 2014) and the recent Chemistry-Climate Model Initiative (CCMI) intercomparison (Bednarz et al., 2018; Hardiman et al., 2017; Morgenstern et al., 2017). There have been a number of versions of UKCA with defined scopes but we denote the version used in UKESM1 and described here as UKCA StratTrop, to signify its purpose of holistic treatment of composition processes in the troposphere and stratosphere.

As a result of the Chemistry-Climate Model Validation Activity (CCMVal), it was recommended that models which are aimed at simulating the coupled ozone-climate problem should include processes to enable interactive ozone in the troposphere and stratosphere (Morgenstern et al., 2010). In Chemistry-Climate Models (CCMs), the chemistry schemes are used to describe the reactions that chemical compounds undergo. These chemistry schemes can be constructed to explicitly model a specific chemical reaction system (Aumont et al., 2005) but in most applications the chemistry schemes are heavily simplified. Until recently, models of atmospheric chemistry tended to focus on chemistry schemes formulated for limited regions of the atmosphere; detailed schemes have been constructed to examine phenomena in the stratosphere, such as ozone depletion, whereas other schemes that focus on the troposphere have been developed to examine phenomena such as air pollution. An example of this using the UKCA model framework are two studies of the effects of the eruption of Mt. Pinatubo, where Telford et al. (2009) used the stratospheric scheme of Morgenstern et al. (2009) to study the effects of the eruption on stratospheric ozone, whereas Telford et al. (2010) used the tropospheric scheme of O'Connor et al. (2014) to examine the effects on tropospheric oxidising capacity. Whilst the chemical schemes described in O'Connor et al. (2014) (hereafter



1 OC14) and Morgenstern et al. (2009) (hereafter MO09) have some overlap (for example the
2 use of some common reactions) the schemes were developed with specific applications in
3 scope. The reason for partitioning chemical complexity up like this is to reduce the
4 computational resources required. Moreover, simulations with these process limitations were
5 found to be able to capture the phenomena of interest.

6 However, increases in computational power and a drive to answer a greater number of
7 questions from model simulations have allowed models that simulate both the stratosphere
8 and troposphere to be developed and which are now widely used (e.g. Pitari et al., 2002;
9 Jockel et al., 2006; Lamarque et al., 2008; Morgenstern et al., 2012). The removal of the need
10 for prescribed upper boundary conditions (for the stratosphere), and a more comprehensive
11 chemistry scheme, make their increased cost worth bearing. In this work, we describe the
12 implementation of a combined chemistry scheme suitable for simulating the stratosphere and
13 the troposphere within the UKCA model as used in UKESM1 (Sellar et al., 2019a). This
14 scheme, UKCA StratTrop, builds on and combines the existing stratospheric (MO09) and
15 tropospheric schemes (OC14). In various configurations of UKCA (under the names
16 HadGEM3-ES, UMuKCA-UCAM, NIWA-UKCA, ACCESS), this combined chemical scheme
17 has already been used to study: stratospheric ozone and its sensitivity to changes in bromine
18 (Yang et al., 2014), subsequent circulation changes (Braesicke et al., 2013), and how it may
19 be impacted by certain forms of geoengineering (Tang et al., 2014); the role of ozone radiative
20 feedback on temperature and humidity biases at the tropical tropopause layer (TTL)
21 (Hardiman et al., 2015); the effects on tropospheric and stratospheric ozone changes under
22 climate and emissions changes following the Representative Concentration Pathways (RCPs)
23 (Banerjee et al., 2015; Dhomse et al., 2018); climate induced changes in lightning (Banerjee
24 et al., 2014) and changes in methane chemistry between the present day and the last
25 interglacial (Quiquet et al., 2015). The scheme has been included in model simulations as part
26 of the CCMI project (Eyring et al., 2013; Hardiman et al., 2017; Morgenstern et al., 2017;
27 Dhomse et al., 2018) as well as all future Earth System modelling studies using the UKESM1
28 model (Sellar et al., 2019a).

29
30 This paper is organised in the following sections: In Section 2, we present a thorough
31 description of UKCA StratTrop, including the physical model and details of the chemistry
32 scheme, followed by a detailed description of the emissions used in the StratTrop scheme and
33 some notes on the historical development of the scheme. In Section 3, we describe the two
34 15-year simulations we have performed with UKCA StratTrop in an atmosphere-only
35 configuration of UKESM1. In Section 4, we use these simulations to review the performance
36 of UKCA StratTrop, focusing on the model's ability to simulate key features of tropospheric
37 and stratospheric chemistry as simulated by other models or observed using in situ and remote
38 sensing measurements. Finally, in Section 5, we discuss the performance of the model and
39 make some recommendations for further targeted studies.

40

41

42 2.0 Model Description



1 In this section, we present a thorough description of UKCA StratTrop, from the host physical
2 model to the detailed process representation of the StratTrop chemistry scheme.

3 4 **2.1 Physical Model**

5 The physical model to which the UKCA StratTrop chemistry scheme has been coupled is the
6 Global Atmosphere 7.1/Global Land 7.0 (GA7.1/GL7.0; Walters et al., 2019) configuration of
7 the Hadley Centre Global Environment Model version 3 (HadGEM3; Hewitt et al., 2011).

8
9 The coupling between the UKCA StratTrop chemistry scheme and the GA7.1/GL7.0
10 configuration of HadGEM3 is based on the Met Office's Unified Model (MetUM; Brown et al.,
11 2012). As a result, UKCA uses aspects of MetUM for the large-scale advection, convective
12 transport, and boundary layer mixing of its tracers. The large-scale advection makes use of
13 the semi-implicit semi-Lagrangian formulation of the ENDGame dynamical core (Wood et al.,
14 2014) to solve the non-hydrostatic, fully compressible deep-atmosphere equations of motion.
15 These are discretized on to a regular latitude-longitude grid, with Arakawa C-grid staggering
16 (Arakawa and Lamb, 1977). The discretization in the vertical uses Charney–Phillips staggering
17 (Charney and Phillips, 1953) with terrain-following hybrid height coordinates. Although
18 GA7.1/GL7.0 can be run at a variety of resolutions, as detailed in Walters et al. (2019), the
19 resolution here is N96L85 (1.875° x 1.25° longitude-latitude) i.e. approximately 135 km
20 resolution in the horizontal and with 85 levels covering the altitude range from the surface to
21 85 km. Of the 85 terrain-following model levels, 50 lie below 18 km and 35 levels are above
22 18 km (Walters et al., 2019). Mass conservation of UKCA tracers is achieved with the
23 optimised conservative filter (OCF) scheme (Zerroukat and Allen, 2015); use of this scheme
24 for virtual dry potential temperature resulted in reducing the warm bias at the tropical
25 tropopause layer (TTL) (Hardiman et al., 2015; Walters et al., 2019). This conservation
26 scheme is also used for moist prognostics (e.g. water vapour mass mixing ratio and prognostic
27 cloud fields). Although it makes the conservation scheme for moist prognostics consistent with
28 the treatment of UKCA tracers and virtual dry potential temperature, Walters et al. (2019)
29 found that it had little impact on moisture biases in the lower stratosphere.

30
31 The convective transport of UKCA tracers is treated within the MetUM convection scheme. It
32 is essentially the mass flux scheme of Gregory and Rowntree (1990) but with updates for
33 downdrafts (Gregory and Allen, 1991), convective momentum transport (Gregory et al., 1997),
34 and Convective Available Potential Energy closure. The scheme involves diagnosis of
35 possible convection from the boundary layer, followed by a call to shallow or deep convection
36 on selected grid points based on the diagnosis from step one, and then a call to the mid-level
37 convection scheme at all points. One key difference between the convective treatment of
38 UKCA chemical and aerosol tracers is that convective scavenging of aerosols (simulated with
39 GLOMAP-mode) is coupled with the convective transport following Kipling et al. (2013),
40 whereas for chemical tracers, convective transport and scavenging are treated independently.
41 Further details on the convection scheme in GA7.1 can be found in Walters et al. (2019).
42 Finally, mixing over the full depth of the troposphere is carried out by the so-called “boundary-
43 layer” scheme in GA7.1; this scheme is that of Lock et al. (2000), but with updates from Lock
44 (2001) and Brown et al. (2008).

45
46 The GA7.1/GL7.0 configuration described in Walters et al. (2019) already includes the two-
47 moment GLOMAP-mode aerosol scheme from UKCA (Mann et al., 2010; Mulcahy et al., 2018;



1 Mulcahy et al., 2019), in which sulphate and secondary organic aerosol (SOA) formation is
2 driven by prescribed oxidant fields. In the UKCA-StratTrop configuration described here, the
3 oxidants driving secondary aerosol formation are fully interactive; this coupling between UKCA
4 chemistry and GLOMAP-mode is fully described in Mulcahy et al. (2019). Together with
5 dynamic vegetation and a terrestrial carbon/nitrogen scheme (Sellar et al., 2019a),
6 GA7.1/GL7.0 and UKCA StratTrop make up the atmospheric and land components of the UK
7 Earth System Model, UKESM1 (Sellar et al., 2019a) which will be used as part of the UK
8 contribution to the 6th Coupled Model Intercomparison Project (CMIP6; Eyring et al., 2016).

9

10 **2.2 Chemistry scheme**

11 The UKCA StratTrop scheme is based on a merger between the stratospheric scheme of
12 MO09 and the tropospheric “Troplisop” scheme of OC14. StratTrop simulates the O_x , HO_x
13 and NO_x chemical cycles and the oxidation of carbon monoxide, ethane, propane, and
14 isoprene in addition to Cl and Br chemistry, including heterogeneous processes on polar
15 stratospheric clouds (PSCs) and liquid sulphate aerosols (SAs). The level of detail of the
16 VOC oxidation is far from the complexity of explicit representations (Aumont et al., 2005) but
17 the VOCs simulated are treated as discrete species.

18

19 Wet deposition is parameterised using the approach of Giannakopoulos et al. (1999). Dry
20 deposition is parameterised employing a resistance type model (Wesely, 1989) using the
21 implementation described in OC14, updated to account for advancements in the Joint UK Land
22 Environment Simulator (JULES; Best et al., 2011), in particular a significant increase in land
23 surface types (an increase from 9 to 27; see below for more details). Interactive photolysis is
24 represented with the Fast-JX scheme (Neu et al., 2007), as implemented in Telford et al.
25 (2013). Fast-JX covers the wavelength range of 177 to 750 nm. For shorter wavelengths,
26 effective above 60 km of altitude, a correction is applied to the photolysis rates following the
27 formulation of Lary and Pyle (1991).

28

29 The StratTrop scheme includes emissions of 12 chemical species: nitrogen oxide (NO),
30 carbon monoxide (CO), formaldehyde (HCHO), ethane (C_2H_6), propane (C_3H_8), acetaldehyde
31 (CH_3CHO), acetone ($(CH_3)_2CO$), methanol (CH_3OH) and isoprene (C_5H_8) in addition to trace
32 gas aerosol-precursor emissions (dimethyl sulphide (DMS), sulphur dioxide (SO_2), and
33 monoterpenes). For the implementation used in UKESM1, emissions may be prescribed or
34 interactive and are described in more detail in Sections 2.6.1 to 2.6.3. A further 7 species
35 (N_2O , CF_2Cl_2 , $CFCl_3$, CH_3Br , COS, H_2 , and CH_4) are constrained by lower boundary conditions;
36 for more details see Section 2.6.4.

37

38 UKCA StratTrop was developed by starting with the stratospheric chemistry scheme (MO09)
39 and adding aspects of chemistry unique to the tropospheric scheme (OC14). In most cases
40 the formulation and reaction coefficients are taken from reference evaluations (JPL and
41 IUPAC) or the Master Chemical Mechanism, as detailed in OC14. Table 1 provides a list of
42 the chemical tracers included in the StratTrop configuration used in UKESM1. Tables 2-5
43 include lists of the bi-molecular, ter-molecular, photolysis and heterogeneous reactions
44 included in the model configuration. In total the model employs 84 tracers and represents the
45 chemistry of 81 of these (Table 1). O_2 , N_2 and CO_2 are not treated as chemically active species.



1 This chemistry scheme accounts for 199 bimolecular reactions (Table 2), 25 uni- and
2 termolecular reactions (Table 3), 59 photolytic reactions (Table 4), 5 heterogeneous reactions
3 (Table 5) and 3 aqueous phase reactions for the Sulfur cycle (Table 6). Hence, UKCA-
4 StratTrop describes the oxidation of the organic compounds – methane, ethane, propane and
5 isoprene and their oxidation products – coupled to the inorganic chemistry of O_x, NO_x, HO_x,
6 ClO_x and BrO_x, using a continuous set of equations with no artificial boundaries imposed on
7 where to stop performing chemistry. The top model levels, where dynamics isn't fully resolved,
8 act as a dynamical sponge where species' concentrations are overwritten. The time dependent
9 chemical reactions are integrated forward in time using the iterative Newton Raphson solver
10 described in Essenturk et al. (2018), with a time step of 60 minutes throughout the atmosphere.

11

12 **Table 1.** List of chemical species in UKCA StratTrop. Species in italics are not advected tracers but
13 are calculated using a steady state approximation. Species in bold are set as constant values
14 throughout the atmosphere. [†]The molecular mass of Sec_Org is set to 150 g/mol.

Name	Formula	Dry Deposit ed	Wet Deposited	Emitted or LBC
O(3P)	O(³ P)	No	No	No
<i>O(1D)</i>	<i>O(¹D)</i>	No	No	No
O3	O ₃	Yes	No	No
N	N	No	No	No
NO	NO	Yes	No	Emitted
NO3	NO ₃	Yes	Yes	No
NO2	NO ₂	Yes	No	No
N2O5	N ₂ O ₅	Yes	Yes	No
HO2NO2	HO ₂ NO ₂	Yes	Yes	No
HONO2	HONO ₂	Yes	Yes	No
H2O2	H ₂ O ₂	Yes	Yes	No
CH4	CH ₄	No	No	LBC
CO	CO	Yes	No	Emitted
HCHO	HCHO	Yes	Yes	Emitted
MeOO	CH ₃ OO	No	Yes	No
MeOOH	CH ₃ OOH	Yes	Yes	No
H	H	No	No	No
H2O	H ₂ O	No	No	No
OH	OH	No	No	No
HO2	HO ₂	No	Yes	No
Cl	Cl	No	No	No
Cl2O2	Cl ₂ O ₂	No	No	No
ClO	ClO	No	No	No
OCIO	OCIO	No	No	No
Br	Br	No	No	No
BrO	BrO	No	No	No
BrCl	BrCl	No	No	No



BrONO2	BrONO ₂	No	Yes	No
N2O	N ₂ O	No	No	LBC
HCl	HCl	Yes	Yes	No
HOCl	HOCl	Yes	Yes	No
HBr	HBr	Yes	Yes	No
HOBr	HOBr	Yes	Yes	No
ClONO2	ClONO ₂	No	Yes	No
CFCl3	CFCl ₃	No	No	LBC
CF2Cl2	CF ₂ Cl ₂	No	No	LBC
MeBr	CH ₃ Br	No	No	LBC
HONO	HONO	Yes	Yes	No
C2H6	C ₂ H ₆	No	No	Emitted
EtOO	C ₂ H ₅ OO	No	No	No
EtOOH	C ₂ H ₅ OOH	Yes	Yes	No
MeCHO	CH ₃ CHO	Yes	No	Emitted
MeCO3	CH ₃ C(O)OO	No	No	No
PAN	PAN	Yes	No	No
C3H8	C ₃ H ₈	No	No	Emitted
n-PrOO	C ₃ H ₇ OO	No	No	No
i-PrOO	CH ₃ CH(OO)CH ₃	No	No	No
n-PrOOH	C ₃ H ₇ OOH	Yes	Yes	No
i-PrOOH	CH ₃ CH(OOH)CH ₃	Yes	Yes	No
EtCHO	C ₂ H ₅ CHO	Yes	No	No
EtCO3	C ₂ H ₅ C(O)OO	No	No	No
Me2CO	CH ₃ C(O)CH ₃	No	No	Emitted
MeCOCH2O				
O	CH ₃ C(O)CH ₂ OO	No	No	No
MeCOCH2O				
OH	CH ₃ C(O)CH ₂ OOH	Yes	Yes	No
PPAN	PPAN	Yes	No	No
MeONO2	MeONO ₂	No	No	No
C5H8	C ₅ H ₈	No	No	Emitted
ISO2	HOC ₅ H ₈ OO	No	No	No
ISOOH	HOC ₅ H ₈ OOH	Yes	Yes	No
ISON	ISON	Yes	Yes	No
MACR	C ₄ H ₆ O	Yes	No	No
MACRO2	C ₄ H ₆ O(OO)	No	No	No
MACROOH	C ₄ H ₆ O(OOH)	Yes	Yes	No
MPAN	MPAN	Yes	No	No
HACET	CH ₃ C(O)CH ₂ OH	Yes	Yes	No
MGLY	CH ₃ COCHHO	Yes	Yes	No
NALD	NALD	Yes	No	No
HCOOH	HC(O)OH	Yes	Yes	No
MeCO3H	CH ₃ C(O)OOH	Yes	Yes	No
MeCO2H	CH ₃ C(O)OH	Yes	Yes	No
H2	H ₂	No	No	LBC
MeOH	CH ₃ OH	Yes	Yes	Emitted



CO2	CO₂	No	No	No
O2	O₂	No	No	No
N2	N₂	No	No	No
DMS	CH ₃ SCH ₃	No	No	Emitted
SO2	SO ₂	Yes	Yes	Emitted
H2SO4	H ₂ SO ₄	Yes	No	No
MSA	MSA	No	No	No
DMSO	DMSO	Yes	Yes	No
COS	COS	No	No	Emitted
SO3	SO ₃	No	No	No
Monoterp	C ₁₀ H ₁₆	Yes	No	Emitted
Sec_Org	†Sec_Org	Yes	Yes	No

1

2 **Table 2.** List of bi-molecular reactions in UKCA-StratTrop. Reactions with a † next to them have
 3 additional code to account for branching of reaction as, for example, a function of pressure (CO+OH)
 4 or H₂O (HO₂ + HO₂). The temperature dependent rate coefficient can be calculated for each grid box at
 5 each chemistry timestep through: $k_{(T)} = A \left(\frac{T}{300}\right)^\alpha \exp\left(\frac{-E_a}{RT}\right)$ where T refers to the grid box temperature
 6 (K).

Reactants	Products	A	α	-E _a /R
Br + Cl ₂ O ₂	BrCl + Cl + O ₂	5.90E-12	0	170
Br + HCHO	HBr + CO + HO ₂	1.70E-11	0	800
Br + HO ₂	HBr + O ₂	4.80E-12	0	310
Br + O ₃	BrO + O ₂	1.60E-11	0	780
Br + OClO	BrO + ClO	2.60E-11	0	1300
BrO + BrO	Br + Br + O ₂	2.40E-12	0	-40
BrO + ClO	Br + Cl + O ₂	2.30E-12	0	-260
BrO + ClO	Br + OClO	9.50E-13	0	-550
BrO + ClO	BrCl + O ₂	4.10E-13	0	-290
BrO + HO ₂	HOBr + O ₂	4.50E-12	0	-460
BrO + NO	Br + NO ₂	8.80E-12	0	-260
BrO + OH	Br + HO ₂	1.70E-11	0	-250
CF ₂ Cl ₂ + O(¹ D)	Cl + ClO	1.40E-10	0	0
CFC ₃ + O(¹ D)	Cl + Cl + ClO	2.30E-10	0	0
Cl + CH ₄	HCl + MeOO	7.30E-12	0	1280
Cl + Cl ₂ O ₂	Cl + Cl + Cl	7.60E-11	0	-65
Cl + ClONO ₂	Cl + Cl + NO ₃	6.50E-12	0	-135
Cl + H ₂	HCl + H	3.05E-11	0	2270
Cl + H ₂ O ₂	HCl + HO ₂	1.10E-11	0	980
Cl + HCHO	HCl + CO + HO ₂	8.10E-11	0	30
Cl + HO ₂	ClO + OH	3.65E-11	0	375
Cl + HO ₂	HCl + O ₂	1.40E-11	0	-270
Cl + HOCl	Cl + Cl + OH	3.40E-12	0	130
Cl + NO ₃	ClO + NO ₂	2.40E-11	0	0
Cl + O ₃	ClO + O ₂	2.30E-11	0	200
Cl + OClO	ClO + ClO	3.40E-11	0	-160



Cl + MeOOH	HCl + MeOO	5.70E-11	0	0
ClO + ClO	Cl + Cl + O ₂	1.00E-12	0	1590
ClO + ClO	Cl + Cl + O ₂	3.00E-11	0	2450
ClO + ClO	Cl + OCIO	3.50E-13	0	1370
ClO + HO ₂	HOCl + O ₂	2.60E-12	0	-290
ClO + MeOO	Cl + HCHO + HO ₂	3.30E-12	0	115
ClO + NO	Cl + NO ₂	6.40E-12	0	-290
ClO + NO ₃	Cl + O ₂ + NO ₂	4.60E-13	0	0
EtCO ₃ + NO	EtOO + CO ₂ + NO ₂	6.70E-12	0	-340
EtCO ₃ + NO ₃	EtOO + CO ₂ + NO ₂	4.00E-12	0	0
EtOO + MeCO ₃	MeCHO + HO ₂ + MeOO	4.40E-13	0	-1070
EtOO + NO	MeCHO + HO ₂ + NO ₂	2.55E-12	0	-380
EtOO + NO ₃	MeCHO + HO ₂ + NO ₂	2.30E-12	0	0
H + HO ₂	H ₂ + O ₂	6.90E-12	0	0
H + HO ₂	O(³ P) + H ₂ O	1.62E-12	0	0
H + HO ₂	OH + OH	7.20E-11	0	0
H + NO ₂	OH + NO	4.00E-10	0	340
H + O ₃	OH + O ₂	1.40E-10	0	470
HO ₂ + HO ₂ †	H ₂ O ₂	3.00E-13	0	-460
HO ₂ + MeOO†	MeOOH	3.80E-13	0	-780
HO ₂ + NO	OH + NO ₂	3.30E-12	0	-270
HO ₂ + NO ₃	OH + NO ₂ + O ₂	3.50E-12	0	0
HO ₂ + O ₃	OH + O ₂ + O ₂	2.03E-16	4.57	-693
HO ₂ + EtCO ₃	O ₂ + EtCO ₃ H	4.40E-13	0	-980
HO ₂ + EtCO ₃	O ₃ + EtCO ₂ H	7.80E-14	0	-980
HO ₂ + EtOO	EtOOH	6.40E-13	0	-710
HO ₂ + ISO ₂	ISOOH	2.05E-13	0	-1300
HO ₂ + MACRO ₂	MACROOH	1.82E-13	0	-1300
HO ₂ + MeCO ₃	MeCO ₂ H + O ₃	7.80E-14	0	-980
HO ₂ + MeCO ₃	MeCO ₃ H	2.13E-13	0	-980
HO ₂ + MeCO ₃	OH + MeOO	2.29E-13	0	-980
HO ₂ + MeCOCH ₂ OO	MeCOCH ₂ OOH	9.00E-12	0	0
HO ₂ + MeOO†	HCHO	3.80E-13	0	-780
HO ₂ + i-PrOO	i-PrOOH	1.51E-13	0	-1300
HO ₂ + n-PrOO	n-PrOOH	1.51E-13	0	-1300
i-PrOO + NO	Me ₂ CO + HO ₂ + NO ₂	2.70E-12	0	-360
i-PrOO + NO ₃	Me ₂ CO + HO ₂ + NO ₂	2.70E-12	0	-360
ISO ₂ + ISO ₂	MACR + MACR + HCHO + HO ₂	2.00E-12	0	0
MACRO ₂ + MACRO ₂	HACET + MGLY + 0.5*HCHO + 0.5*CO + HO ₂	2.00E-12	0	0
MeBr + Cl	Br + HCl	1.40E-11	0	1030
MeBr + O(¹ D)	Br + OH	1.80E-10	0	0
MeBr + OH	Br + H ₂ O	2.35E-12	0	1300
MeCO ₃ + NO	MeOO + CO ₂ + NO ₂	7.50E-12	0	-290
MeCO ₃ + NO ₃	MeOO + CO ₂ + NO ₂	4.00E-12	0	0



MeCOCH ₂ OO + NO	MeCO ₃ + HCHO + NO ₂	2.70E-12	0	-360
MeCOCH ₂ OO + NO ₃	MeCO ₃ + HCHO + NO ₂	2.30E-12	0	0
MeOO + NO	HO ₂ + HCHO + NO ₂	2.30E-12	0	-360
MeOO + MeOO†	HO ₂ + HO ₂ + HCHO + HCHO	1.03E-13	0	-365
MeOO + MeCO ₃	HO ₂ + HCHO + MeOO	1.80E-12	0	-500
MeOO + MeCO ₃	MeCO ₂ H + HCHO	2.00E-13	0	-500
MeOO + MeOO†	MeOH + HCHO	1.03E-13	0	-365
MeOO + NO	MeONO ₂	2.30E-15	0	-360
MeOO + NO ₃	HO ₂ + HCHO + NO ₂	1.20E-12	0	0
N + NO	N ₂ + O(³ P)	2.10E-11	0	-100
N + NO ₂	N ₂ O + O(³ P)	5.80E-12	0	-220
N + O ₂	NO + O(³ P)	1.50E-11	0	3600
n-PrOO + NO	EtCHO + HO ₂ + NO ₂	2.90E-12	0	-350
n-PrOO + NO ₃	EtCHO + HO ₂ + NO ₂	2.70E-12	0	-360
N ₂ O ₅ + H ₂ O	HONO ₂ + HONO ₂	2.50E-22	0	0
NO + NO ₃	NO ₂ + NO ₂	1.50E-11	0	-170
NO + O ₃	NO ₂	3.00E-12	0	1500
NO + ISO2	ISON	1.12E-13	0	-360
NO + ISO2	NO ₂ + MACR + HCHO + HO ₂	2.43E-12	0	-360
NO + MACRO2	NO ₂ + 0.25*MeCO ₃ + 0.25*HACET + 0.25*CO + 0.5*MGLY + 0.75*HCHO + 0.75*HO ₂	2.54E-12	0	-360
NO ₂ + NO ₃	NO + NO ₂ + O ₂	4.50E-14	0	1260
NO ₂ + O ₃	NO ₃	1.20E-13	0	2450
NO ₃ + Br	BrO + NO ₂	1.60E-11	0	0
NO ₃ + HCHO	HONO ₂ + HO ₂ + CO	2.00E-12	0	2440
NO ₃ + C ₅ H ₈	ISON	3.15E-12	0	450
NO ₃ + EtCHO	HONO ₂ + EtCO ₃	6.30E-15	0	0
NO ₃ + MGLY	MeCO ₃ + CO + HONO ₂	3.36E-12	0	1860
NO ₃ + Me ₂ CO	HONO ₂ + MeCOCH ₂ OO	3.00E-17	0	0
NO ₃ + MeCHO	HONO ₂ + MeCO ₃	1.40E-12	0	1860
O(¹ D) + CH ₄	HCHO + H ₂	9.00E-12	0	0
O(¹ D) + CH ₄	OH + MeOO	1.31E-10	0	0
O(¹ D) + CO ₂	O(³ P) + CO ₂	7.50E-11	0	-115
O(¹ D) + H ₂	OH + H	1.20E-10	0	0
O(¹ D) + H ₂ O	OH + OH	1.63E-10	0	-60
O(¹ D) + HBr	HBr + O(³ P)	3.00E-11	0	0
O(¹ D) + HBr	OH + Br	1.20E-10	0	0
O(¹ D) + HCl	H + ClO	3.60E-11	0	0
O(¹ D) + HCl	O(³ P) + HCl	1.35E-11	0	0
O(¹ D) + HCl	OH + Cl	1.01E-10	0	0
O(¹ D) + N ₂	O(³ P) + N ₂	2.15E-11	0	-110
O(¹ D) + N ₂ O	N ₂ + O ₂	4.60E-11	0	-20
O(¹ D) + N ₂ O	NO + NO	7.30E-11	0	-20



O(¹ D) + O ₂	O(³ P) + O ₂	3.30E-11	0	-55
O(¹ D) + O ₃	O ₂ + O(³ P) + O(³ P)	1.20E-10	0	0
O(¹ D) + O ₃	O ₂ + O ₂	1.20E-10	0	0
O(¹ D) + CH ₄	HCHO + HO ₂ + HO ₂	3.45E-11	0	0
O(³ P) + BrO	O ₂ + Br	1.90E-11	0	-230
O(³ P) + ClO	Cl + O ₂	2.80E-11	0	-85
O(³ P) + ClONO ₂	ClO + NO ₃	3.60E-12	0	840
O(³ P) + H ₂	OH + H	9.00E-18	0	0
O(³ P) + H ₂ O ₂	OH + HO ₂	1.40E-12	0	2000
O(³ P) + HBr	OH + Br	5.80E-12	0	1500
O(³ P) + HCHO	OH + CO + HO ₂	3.40E-11	0	1600
O(³ P) + HCl	OH + Cl	1.00E-11	0	3300
O(³ P) + HO ₂	OH + O ₂	2.70E-11	0	-224
O(³ P) + HOCl	OH + ClO	1.70E-13	0	0
O(³ P) + NO ₂	NO + O ₂	5.10E-12	0	-210
O(³ P) + NO ₃	O ₂ + NO ₂	1.70E-11	0	0
O(³ P) + O ₃	O ₂ + O ₂	8.00E-12	0	2060
O(³ P) + OCIO	O ₂ + ClO	2.40E-12	0	960
O(³ P) + OH	O ₂ + H	1.80E-11	0	-180
	0.25*HO ₂ + 0.25*OH + 0.65*MACR + 0.58*HCHO + 0.1*MACRO ₂ + 0.1*MeCO ₃ + 0.08*MeOO + 0.28*HCOOH + 0.14*CO + 0.09*H ₂ O ₂			
O ₃ + C ₅ H ₈	0.9*MGLY + 0.45*HCOOH + 0.32*HO ₂ + 0.22*CO + 0.19*OH + 0.1*MeCO ₃	9.99E-15	0	1995
O ₃ + MACR	0.9*MGLY + 0.45*HCOOH + 0.32*HO ₂ + 0.22*CO + 0.19*OH + 0.1*MeCO ₃	4.26E-16	0	1520
O ₃ + MACR	0.19*OH + 0.1*MeCO ₃	7.00E-16	0	2100
OCIO + NO	NO ₂ + ClO	2.50E-12	0	600
OH + CH ₄	H ₂ O + MeOO	2.45E-12	0	1775
OH + CO†	H + CO ₂	1.44E-13	0	0
OH + ClO	HCl + O ₂	6.00E-13	0	-230
OH + ClO	HO ₂ + Cl	7.40E-12	0	-270
OH + ClONO ₂	HOCl + NO ₃	1.20E-12	0	330
OH + H ₂	H ₂ O + H	2.80E-12	0	1800
OH + HBr	H ₂ O + Br	5.50E-12	0	-200
OH + HCHO	H ₂ O + HO ₂ + CO	5.40E-12	0	-135
OH + HCl	H ₂ O + Cl	1.80E-12	0	250
OH + HO ₂	H ₂ O + O ₂	4.80E-11	0	-250
OH + H ₂ O ₂	HO ₂ + H ₂ O	2.90E-12	0	160
OH + HO ₂ NO ₂	H ₂ O + NO ₂ + O ₂	3.20E-13	0	-690
OH + HOCl	ClO + H ₂ O	3.00E-12	0	500
OH + HONO ₂ †	H ₂ O + NO ₃	2.40E-14	0	-460
OH + MeOOH	H ₂ O + MeOO	1.89E-12	0	-190
OH + NO ₃	HO ₂ + NO ₂	2.20E-11	0	0
OH + O ₃	HO ₂ + O ₂	1.70E-12	0	940



OH + OCIO	HOCl + O ₂	1.40E-12	0	-600
OH + OH	H ₂ O + O(³ P)	6.31E-14	2.6	-945
OH + C ₂ H ₆	H ₂ O + EtOO	6.90E-12	0	1000
OH + C ₃ H ₈ †	i-PrOO + H ₂ O	7.60E-12	0	585
OH + C ₃ H ₈ †	n-PrOO + H ₂ O	7.60E-12	0	585
OH + C ₅ H ₈	ISO2	2.70E-11	0	-390
OH + EtCHO	H ₂ O + EtCO3	4.90E-12	0	-405
OH + EtOOH	H ₂ O + EtOO	1.90E-12	0	-190
OH + EtOOH	H ₂ O + MeCHO + OH	8.01E-12	0	0
OH + HACET	MGLY + HO ₂	1.60E-12	0	-305
OH + HCOOH	HO ₂	4.50E-13	0	0
OH + HONO	H ₂ O + NO ₂	2.50E-12	0	-260
OH + ISON	HACET + NALD	1.30E-11	0	0
OH + ISOOH	MACR + OH	1.00E-10	0	0
OH + MACR	MACRO2	1.30E-12	0	-610
OH + MACR	MACRO2	4.00E-12	0	-380
OH + MACROOH	MACRO2	3.77E-11	0	0
OH + MGLY	MeCO3 + CO	1.90E-12	0	-575
OH + MPAN	HACET + NO ₂	2.90E-11	0	0
OH + Me2CO	H ₂ O + MeCOCH ₂ OO	1.70E-14	0	-423
OH + Me2CO	H ₂ O + MeCOCH ₂ OO	8.80E-12	0	1320
OH + MeCHO	H ₂ O + MeCO3	4.70E-12	0	-345
OH + MeCO2H	MeOO	8.00E-13	0	0
OH + MeCO3H	MeCO3	3.70E-12	0	0
OH + MeCOCH ₂ OOH	H ₂ O + MeCOCH ₂ OO	1.90E-12	0	-190
OH + MeCOCH ₂ OOH	OH + MGLY	8.39E-12	0	0
OH + MeOH	HO ₂ + HCHO	2.85E-12	0	345
OH + MeONO ₂	HCHO + NO ₂ + H ₂ O	4.00E-13	0	845
OH + MeOOH	H ₂ O + HCHO + OH	2.12E-12	0	-190
OH + NALD	HCHO + CO + NO ₂	4.70E-12	0	-345
OH + PAN	HCHO + NO ₂ + H ₂ O	3.00E-14	0	0
OH + PPAN	MeCHO + NO ₂ + H ₂ O	1.27E-12	0	0
OH + i-PrOOH	Me2CO + OH	1.66E-11	0	0
OH + i-PrOOH	i-PrOO + H ₂ O	1.90E-12	0	-190
OH + n-PrOOH	EtCHO + H ₂ O + OH	1.10E-11	0	0
OH + n-PrOOH	n-PrOO + H ₂ O	1.90E-12	0	-190
DMS + OH	SO ₂	1.20E-11	0	260
DMS + OH	MSA + SO ₂	3.04E-12	0	-350
DMS + NO ₃	SO ₂	1.90E-13	0	-500
DMS + O(³ P)	SO ₂	1.30E-11	0	-410
COS + O(³ P)	CO + SO ₂	2.10E-11	0	2200
COS + OH	CO ₂ + SO ₂	1.10E-13	0	1200
SO ₂ + O ₃	SO ₃	3.00E-12	0	7000
SO ₃ + H ₂ O	H ₂ SO ₄ + H ₂ O	8.50E-41	0	-6540
Monoterp + OH	0.13*Sec_Org	1.20E-11	0	-444



Monoterp + O ₃	0.13*Sec_Org	1.01E-15	0	732
Monoterp + NO ₃	0.13*Sec_Org	1.19E-12	0	-925

1

2 **Table 3:** Termolecular reactions used in UKCA StratTrop as implemented in UKESM1.

Reactants	Products	F _c	k ₁	α ₁	β ₁	k ₂	α ₂	β ₂
O(³ P) + O ₂	O ₃	0.00	6.00E-34	-2.5	0	0.00E+00	0	0
O(³ P) + NO	NO ₂	0.60	9.00E-32	-1.5	0	3.00E-11	0	0
O(³ P) + NO ₂	NO ₃	0.60	2.50E-31	-1.8	0	2.20E-11	-0.7	0
O(¹ D) + N ₂	N ₂ O	0.00	2.80E-36	-0.9	0	0.00E+00	0	0
BrO + NO ₂	BrONO ₂	0.60	5.20E-31	-3.2	0	6.90E-12	0	0
ClO + ClO	Cl ₂ O ₂	0.60	1.60E-32	-4.5	0	3.00E-12	-2	0
Cl ₂ O ₂	ClO + ClO	0.45	3.70E-07	0.0	7690	1.80E+14	0	7690
ClO + NO ₂	ClONO ₂	0.60	1.80E-31	-3.4	0	1.50E-11	0	0
H + O ₂	HO ₂	0.60	4.40E-32	-1.3	0	7.50E-11	0	0
HO ₂ + HO ₂ [†]	H ₂ O ₂ + O ₂	0.00	2.10E-33	0.0	-920	0.00E+00	0	0
HO ₂ + NO ₂	HO ₂ NO ₂	0.60	2.00E-31	-3.4	0	2.90E-12	0	0
HO ₂ NO ₂	HO ₂ + NO ₂	0.50	4.10E-05	0.0	10650	4.80E+15	0	11170
OH + NO	HONO	0.60	7.00E-31	-2.6	0	3.60E-11	-0.1	0
OH + NO ₂	HONO ₂	0.60	1.80E-30	-3.0	0	2.80E-11	0	0
OH + OH	H ₂ O ₂	0.60	6.90E-31	-1.0	0	2.60E-11	0	0
MeCO ₃ + NO ₂	PAN	0.30	2.70E-28	-7.1	0	1.20E-11	-0.9	0
PAN	MeCO ₃ + NO ₂	0.30	4.90E-03	0.0	12100	5.40E+16	0	13830
EtCO ₃ + NO ₂	PPAN	0.30	2.70E-28	-7.1	0	1.20E-11	-0.9	0
PPAN	EtCO ₃ + NO ₂	0.30	4.90E-03	0.0	12100	5.40E+16	0	13830
MACRO ₂ + NO ₂	MPAN	0.30	2.70E-28	-7.1	0	1.20E-11	-0.9	0
MPAN	MACRO ₂ + NO ₂	0.30	4.90E-03	0.0	12100	5.40E+16	0	13830
NO ₂ + NO ₃	N ₂ O ₅	0.35	3.60E-30	-4.1	0	1.90E-12	0.2	0
N ₂ O ₅ + M	NO ₂ + NO ₃	0.35	1.30E-03	-3.5	11000	9.70E+14	0.1	11080
NO + NO	NO ₂ + NO ₂	0.00	3.30E-39	0.0	-530	0.00E+00	0	0
SO ₂ + OH	SO ₃ + HO ₂	0.60	3.00E-31	-3.3	0	1.50E-12	0	0

$$k_0 = k_1 \times (T/300)^{\alpha_1} \times \exp(-\beta_1/T)$$

$$k_\infty = k_2 \times (T/300)^{\alpha_2} \times \exp(-\beta_2/T)$$

$$k_{([M],T)} = \left(\frac{k_0[M]}{1 + \frac{k_0[M]}{k_\infty}} \right) F_c \left\{ 1 + \left[\log_{10} \left(\frac{k_0[M]}{k_\infty} \right) \right]^2 \right\}^{-1}$$

[†]Indicates that extra code is used to account for water dependence of this reaction.
 M is used to represent a third body (calculated from the grid box pressure and temperature).

3
 4
 5
 6
 7



1 **Table 4.** Photodissociation reactions used in UKCA-StratTrop. For details of the cross-section and
 2 quantum yield information please see Telford et al. (2013).

Reactants	Products
BrCl + hv	Br + Cl
BrO + hv	Br + O(³ P)
BrONO ₂ + hv	Br + NO ₃
BrONO ₂ + hv	BrO + NO ₂
CF ₂ Cl ₂ + hv	Cl + Cl
CFCl ₃ + hv	Cl + Cl + Cl
CH ₄ + hv	MeOO + H
Cl ₂ O ₂ + hv	Cl + Cl + O ₂
ClONO ₂ + hv	Cl + NO ₃
ClONO ₂ + hv	ClO + NO ₂
CO ₂ + hv	CO + O(³ P)
COS + hv	CO + SO ₂
EtCHO + hv	EtOO + HO ₂ + CO
EtOOH + hv	MeCHO + HO ₂ + OH
H ₂ O + hv	OH + H
H ₂ O ₂ + hv	OH + OH
H ₂ SO ₄ + hv	SO ₃ + OH
HACET + hv	MeCO ₃ + HCHO + HO ₂
HCHO + hv	HO ₂ + HO ₂ + CO
HCHO + hv	H ₂ + CO
HCl + hv	H + Cl
HO ₂ NO ₂ + hv	HO ₂ + NO ₂
HO ₂ NO ₂ + hv	OH + NO ₃
HOBBr + hv	OH + Br
HOCl + hv	OH + Cl
HONO + hv	OH + NO
HONO ₂ + hv	OH + NO ₂
i-PrOOH + hv	Me ₂ CO + HO ₂ + OH NO ₂ + MACR + HCHO + HO ₂
ISON + hv	OH + MACR + HCHO + HO ₂
ISOOH + hv	MeCO ₃ + HCHO + CO + HO ₂
MACR + hv	HO ₂
MACROOH + hv	OH + HO ₂ + OH + HO ₂ HACET + CO + MGLY + HCHO
MACROOH + hv	HCHO
Me ₂ CO + hv	MeCO ₃ + MeOO
MeBr + hv	Br + H
MeCHO + hv	MeOO + HO ₂ + CO
MeCHO + hv	CH ₄ + CO
MeCO ₃ H + hv	MeOO + OH
MeCOCH ₂ OOH + hv	MeCO ₃ + HCHO + OH



MeONO ₂ + hv	HO ₂ + HCHO + NO ₂
MeOOH + hv	HO ₂ + HCHO + OH
MGLY + hv	MeCO ₃ + CO + HO ₂
MPAN + hv	MACRO ₂ + NO ₂
N ₂ O + hv	N ₂ + O(¹ D)
N ₂ O ₅ + hv	NO ₂ + NO ₃
NALD + hv	HCHO + CO + NO ₂ + HO ₂
NO + hv	N + O(³ P)
NO ₂ + hv	NO + O(³ P)
NO ₃ + hv	NO + O ₂
NO ₃ + hv	NO ₂ + O(³ P)
n-PrOOH + hv	EtCHO + HO ₂ + OH
O ₂ + hv	O(³ P) + O(³ P)
O ₂ + hv	O(³ P) + O(¹ D)
O ₃ + hv	O ₂ + O(¹ D)
O ₃ + hv	O ₂ + O(³ P)
OCIO + hv	O(³ P) + ClO
PAN + hv	MeCO ₃ + NO ₂
PPAN + hv	EtCO ₃ + NO ₂
SO ₃ + hv	SO ₂ + O(³ P)

1

2

3 **Table 5.** Heterogeneous reaction list used in UKCA StratTrop in UKESM1. Uptake coefficients are
 4 denoted *f* when not constant; see Denison et al. (2018) for full references and formulation.

Reactants	Products	Uptake coefficient (γ)		
		Liquid aerosol	Nat	Ice
ClONO ₂ + HCl	Cl + Cl + HONO ₂	<i>f</i>	0.3	0.3
ClONO ₂ + H ₂ O	HOCl + HONO ₂		0.006	0.3
N ₂ O ₅ + H ₂ O	HONO ₂ + HONO ₂	0.1	0.0006	0.03
N ₂ O ₅ + HCl	Cl + NO ₂ + HONO ₂		0.003	0.03
HOCl + HCl	Cl + Cl + H ₂ O	<i>f</i>	0.3	0.3

5



1

2 **Table 6.** Aqueous phase Sulfur cycle reactions used in UKCA StratTrop in UKESM1 (after
3 Kreidenweis et al (2003)).

Reactants	Products	Rate expression /cm ³ molecule ⁻¹ s ⁻¹
HSO ₃ ⁻ (aq) + H ₂ O ₂ (aq)	SO ₄ ²⁻ (aq)	2.1295E+14*exp(-4430.0/T)*([H ⁺]/(1.0 + 13.0*[H ⁺]))
HSO ₃ ⁻ (aq) + O ₃ (aq)	SO ₄ ²⁻ (aq)	4.0113E+13*exp(-5530.0/T)
SO ₃ ²⁻ (aq) + O ₃ (aq)	SO ₄ ²⁻ (aq)	7.43E+16*exp(-5280.0/T)

4

5 [H⁺] is prescribed in UKCA StratTrop in UKESM1 at 1E-5 molecules cm⁻³.

6

7 The stratospheric sulfate aerosol optical depth, used in the radiation scheme of MetUM, is
8 modified to be consistent with the aerosols seen in the heterogeneous chemistry which, by
9 default, are taken from a surface aerosol density climatology prepared for the CMIP6 model
10 intercomparison (Luo, personal communication). The surface aerosol density is converted to
11 mass mixing ratio, using a climatology of particle size (Thomason and Peter, 2006) and
12 assuming a density of 1700 kg/m³.

13

14 2.3 Photolysis

15 The most significant new development relative to MO09 and OC14 in the UKCA-StratTrop
16 scheme used in UKESM1 is the interactive Fast-JX photolysis scheme which is applied to
17 derive photolysis rates between 177 and 750 nm (Neu et al., 2007) as described in Telford et
18 al. (2013). This is an important new addition as it enables interactive treatment of photolysis
19 rates (key drivers for the photochemistry of the atmosphere) under changing climate and
20 atmospheric composition. For shorter wavelengths, relevant above 60 km, a correction is
21 added, to account for photolysis occurring between 112 and 177 nm, following Lary and Pyle
22 (1991).

23

24 In older versions of UKCA (i.e. MO09 and OC14) precalculated photolysis frequencies were
25 applied in the model by default. Sellar et al (2019) shows a comparison of these and we note
26 here that the switch from pre-calculated to on-line interactive photolysis calculations has had
27 a significant effect on shortening the model simulated methane lifetime and increasing the
28 tropospheric mean [OH] (Telford et al., 2013; O'Connor et al., 2014; Voulgarakis et al., 2009),
29 as shown in Figure 4.

30

31 2.4 Dry deposition

32 In UKCA the representation of dry deposition follows the resistance-in-series model as
33 described by Wesley (1989) in which the removal of material at the surface is described by
34 three resistances, r_a , r_b , and r_c . The deposition velocity v_d (m s⁻¹) is then a function of these
35 three resistance terms according to:

36

$$37 \quad v_d = \frac{1}{r_a + r_b + r_c},$$

38

39 where r_a denotes the aerodynamic resistance to dry deposition, r_b is the quasi-laminar
40 resistance term, and r_c represents the resistance to uptake at the surface. Of these three terms



1 r_c tends to be the most complex because it encompasses a variety of exchange fluxes, such
2 as stomatal and cuticular uptake, assimilation by soil microbes, etc. The uptake at the surface
3 also depends strongly on the presence of dew, rain, or snow which can interrupt the deposition
4 process altogether.

6 **2.4.1 Dry deposition of gas-phase species**

7 Surface dry deposition is calculated interactive at every time step for a number of atmospheric
8 gas-phase species (c.f., Table 1 for a list of deposited species). The aerodynamic resistance
9 r_a is given by:

$$11 \quad r_a = \frac{\ln\left(\frac{z}{z_0}\right) - \Psi}{k \times u^*},$$

12
13 where z_0 is the roughness length, Ψ denotes the Businger dimensionless stability function, k
14 is the von Karman constant, and u^* is the friction velocity. r_a represents the resistance to
15 turbulent mixing in the boundary layer and therefore depends crucially on the stability of the
16 boundary layer. It is independent of the chemical species that is deposited.

17
18 The quasi-laminar resistance r_b , on the other hand, depends on the chemical and physical
19 properties of the deposited species. It describes the transport through the thin, laminar layer
20 of air closest to the surface. Transport through this layer is diffusive due to the absence of
21 turbulent mixing.

22
23 The third resistance term r_c depends on both the physico-chemical properties of the deposited
24 species and the properties and condition of the respective surface to which deposition occurs.
25 The surface can be anything from bare soil or rock to vegetation and even urban environments.
26 Surface uptake varies with season, time of day and current meteorological conditions. The
27 largest individual surface type is water in the form of the world's oceans. In this latter case
28 solubility obviously plays the key role (Hardacre et al., 2015; Luhar et al., 2017).

29
30 A particularly important surface uptake process is the deposition flux to the terrestrial
31 vegetation. In this case a number of pathways exist which are commonly integrated into the
32 so-called "Big-leaf" model (Smith et al., 2000; Seinfeld and Pandis, 2006). Of all the deposition
33 pathways manifesting in vegetated regions, for most species the most important is uptake
34 through the stomata. Through these tiny pores in the leaf surface plants take up carbon dioxide
35 from the atmosphere and exchange water vapour and oxygen with it. This exchange also
36 includes all other species that make up the ambient air, including pollutants such as for
37 instance ozone. For this, the specific type of vegetation is crucial. Ozone deposition fluxes, for
38 instance, vary widely between forests and grasslands.

39
40 The calculation of the surface resistance term and land surface type information provided by
41 the dynamic vegetation model JULES (Best et al., 2011; Clark et al., 2011) is utilised in UKCA.
42 JULES forms part of the UKESM1 Earth system model and is thus coupled with UKCA. Within
43 JULES, various land surface type configurations may be selected. In the most simple
44 configuration, which was also used in the UKESM1 predecessor model HadGEM2-ES, any
45 land-based grid box at the surface can be subdivided into variable-sized fractions assigned to
46 any of 9 different surface types: broadleaf trees, needleleaf trees, C3 grasses, C4 grasses,



1 shrubs, bare spoil, rivers and lakes, urban environments and ice. Non-land grid boxes are
2 treated separately.

3
4 Since then, the number of land surface types in JULES has increased substantially (c.f. Harper
5 et al., 2018). Apart from the original 9-tile version (5 vegetation and 4 non-vegetation types),
6 13, 17, and also 27-tile configurations are now included. The upgrade to the 13-tile
7 configuration increases the number of vegetation types by introducing 3 broadleaf plant
8 functional types (PFTs), 2 needleleaf PFTs, and 2 shrub PFTs; the number of grass-related
9 PFTs as well as the number of non-vegetation type remains the same. In this configuration,
10 The 17-tile configuration further extends the number of PFTs by introducing 4 cropland types,
11 two C3-grass related and two C4-grass related PFTs; again, the number of non-vegetation
12 types remains the same. Finally, the 27-tile land surface configuration, corresponding to the
13 UKESM1 release configurations and the configurations used for this manuscript, introduces a
14 substantial number of additional land ice tiles. Each of these land surface and PFT tiles offers
15 a specific resistance to dry deposition of atmospheric gas-phase species.

16
17 For dry deposition of aerosols a slightly different treatment is taken to that described above
18 and we direct the reader to Mulchay et al. (2019) and references therein for more details.

19

20 **2.5 Wet deposition**

21 The wet deposition scheme employed in UKCA for the removal of tropospheric gas-phase
22 species through convective and stratiform precipitation is the same as that described in
23 O'Connor et al., 2014. The original scheme was implemented from the TOMCAT chemistry
24 transport model (CTM) where it previously had been validated by Giannakopoulos (1998) and
25 Giannakopoulos et al. (1999). In this paper we provide a brief description of the scheme but
26 will not present an evaluation because there have been no changes since the last published
27 version. For an in-depth performance evaluation in UKCA we refer to section 3.4 in O'Connor
28 et al. (2014).

29

30 Following a scheme originally developed by Walton et al. (1988) wet deposition is
31 parameterized as a first-order loss process which is calculated as a function of the three-
32 dimensional convective and stratiform precipitation. The climate model provides the required
33 precipitation activity to UKCA. The wet scavenging rate r is calculated at every grid box and
34 time step according to:

35

$$36 \quad r = S_j \times p_j(l)$$

37

38 where S_j is the wet scavenging coefficient for precipitation type j (cm^{-1}) and $p_j(l)$ is the
39 precipitation rate for type j (convective or stratiform), provided by the climate model at model
40 level l (cm h^{-1}).

41

42 Scavenging coefficients for nitric acid (HNO_3) of 2.4 cm^{-1} and 4.7 cm^{-1} for stratiform and
43 convective precipitation, respectively, are applied (c.f., Penner et al., 1991). These parameters
44 are scaled down for individual species using the fraction of each species in the aqueous phase,
45 f_{aq} , calculated by:

46



1
2
3
4
5
6
7
8
9
10
11
12
13
14

$$f_{aq} = \frac{L \times H_{eff} \times R \times T}{1 + L \times H_{eff} \times R \times T}$$

where L represents the liquid water content, R the universal gas constant, T denotes ambient temperature, and H_{eff} is the effective Henry's Law constant for each species. H_{eff} includes the effects of solubility, dissociation, and complex formation. Tables 7, 8 and 9 summarise the parameters used in the UKCA wet deposition scheme for each soluble species included in the StratTrop chemical mechanism.

Furthermore, in the scheme precipitation only occurs over a fraction of the grid box. This fraction is assumed to be 1.0 and 0.3 for stratiform and convective precipitation, respectively. These fractions are applied in the calculation of the grid box mean wet scavenging rate for both precipitation types after which point the two rates are added together.

Table 7. Values required to calculate the effective Henry's Law coefficient for the soluble tropospheric species included in the UKCA strat-trop scheme, where Me=CH₃, Et=C₂H₅, Pr=C₃H₇.

Species	Henry's Law Data		Dissociation Data	
	$K_H(298\text{ K})$	$-\Delta H/R$	$K_a(298\text{ K})$	$-\Delta H/R$
	M atm ⁻¹	K ⁻¹	M	K ⁻¹
NO ₃	2.0E+00	2000.0	0.0E+00	0.0
N ₂ O ₅	2.1E+05	8700.0	2.0E+01	0.0
HO ₂ NO ₂	1.3E+04	6900.0	1.0E-05	0.0
HONO ₂	2.1E+05	8700.0	2.0E+01	0.0
HO ₂	4.0E+03	5900.0	2.0E-05	0.0
H ₂ O ₂	8.3E+04	7400.0	2.4E-12	-3730.0
HCHO	3.3E+03	6500.0	0.0E+00	0.0
MeOO	2.0E+03	6600.0	0.0E+00	0.0
MeOOH	3.1E+02	5000.0	0.0E+00	0.0
HONO	5.0E+01	4900.0	5.6E-04	-1260.0
EtOOH	3.4E+02	5700.0	0.0E+00	0.0
n-PrOOH	3.4E+02	5700.0	0.0E+00	0.0
i-PrOOH	3.4E+02	5700.0	0.0E+00	0.0
MeCOCH ₂ OOH	3.4E+02	5700.0	0.0E+00	0.0
ISOOH	1.7E+06	9700.0	0.0E+00	0.0



ISON	3.0E+03	7400.0	0.0E+00	0.0
MACROOH	1.7E+06	9700.0	0.0E+00	0.0
HACET	1.4E+02	7200.0	0.0E+00	0.0
MGLY	3.5E+03	7200.0	0.0E+00	0.0
HCOOH	6.9E+03	5600.0	1.8E-04	-1510.0
MeCO ₃ H	7.5E+02	5300.0	6.3E-09	0.0
MeCO ₂ H	4.7E+03	6000.0	1.8E-05	0.0
MeOH	2.3E+02	4900.0	0.0E+00	0.0

1
 2
 3

Table 8. Values required to calculate the effective Henry's Law coefficient for the soluble stratospheric species included in the UKCA strat-trop scheme, where Me=CH₃, Et=C₂H₅, Pr=C₃H₇.

Species	Henry's Law Data		Dissociation Data	
	$K_H(298\text{ K})$	$-\Delta H/R$	$K_a(298\text{ K})$	$-\Delta H/R$
	M atm ⁻¹	K ⁻¹	M	K ⁻¹
BrONO ₂	2.1E+05	8700.0	1.57E+02	0.0
HCl	1.9E+01	600.0	1.0E+04	0.0
HOCl	9.2E+02	5900.0	3.2E+06	0.0
HBr	1.3E+00	10,200.0	1.0E+09	0.0
HOBr	6.1E+04	0.0	0.0E+00	0.0
ClONO ₂	2.1E+05	8700.0	1.57E+01	0.0

4
 5
 6
 7

Table 9. Values required to calculate the effective Henry's Law coefficient for the soluble aerosol precursor species included in the UKCA strat-trop scheme, where Me=CH₃, Et=C₂H₅, Pr=C₃H₇.

Species	Henry's Law Data		Dissociation Data	
	$K_H(298\text{ K})$	$-\Delta H/R$	$K_a(298\text{ K})$	$-\Delta H/R$
	M atm ⁻¹	K ⁻¹	M	K ⁻¹
O ₃	1.13E-02	2300.0	0.0E+00	0.0
SO ₂	1.23E+00	3020.0	1.23E-02	2010.00
DMSO	5.0E+04	6425.0	0.0E+00	0.0

8
 9
 10

2.6 Emissions



1 In this section, the implementation of tropospheric ozone precursor emissions used in the
2 UKCA StratTrop scheme are described in detail. The StratTrop scheme includes the
3 emissions of nine chemical species: nitrogen oxide (NO), carbon monoxide (CO),
4 formaldehyde (HCHO), ethane (C₂H₆), propane (C₃H₈), acetaldehyde (MeCHO), acetone
5 (Me₂CO), isoprene (C₅H₈), and methanol (MeOH). Emissions to UKCA can be broadly
6 classified into two categories: *offline*, where pre-computed fluxes are read from input files; and
7 *online*, where fluxes are computed in real-time during the simulation making use of online
8 meteorological variables from the MetUM. The implementation of *offline* emissions will be
9 described in Section 2.6.1. Examples of *online* emissions currently in UKCA StratTrop are
10 biogenic volatile organic compound (BVOC) emissions (Section 2.6.2) and lightning NO_x
11 (Section 2.6.3).

12
13 When UKCA StratTrop is coupled to the UKCA aerosol scheme, GLOMAP-mode (Mann et al.,
14 2010) as here, there are additional trace gas aerosol-precursor emissions for dimethyl
15 sulphide (DMS), sulphur dioxide (SO₂), and monoterpenes (C₁₀H₁₆). These emissions will be
16 discussed in the context of the UKESM1 aerosol performance in Mulcahy et al. (2019); the
17 focus here will solely be on the tropospheric ozone precursor emissions. Table 11 and Figures
18 5-8 summarise the mean global annual emissions totals for the time period considered here
19 (2005-2014) and their global and seasonal distributions.

22 **2.6.1 Offline Anthropogenic and Natural Emissions**

23 *Offline* tropospheric ozone precursor emissions are either injected into the model's lowest
24 layer or, in the case of aircraft emissions and some biomass burning emissions, injected into
25 a number of model levels. The emissions are added to the appropriate UKCA tracers (see
26 Table 1) and mixed simultaneously by the boundary-layer mixing scheme (Section 2.1). Boreal
27 and temperate forest and deforestation emissions are considered 'high-level' and are spread
28 uniformly up to level 20 (~3 km in L85).

29
30 For anthropogenic emissions, we make use of historical (1750–2014) annual emissions of
31 reactive gases from the Community Emissions Data System (CEDS; Hoesly et al., 2018) that
32 were prepared for use in CMIP6. The CEDS emissions are generally greater than those of
33 other emission datasets (e.g. Lamarque et al., 2010) for the years that are used in the
34 simulations evaluated here (i.e. 2005-2014). Biomass burning emissions are taken from van
35 Marle et al. (2017). They combined satellite observations from 1997 with various proxies and
36 output from six fire models participating in the Fire Model Intercomparison Project (FireMIP;
37 Rabin et al., 2017) to provide a complete dataset of biomass burning emissions from 1750 to
38 2014 for use in CMIP6. As was the case for anthropogenic emissions, emissions from the
39 years 2005-2014 are used here. For both anthropogenic and biomass burning, the emissions
40 were re-gridded from their native resolution to N96L85 while conserving global annual totals
41 and seasonal cycles. For VOCs, emissions of all C₂ and C₃ VOCs are included as ethane and
42 propane, respectively.

43
44 For natural emissions which are not simulated, *offline* emissions are prescribed through the
45 provision of pre-computed fluxes. For example, oceanic emissions of CO, ethane (including
46 ethene (C₂H₄)), propane (including propene (C₃H₆)) are taken from the POET (Granier et al.,
47 2005) inventory for the year 1990 which contains one annual cycle with 12 monthly fluxes.
48 These fluxes are applied perpetually to all years of the time series. Biogenic emissions of



1 acetaldehyde (MeCHO) make use of combined emissions of MeCHO and other aldehydes
2 from the MACCity-MEGAN emissions inventory (Sindelarova et al., 2014); biogenic emissions
3 of CO, HCHO, MeOH, and propane (including C₃H₆) are also taken from this inventory. For
4 biogenic acetone emissions, emissions of acetone and *other* ketones from the MACCity-
5 MEGAN emissions inventory (Sindelarova et al., 2014) are combined. Based on the years
6 2001-2010, a monthly mean climatology is derived and applied to all years (see Section 3 for
7 the implementation of the emission in the model). Finally, soil emissions of NO_x are distributed
8 according to Yienger and Levy (1995) and scaled to give a global annual total of 12.0 Tg NO/yr
9 and again perpetually applied to all years.

10

11 **2.6.2 Biogenic VOC emissions**

12 In the standard configuration of UKCA StratTrop in UKESM1, emissions of organic compounds
13 from the natural environment (BVOC) are added to UKCA interactively (Sellar et al., 2019a).
14 Specifically, emissions of isoprene (C₅H₈) and (mono-)terpenes are *online*, the latter
15 represented by a lumped compound in UKCA with the formula C₁₀H₁₆ and a corresponding
16 molecular weight of 136 g mol⁻¹, are calculated by the interactive biogenic VOC (iBVOC)
17 emission model (Pacifico et al., 2011). Emission fluxes are passed to UKCA at every model
18 time step.

19

20 In iBVOC the emissions of isoprene are coupled to the gross primary productivity of the
21 terrestrial vegetation (Arneth et al., 2007; Pacifico et al., 2011). The biogenic emission of all
22 other organic compounds included in the iBVOC model, i.e., (mono-)terpenes, methanol, and
23 acetone, follow the original model described in Guenther et al. (1995). Note that the current
24 configuration of UKCA used in UKESM1 does not make use of the interactive emissions of
25 methanol or acetone; these are *offline* as discussed in Section 2.6.1. To the best of our
26 knowledge, in the case of the non-isoprene biogenic VOCs there exists no equivalent process-
27 based formulation for an interactive BVOC emission model applicable to Earth System Models
28 (ESMs).

29

30 For present-day conditions total global annual emissions of isoprene amount to 495.9 (±13.6)
31 Tg(C) yr⁻¹. This number represents the 10-year average annual total emission strength and
32 the uncertainty quantified by the standard deviation over the 10-year period between 2005
33 and 2014 taken from a historic run with UKESM1 (Sellar et al., 2019a). This is in good
34 agreement with estimates reported for other emission models (e.g. Arneth et al., 2008;
35 Guenther et al., 2012; Messina et al., 2016; Müller et al., 2008; Sindelarova et al., 2014;
36 Stavrakou et al., 2009; Young et al., 2009). However, it has been argued that wide model
37 agreement is achieved rather due to model tuning than due to a high level of process
38 understanding (c.f., Arneth et al., 2008). For the global annual total (mono-)terpene emissions,
39 iBVOC calculates 115.1 (±1.6) Tg(C) yr⁻¹ over the same period of model simulation. This model
40 estimate is in reasonable good agreement with the literature (e.g., Folberth et al., 2006;
41 Lathière et al., 2006; Arneth et al., 2007, 2011; Acosta Navarro et al., 2014; Sindelarova et al.,
42 2014; Bauwens et al., 2016; Messina et al., 2016).

43

44 In the configuration of UKCA StratTrop used in UKESM1, isoprene is included in the gas-
45 phase chemistry but does not contribute to the formation of secondary organic aerosol (SOA).
46 Emissions of (mono-)terpenes are oxidised using a fixed yield approach (e.g. Kelly et al., 2018)
47 to form SOA in the GLOMAP-mode aerosol scheme - see Table 2 and Mulcahy et al., 2019
48 for a detailed description and evaluation.



1

2 **2.6.3 Emissions of NO_x from lightning**

3 The lightning NO_x emissions scheme in UKCA StratTrop is based on the cloud top
4 parameterisation proposed by Price and Rind (1992). Based on satellite data and storm
5 measurements, the lightning flash density is parameterised as:

6

$$7 \quad F_l = 3.44 \times 10^{-5} H^{4.9} \quad \text{Eq 1.}$$

$$8 \quad F_o = 6.2 \times 10^{-4} H^{1.3} \quad \text{Eq 2.}$$

9

10 where F is the flash density (flash min⁻¹), H is the cloud top height (km), and the l and o
11 subscripts are used to represent the land and ocean, respectively, and distinguish between
12 the updraft velocities experienced over the two surfaces. The scheme also differentiates
13 between cloud-to-cloud and cloud-to-ground flashes based on the grid cell latitude (Price and
14 Rind, 1993) and is resolution-independent by the implementation of a spatial calibration factor
15 (Prince and Rind, 1994). A minimum cloud depth of 5 km is required for NO_x emissions to be
16 activated and is diagnosed on a timestep basis from the physical model's convection scheme.
17 For NO_x production, the parameterisation assumes that the production efficiency per unit of
18 energy discharged is 25x10¹⁶ molec (NO) J⁻¹, with the energy discharged from cloud-to-ground
19 flashes being 3 times greater than that for cloud-to-cloud flashes.

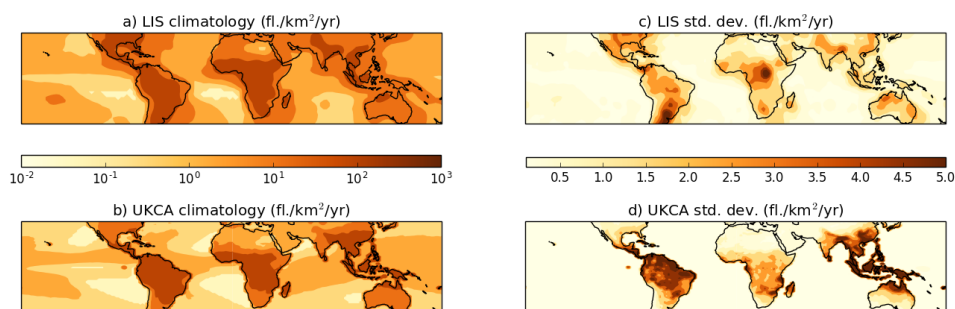
20

21 This implementation is identical to that implemented in HadGEM2-ES (Collins et al., 2011) by
22 O'Connor et al. (2014) except that NO_x emissions are now distributed linearly in altitude in
23 log(pressure) rather than linearly in pressure. Whereas global annual lightning emissions in
24 HadGEM2-ES were inadvertently too low (O'Connor et al., 2014; Young et al., 2013), here,
25 the emissions have been scaled to give an average global annual emission rate of 5.93 and
26 5.98 TgN yr⁻¹ over the period 2005 to 2014 in the free-running and nudged simulations,
27 respectively. When compared with anthropogenic, biomass burning and natural emissions,
28 lightning contributes approximately 10 % to the global annual NO_x emission rate, consistent
29 with estimates from Schumann and Huntrieser (2007).

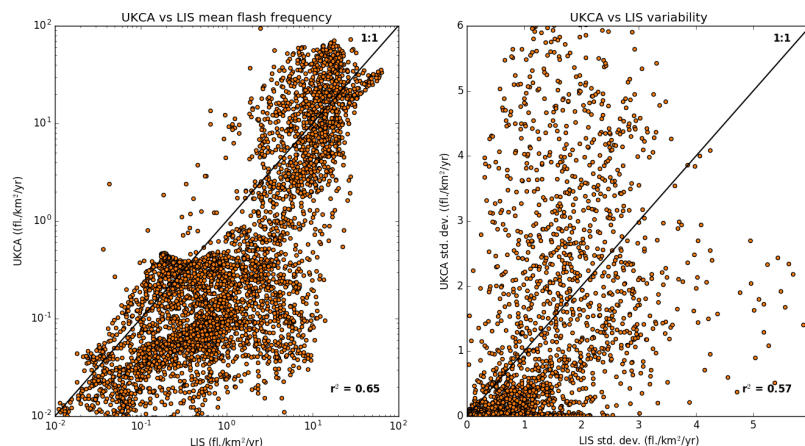
30

31 Figure 1 shows tropical distributions of decadal mean annual flash density as observed by the
32 Lightning Imaging Sensor (LIS) on board the Tropical Rainfall Measuring Mission (TRMM)
33 satellite (Mack et al., 2007) in comparison with the free-running simulation being evaluated
34 here (see section 3 for details). It demonstrates that UKCA is capable of capturing the broad
35 features of the observed climatology, with peak densities over S. America, Africa, and East
36 Asia; the spatial coefficient of determination (R²) between the modelled and observed
37 climatology is 0.65 and 0.69 in the free-running and nudged (not shown) simulations,
38 respectively. However, the model tends to be biased low in regions of low flash density (e.g.
39 over the oceans and towards the extra tropics) than compared to the observations (Figure 2),
40 consistent with the assessment of Finney et al. (2014). In considering the variability, the spatial
41 R² between the modelled and observed variability is 0.57 and 0.59 in the free-running and
42 nudged simulations, respectively. The variability from UKCA is comparable in magnitude to
43 that observed over Africa, albeit displaced geographically. Over the Maritime continent and S.
44 America, for example, UKCA overestimates the variability relative to the LIS observations.

45



1
2 **Figure 1.** Tropical distribution of the LIS-observed climatological annual mean lightning flash density
3 over the period 1999-2013 in a) in comparison with the modelled annual mean climatology from the
4 period 2005-2014 in b). The corresponding standard deviation of the observed and modelled
5 climatologies are shown in c) and d), respectively.
6



7
8 **Figure 2.** Scatter plot of the modelled versus the LIS-observed multi-annual annual mean lightning
9 flash density (left) and the standard deviation (right).
10

11 Whilst the skill of the cloud top parameterisation is good relative to other parameterisations,
12 (Finney et al., 2014) and the performance here in the free-running and nudged model
13 simulations is consistent with that assessment, raising the diagnosed cloud top height over
14 land to the power of 4.9 makes the cloud top parameterisation susceptible to model biases in
15 cloud top height, as noted by Allen and Pickering (2002) and Tost et al. (2007). Lightning is
16 potentially a key chemistry-climate interaction in Earth System Models but the sensitivity to
17 how it is represented (i.e. using cloud top height (Banerjee et al., 2014) or ice-flux based
18 parameterisations (Finney et al., 2018)) warrants further investigation. Indeed, Hakim et al.
19 (2019) recently identified uncertainty in modelled lightning NO_x in the Indian subcontinent as
20 being an important source of uncertainty in model simulations of tropospheric ozone in that
21 region.
22



1 **2.6.4 Lower boundary conditions**

2 Lower boundary conditions are provided at the surface for the chemical species CH₄, N₂O,
3 CFC-11 (CFCl₃), CFC-12 (CF₂Cl₂), CH₃Br, H₂, and COS. Values for H₂ and COS are fixed at
4 500 ppb and 482.8 ppt respectively (invariant with time). Values for the remaining species are
5 specified using time series data provided for the 5th Coupled Model Intercomparison Project
6 (CMIP5) for the greenhouse gas concentrations (see *RCP webpage in references*). The values
7 provided are valid on the 1st July for each year specified, and are linearly interpolated in time
8 to give daily values if data for more than one time-point is defined. CFC-11, CFC-12, and
9 CH₃Br also contain contributions from other Cl and Br containing species to ensure that there
10 is the correct stratospheric chlorine and bromine loading, with these contributing species given
11 in Table 10. These values are converted into a two-dimensional “effective emission” field at
12 each timestep that is used to fix the surface concentrations of these species.

13
14 **Table 10.** List of species contributing to the lower boundary conditions of CFC-11, CFC-12, and
15 CH₃Br. Note that H-1211 contributes to both CFC-11 and CH₃Br as it contains both Cl and Br.
16 Contributions are included by moles of Cl or Br.

CFC-11	CFC-12	CH ₃ Br
CCl ₄	CFC-113	H-1211
CH ₃ CCl ₃	CFC-114	H-1202
HCFC-141b	CFC-115	H-1301
HCFC-142b	HCFC-22	H-2402
H-1211		
CH ₃ Cl		

17
18

19 **2.7 Coupling with other Earth System components**

20 Secondary aerosol formation of sulphate and organic carbon in UKESM1 (Sellar et al., 2019a)
21 is determined by oxidants (OH, O₃, H₂O₂, NO₃) modelled interactively by the UKCA StratTrop
22 chemistry scheme. For further details on the oxidation of sulphate and SOA precursors,
23 chemistry-aerosol coupling, and the scientific performance of the aerosol scheme (GLOMAP-
24 mode; Mann et al., 2010) in UKCA and UKESM1, the reader is referred to Mulcahy et al.
25 (2019).

26

27 In the HadGEM2-ES model (Collins et al., 2011) used for CMIP5, radiative feedbacks between
28 UKCA modelled methane and tropospheric ozone concentrations were active (OC14);
29 stratospheric ozone was prescribed and combined with the modelled interactive tropospheric
30 concentrations. In UKESM1 (Sellar et al., 2019a), however, the coupling between the UKCA
31 modelled radiatively active trace gases and the radiation scheme has been extended to
32 include N₂O and stratospheric ozone (in addition to methane and tropospheric ozone).
33 Although chlorofluorocarbons (CFCs) and hydrochlorofluorocarbons (HCFCs) are modelled in
34 UKCA StratTrop, the radiation scheme cannot handle the speciation. Therefore, separate
35 lumped species (CFC12-eq and HFC134a-eq) are prescribed in the radiation scheme (see
36 Section 2.6.4 on how the lumping/mapping is done).



1
2
3
4
5
6
7
8
9
10
11
12
13
14
15
16
17
18
19
20
21
22
23
24
25
26
27
28
29
30
31
32
33
34
35
36
37
38
39
40
41
42
43
44
45
46
47
48
49
50

2.7.1 Heterogeneous chemistry couplings:

In UKCA StratTrop as implemented in UKESM1, 5 different heterogeneous reactions are included (see Table 5). These reactions occur on the modelled soluble aerosol surface area, which in the troposphere is calculated interactively using GLOMAP-mode by summing over all soluble aerosol modes. In the stratosphere (defined here as being 12 km above the surface) the aerosol surface area comes from the stratospheric sulfate surface area density input climatology, discussed in Sellar et al. (2019b). The combining of the stratospheric aerosol surface area density from the climatology and the interactive components of GLOMAP-mode is calculated at each UKCA time step and only the soluble aerosol modes simulated by GLOMAP are included in the calculation.

Heterogeneous reactions are extremely important for simulating composition change in the stratosphere (Keeble et al., 2014) and there is increasing attention to the simulation of these processes in the troposphere too (e.g. Jacob et al., 2000; Lowe et al., 2015). One of the most important tropospheric heterogeneous reactions is that of N_2O_5 on aerosol surfaces (Jacob et al., 2000). This reaction is complicated because of the dependence of the uptake parameter (γ) on the composition of the aerosol as well as on temperature and relative humidity (Bertram and Thornton 2009). Macintyre and Evans (2010) suggest that models that use high values of $\gamma\text{N}_2\text{O}_5$ (~0.1) overestimate the impact of changing aerosol loadings on tropospheric composition through heterogeneous uptake. In UKCA StratTrop, $\gamma\text{N}_2\text{O}_5$ is set at this higher value, 0.1, throughout the atmosphere. In part this compensates for the fact that there is an important missing aerosol surface in UKESM1 in the troposphere, in the form of nitrate aerosol. The lack of nitrate aerosol is an issue for UKESM1 simulations of particulate matter, particularly in regions with high levels of ammonia emissions. A better understanding of $\gamma\text{N}_2\text{O}_5$ is needed to both understand current composition but also the combined impact of changing gas and aerosol-phase composition. Whilst more sophisticated treatments of $\gamma\text{N}_2\text{O}_5$ are available (e.g. Bertram and Thornton 2009) and have been included in versions of UKCA, further work is required to improve this aspect of the mechanism for UKCA in UKESM1.

2.7.2 Chemical production of H_2O .

There are many chemical reactions which consume or produce water vapour in the troposphere and stratosphere. For example, reactions between the hydroxyl radical (OH) and VOCs usually result in the production of a water molecule:



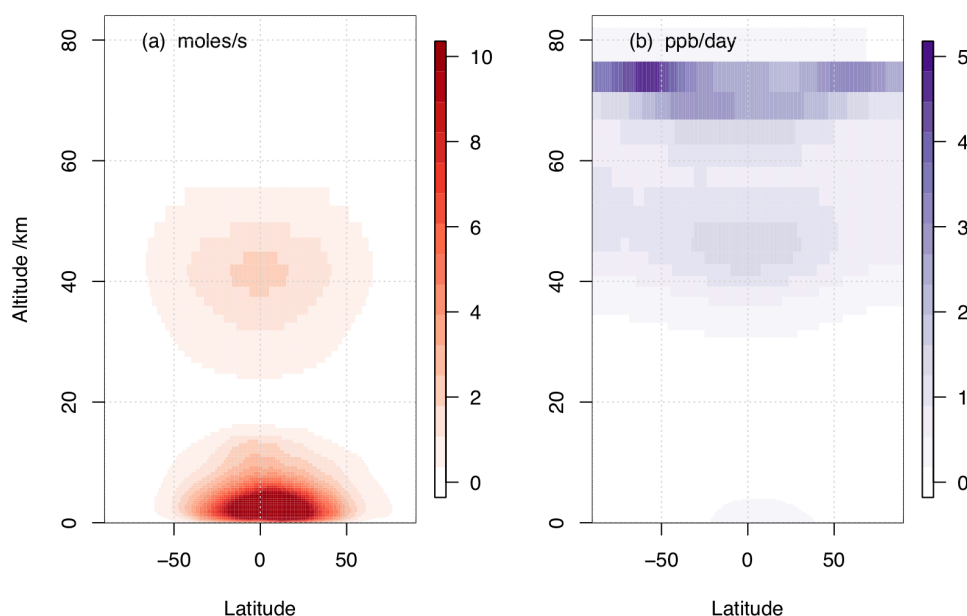
In the troposphere the chemical source of water vapour is negligible compared with that from the oceans and plant evapotranspiration, but given the low temperatures around the tropopause, chemically produced water is very important in the lower stratosphere. Furthermore, the main source of chemical water in the middle to upper stratosphere comes from the oxidation of CH_4 . Complete oxidation of CH_4 to CO_2 can result in the net production of two water molecules.

In previous versions of UKCA, such as that used in HadGEM2-ES, the oxidation of CH_4 to produce chemical water was neglected. Instead stratospheric water vapour was simulated using the following simple relationship:

$$2*[\text{CH}_4] + [\text{H}_2\text{O}] = 3.75 \text{ (ppm)} \quad \text{Eq 4.}$$



1 where UKCA was used to calculate $[\text{CH}_4]$. In UKCA StratTrop as implemented in UKESM1 we
2 now include interactive H_2O production from all chemical reactions in the mechanism. In this
3 way UKCA now passes the water vapour field after the chemistry step back to the main climate
4 model where it is used in other routines. The annual mean zonal mean chemical production
5 of H_2O as simulated by UKESM1 is shown in Figure 3. There are two clear regions which
6 dominate where H_2O chemical production takes place, in the tropical lower troposphere and
7 the tropical upper stratosphere. In both regions the primary source of chemical water is the
8 oxidation of CH_4 . Figure 3 compares the absolute production of chemical water (panel a) and
9 the production of chemical water as expressed in mixing ratio units (panel b). In this sense,
10 panel (b) shows the relative production of chemical water is greatest in the upper stratosphere.
11 The contribution of this source of stratospheric H_2O to the present day forcing of climate
12 relative to the pre-industrial period will be assessed in O'Connor et al. (2019).
13



14
15 **Figure 3.** Multi annual mean zonal mean production of H_2O from the UKCA StratTrop mechanism in
16 UKESM1. Panel (a) shows the production in moles/s and panel (b) in ppb/day, highlighting the larger
17 relative source of water from chemical processes in the upper atmosphere.
18

19 2.7.3 Future couplings.

20 Although UKESM1 (Sellar et al., 2019a) represents a significant enhancement in the
21 representation of atmospheric chemistry and ES interactions, a number of key interactions are
22 not included. For example, the coupling of aerosols with Fast-JX is omitted despite the impact
23 of aerosols on tropospheric photochemical production of ozone (e.g. Xing et al., 2017; Wang
24 et al., 2019). This development is currently underway and will be included in future versions
25 of UKCA and UKESM. Ozone damage to natural and managed ecosystems (e.g. Ashmore,
26 2005) has an important impact on the strength of carbon uptake by vegetation (Sitch et al.,
27 2007; Oliver et al., 2018) and has yet to be implemented. In addition, although the terrestrial
28 carbon cycle considers nitrogen availability/limitation, nitrogen deposition rates are prescribed
29 in UKESM1; future work will include implementing a nitrate aerosol scheme in GLOMAP-mode



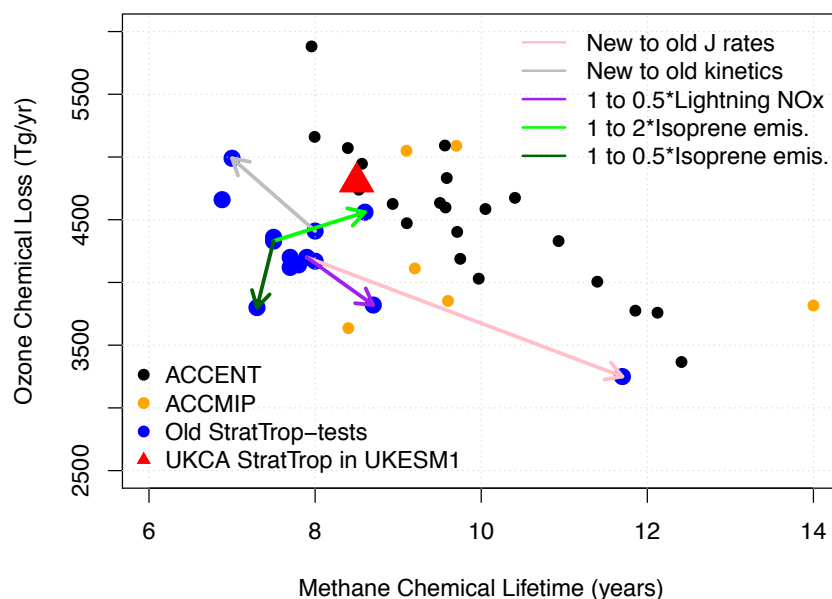
1 and coupling deposition of both oxidised and reduced nitrogen from the atmosphere to the
2 terrestrial biosphere.

3
4

5 **2.8 Historic development of the chemistry scheme**

6 During the development of the StratTrop chemistry scheme, several simulations were run to
7 test the scheme and its sensitivity to different (a) rate coefficients (updating the JPL and IUPAC
8 recommendations), (b) reactions (by looking at the sensitivity to specific reactions associated
9 with isoprene oxidation (Archibald et al., 2011) and the reaction between HO₂ and NO
10 (Butkovzkaya et al., 2005; 2007; 2009), (c) treatment of photolysis, (d) emissions and (e)
11 deposition parameters. These one-at-a-time simulations are outlined in Table S1 in the
12 Supplement. It should be noted that these simulations provide an ensemble of opportunity;
13 they were not designed to probe model sensitivity in a targeted way. However, they result in
14 some useful information which helped the development of the StratTrop mechanism. These
15 simulations made use of an older version of the MetUM and earlier atmosphere only version
16 of UKCA, which is now deprecated. That version of UKCA ran at a lower resolution than the
17 version discussed in this paper and used in UKESM1 (about half the resolution). Results from
18 these simulations are shown in Figure 4 where they are compared against results from model
19 intercomparison studies (further analysis of the model sensitivity tests is presented in the
20 Supplement Figures S1 to S6). Figure 4 focuses on a subset of the full range of experiments
21 performed but contextualises these by comparing to results from the ACCENT simulations
22 discussed in Stevenson et al. (2006) (black dots) and the ACCMIP simulations discussed in
23 Young et al. (2013) (orange dots). In addition to the early sensitivity tests (the blue dots in
24 Figure 4), we also show the results from the simulations presented here, labelled UKESM1
25 (red triangle in Figure 4). The figure focuses on the relationship between methane lifetime and
26 ozone chemical loss, important metrics for representing key sources and sinks of tropospheric
27 OH (Wild 2007). Both metrics are calculated by masking out the stratosphere. The methane
28 lifetime is calculated by dividing the burden of methane in the model by the reaction flux
29 between methane and OH in the troposphere and so represents the lifetime with respect to
30 OH in the troposphere. The ozone loss is calculated by summing the reaction fluxes which are
31 key for O₃ loss in the troposphere (reactions of O₃ with HO_x species and the reaction between
32 O(¹D) and H₂O). The experiments outlined in Table S1 and shown in Figure 4 emphasise that
33 the range in O₃ loss and CH₄ lifetime spanned by changing aspects of the UKCA model span
34 a range as wide as that covered by the ACCMIP models (Young et al., 2013). In other words,
35 the *ensemble of opportunity* from the early tests of the UKCA StratTrop scheme span as wide
36 a range in the metrics presented as the structurally different ACCMIP and ACCENT models.
37 Interestingly, the UKESM1 simulations discussed in this paper in detail lie close to the
38 ACCENT ensemble (black dots), yet the early test simulations using the same chemical
39 mechanism but an earlier version of the MetUM model do not (the blue cluster of dots). This
40 highlights that structural changes in the underlying meteorological model can substantially
41 influence key metrics of atmospheric composition through changes in the distribution of
42 clouds, water vapour and other key variables.

43



1
 2 **Figure 4.** Comparison of early tests of the StratTrop scheme running in an older version of UKCA (blue
 3 dots) with the scheme applied in UKESM1 (red triangle) and other CCMs which took part in the ACCMIP
 4 intercomparison (orange dots) and CTMs which took part in the ACCENT intercomparison (black dots).
 5

6 These sensitivity studies highlight some important points. Simulations using kinetic data
 7 recommendations from IUPAC and JPL updated from 2005 to 2011 led to a decrease in model
 8 methane lifetime and an increase in ozone chemical loss flux (grey arrow), indicating
 9 increased photochemically activity. The attribution of which rate coefficients were dominant in
 10 this behaviour is outside of the scope of this work. Similarly, we note that the metrics analysed
 11 are sensitive to lightning NO_x (Banerjee et al., 2014); decreasing the lightning NO_x emissions
 12 by 50 % (to ~ 3 Tg/yr) results in an increased methane lifetime of ~ 1 year (purple arrow).
 13 Figure 4 also highlights a non-linear response in the simulations to changes in isoprene
 14 emissions; scaling them by a factor of two (100 % increase and 50 % decrease, green arrows)
 15 leads to a highly non-linear response in the metrics analysed. Finally we note that the change
 16 which had the biggest impact on the metrics was switching to the FAST-JX photolysis scheme
 17 (Telford et al., 2013) from pre-calculated photolysis rates and a look-up table (pink arrow). The
 18 main reason for this is that the pre-calculated photolysis rates had underestimated rates for
 19 the photolysis of O₃ to O(¹D). This behaviour has been documented previously (Voulgarakis
 20 et al., 2009; Telford et al., 2013).
 21

22 In addition to the tests described above we found during the testing of the StratTrop scheme
 23 that inclusion of the termolecular reaction:



24 which has been shown to exhibit both pressure and water vapour dependence (Butkovzkaya
 25 et al., 2005; 2007; 2009), led to large changes in the metrics analysed in Figure 4 (see the
 26 Supplement for further details). Previous modelling work highlighted that this could have an
 27



1 important impact on the simulation of ozone (Cariolle et al., 2008). However, owing to
2 uncertainty in its recommendation between the recent evaluations by JPL and IUPAC we have
3 omitted it from the StratTrop scheme used in UKESM1.

4 5 **3.0 Model simulations to evaluate UKCA StratTrop in UKESM1.**

6 In this section, we discuss a series of simulations that have been performed to evaluate the
7 performance of the UKCA StratTrop scheme in UKESM1. These simulations link closely to
8 the UKESM1 Historical and AMIP simulations by using similar inputs, e.g. emissions, and
9 crucially the version of UKCA StratTrop is identical to that used in UKESM1 (Sellar et al.,
10 2019a).

11
12 Simulations analysed in this paper have been carried out with an atmosphere-only
13 configuration of UKESM1 (Sellar et al., 2019a). The sea surface temperatures and sea ice
14 cover used to drive the model are those specified for the historical period by the 6th Coupled
15 Model Intercomparison Project (CMIP6 project; Durack et al., 2016). Land cover fraction,
16 vegetation canopy height and leaf area index (LAI) have been provided as multi-annual
17 monthly mean climatologies, derived from a historical simulation of UKESM1 which includes
18 the dynamic vegetation model TRIFFID (Cox, 2001). Anthropogenic and biomass burning
19 emissions of ozone precursors are prescribed on a monthly basis using a 2005-2014
20 timeseries from Hoesly et al. (2018) (see section 2.6) and van Marle et al. (2017), respectively.
21 Land-based biogenic emissions not simulated within the JULES model (e.g. CO) are provided
22 as monthly climatologies for the period 2001-2010 from the MEGAN-MACC dataset
23 (Sindelarova et al 2014), supplemented by soil NO_x emissions based on Yienger and Levy
24 (1995) and oceanic emissions from POET. Greenhouse gas concentrations for CFC12, CH₄,
25 CO₂, HFC134 and N₂O are derived from the dataset generated by Meinshausen et al (2017)
26 for CMIP6. Concentrations of other CFCs seen only by UKCA are derived from the same
27 dataset but described in more detail under Lower Boundary Conditions (Section 2.6.4). The
28 model is initialised using output after nearly 150 years of the UKESM1 coupled historical
29 simulation. The land surface setup used in this paper is based on a 27 sub-grid tile
30 configuration including 13 plant functional types (three broadleaf tree tiles, two needleleaf tree
31 tiles, three C3-grass tiles including crops, three C4-grass tiles including crops, and two tiles
32 representing shrubs), one water tile (to represent lakes), one tile for bare soil, one urban tile
33 and 11 land ice tiles.

34
35 Two simulations have been carried out using the Atmosphere-only configuration, covering
36 January 1999 to December 2014. The first is a *free-running* (FR) simulation where the
37 meteorology is allowed to evolve independently based on the influence of the aforementioned
38 forcing agents. The second is a *Nudged* (ND) simulation where the meteorology, though under
39 the same forcings as the FR simulation, is in addition relaxed toward the ECMWF's ERA-
40 Interim reanalysis (Dee et al., 2011) using the Nudging functionality in the MetUM (Telford et
41 al., 2008). Nudging is applied to model temperature and winds from about 1.2 km (to be
42 generally free of the boundary layer) to 65 km (maximum height of ERA data), using an e-
43 folding relaxation timescale of 6 hours.

44
45 For both simulations, output from the first 6 years is considered as spin-up and analysis from
46 the years 2005-2014 inclusive is presented in this paper. Model fields used in the analysis
47 have been output mainly as monthly means. In addition, some aerosol-related fields were



1 produced at daily and 6-hourly intervals, while ozone, nitric acid and nitrogen dioxide at the
 2 surface were produced at hourly intervals.

3
 4 Table 11 provides a summary of the sectors contributing to the emissions of the nine
 5 tropospheric ozone precursor species treated in UKCA StratTrop and their corresponding
 6 global annual totals, averaged (mean) over the 2005-2014 time period covered by the two
 7 simulations. Figures 5 and 6 show the multi-annual global annual mean distributions and the
 8 seasonal cycle for different emission sectors and regions for NO and CO, respectively. While
 9 the figures illustrate that the main contribution to NO and CO emissions is of anthropogenic
 10 origin, other sectors are relevant in shaping the yearly cycle. Examples include emissions of
 11 NO from biomass burning in the tropics, soil NO emissions in the extratropics, land biogenic
 12 CO emissions in the extratropics and ocean biogenic CO emissions in the southern
 13 extratropics.

14
 15 **Table 11.** List of emitted tropospheric ozone precursor species in UKCA StratTrop, including the
 16 contributing sectors and the corresponding global annual totals, averaged over the time period of the
 17 simulations i.e. 2005-2014 inclusive.

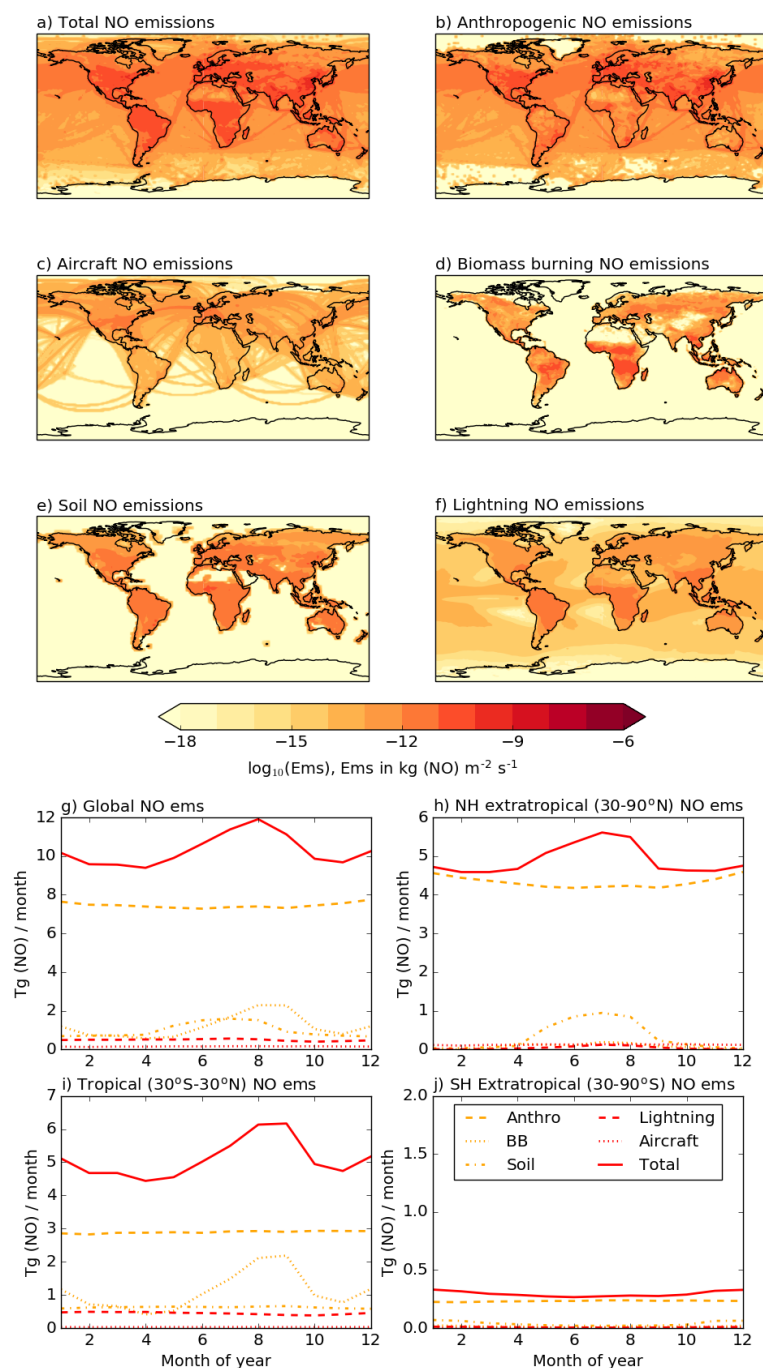
18

Species	Sector	Total
NO _x	Anthropogenic	89.4
	Biomass burning	14.3
	Soil	11.8
	Aircraft	1.9
	Lightning	12.7
	Total (Tg(NO)/year)	130.1
CO	Anthropogenic	603.3
	Biomass burning	347.0
	Land biogenic	88.6
	Ocean biogenic	19.6
	Total (Tg(CO)/year)	1089.5
HCHO	Anthropogenic	2.4
	Biomass burning	4.8
	Land biogenic	4.6
	Total (Tg(HCHO)/year)	11.8
C ₂ H ₆ (including C ₂ H ₄)	Anthropogenic	16.3
	Biomass burning	9.3
	Land biogenic	31.1
	Ocean biogenic	2.4
	Total (Tg(C₂H₆)/year)	59.1
C ₃ H ₈ (including C ₃ H ₆)	Anthropogenic	10.2
	Biomass burning	4.5
	Land biogenic	15.6
	Ocean biogenic	2.8
	Total (Tg(C₃H₈)/year)	33.1
MeCHO (including other aldehydes)	Anthropogenic	1.9
	Biomass burning	7.1



but <i>not</i> HCHO)	Land biogenic Total (Tg(MeCHO)/year)	21.5 30.5
Me ₂ CO	Anthropogenic Biomass burning Land biogenic Total (Tg(Me₂CO)/year)	2.8 3.0 37.4 43.2
MeOH	Anthropogenic Biomass burning Land biogenic Total (Tg(MeOH)/year)	3.8 8.1 129.1 141.0
C ₅ H ₈	Land biogenic Total (Tg(C)/year)	495.9 495.9
C ₁₀ H ₁₆	Land biogenic Total (Tg(C)/year)	115.1 115.1

1
2
3

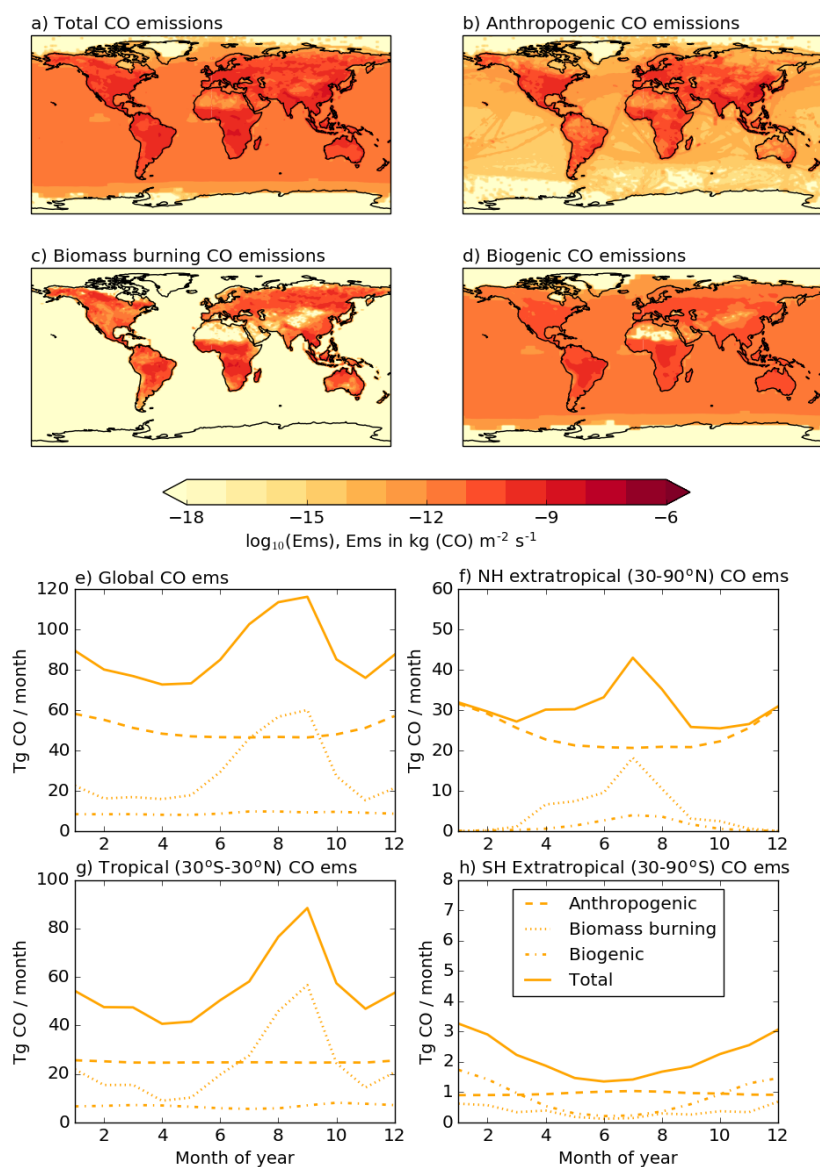


1
 2 **Figure 5.** Multi-annual mean NO emissions distribution (plotted as $\log_{10}(\text{Ems})$, with Ems in $\text{kg}(\text{NO}) \text{m}^{-2} \text{s}^{-1}$) used in the simulations presented here. Panel (a) highlights the total NO emissions, while panels
 3
 4 (b) to (f) show the contributions from anthropogenic, aircraft, biomass burning, soil, and lightning
 5 sources, respectively. Aircraft and lightning emissions have been integrated in the vertical. Panels (g)



1 to (j) show the multi-annual seasonal cycle in $Tg(NO)/month$ over the whole globe, the northern
2 hemisphere (NH) extratropics ($30^{\circ}S-30^{\circ}N$), the tropics ($30^{\circ}S-30^{\circ}N$), and the southern hemisphere (SH)
3 extratropics ($30^{\circ}S-30^{\circ}N$), respectively.

4
5



6
7
8
9
10
11

Figure 6. Multi-annual mean CO emissions distribution (plotted as $\log_{10}(\text{Ems})$, with Ems in $\text{kg (CO) m}^{-2} \text{s}^{-1}$) used in the simulations presented here. Panel (a) highlights the total CO emissions, while panels (b) to (d) show the contributions from anthropogenic, biomass burning and biogenic sources, respectively. Panels (e) to (h) show the multi-annual seasonal cycle in $Tg(\text{CO})/month$ over the whole



1 globe, the northern hemisphere (NH) extratropics (30-90°N), the tropics (30°S-30°N), and the
2 southern hemisphere (SH) extratropics (30-90°S), respectively.

3
4

5 **4.0 Evaluation of model fields**

6 We start our evaluation of UKCA StratTrop in UKESM1 by assessing the performance of the
7 model in the troposphere, against surface observations, and build up the evaluation to focus
8 on tropospheric integrated quantities and stratospheric quantities before concluding with an
9 analysis of transport in the model.

10

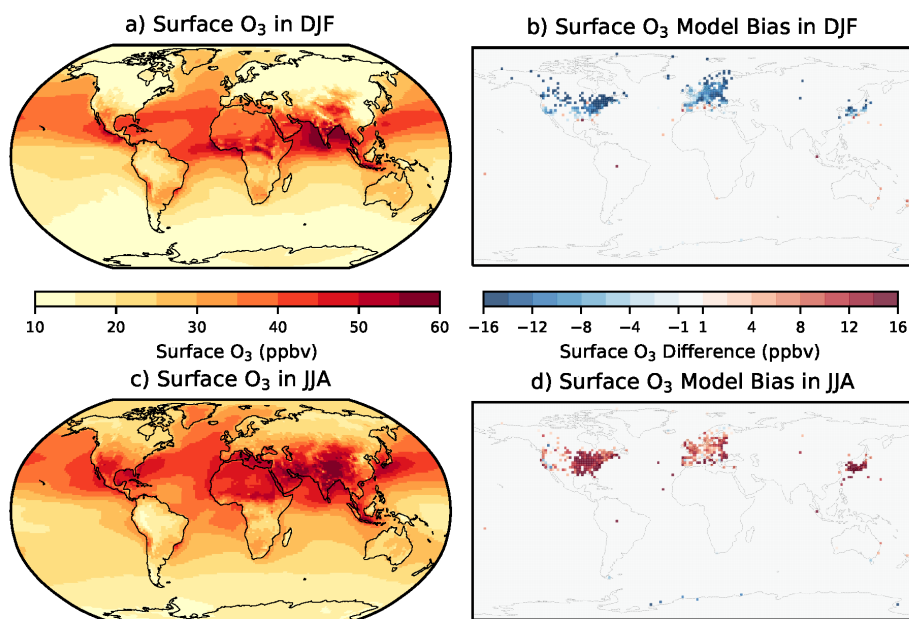
11 **4.1 Evaluation of surface ozone against TOAR observations.**

12 The surface O₃ concentrations in the FR simulations with UKCA StratTrop in UKESM1 for
13 December-January-February (DJF) and June-July-August (JJA) (seasonal means over the
14 2005-2014 period) show elevated values across the tropics in both seasons as well as in the
15 northern mid-latitudes in JJA (Figure 7a and c). Maximum surface O₃ concentrations of more
16 than 60 ppb are simulated across the Middle East, Northern Africa and South Asia in JJA due
17 to large anthropogenic and biogenic sources of O₃ precursors. In DJF, surface O₃
18 concentrations are lower over the continental northern mid-latitudes due to slow O₃ production
19 and an enhanced O₃ removal from elevated NO_x emissions. Meanwhile, surface O₃
20 concentrations are slightly higher over oceanic areas (North Atlantic and North West Pacific)
21 in DJF, probably due to transport from the stratosphere and a reduced chemical sink
22 from weaker photolysis of O₃ (Banerjee et al., 2016). Surface O₃ concentrations are slightly higher
23 over some oceanic areas in JJA, indicating long range transport from polluted continental
24 areas.

25

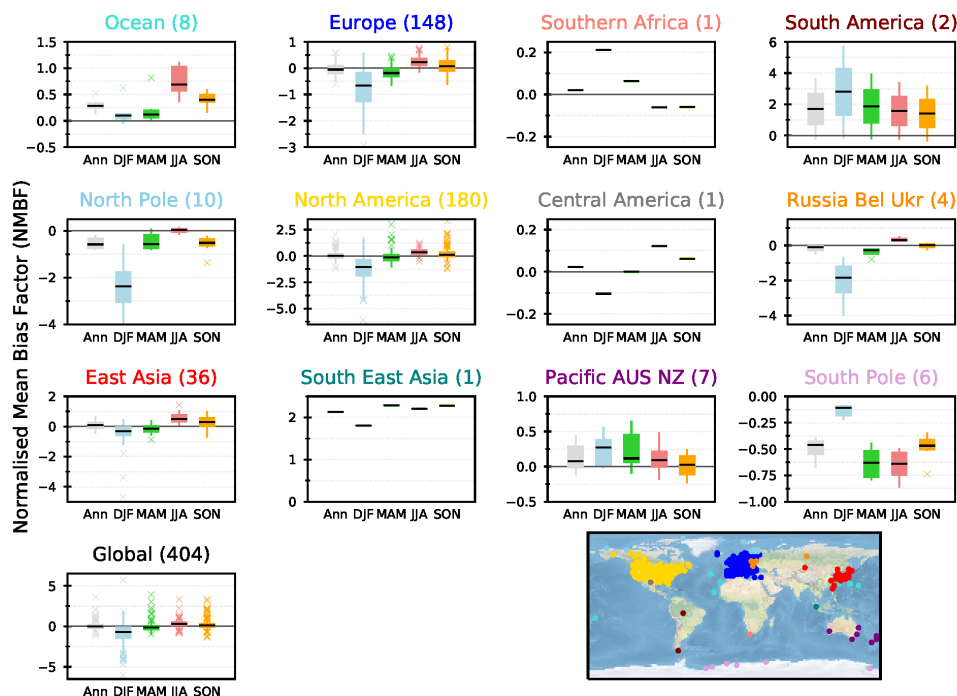
26 Surface O₃ concentrations simulated in the nudged configuration of UKESM1 have been
27 evaluated over the period 2005-2014 by comparing to the gridded rural observations in the
28 TOAR database (Schultz et al., 2017). These data provide a global perspective on surface O₃
29 and is by far the most comprehensive surface O₃ database for use in evaluation of global
30 models. However, the TOAR database does not provide globally uniform coverage and as
31 such the evaluation of the model performance for surface O₃ over key regions, such as South
32 Asia (Hakim et al., 2019), will be analysed in more specific follow up studies making use of
33 bespoke datasets. Figure 7b and d shows that the model underpredicts surface O₃
34 concentrations in DJF and overpredicts O₃ in JJA across the northern midlatitudes, in a similar
35 way to other global models (Young et al., 2018). Potential reasons for these discrepancies
36 could be the coarse model resolution, associated errors in the emissions inventories, errors in
37 the vertical injection of the emissions (for example we inject most of the NO_x near the surface
38 which will titrate O₃), representation of VOCs in the chemistry scheme and uncertainties in O₃
39 loss processes (dry deposition).

40



1
2 **Figure 7.** Simulated seasonal mean surface O₃ concentrations in a) December-January-February (DJF)
3 and c) June-July-August (JJA) over the 2005-2014 period. Difference between simulated and observed
4 surface O₃ from the gridded TOAR database in b) DJF and d) JJA.
5

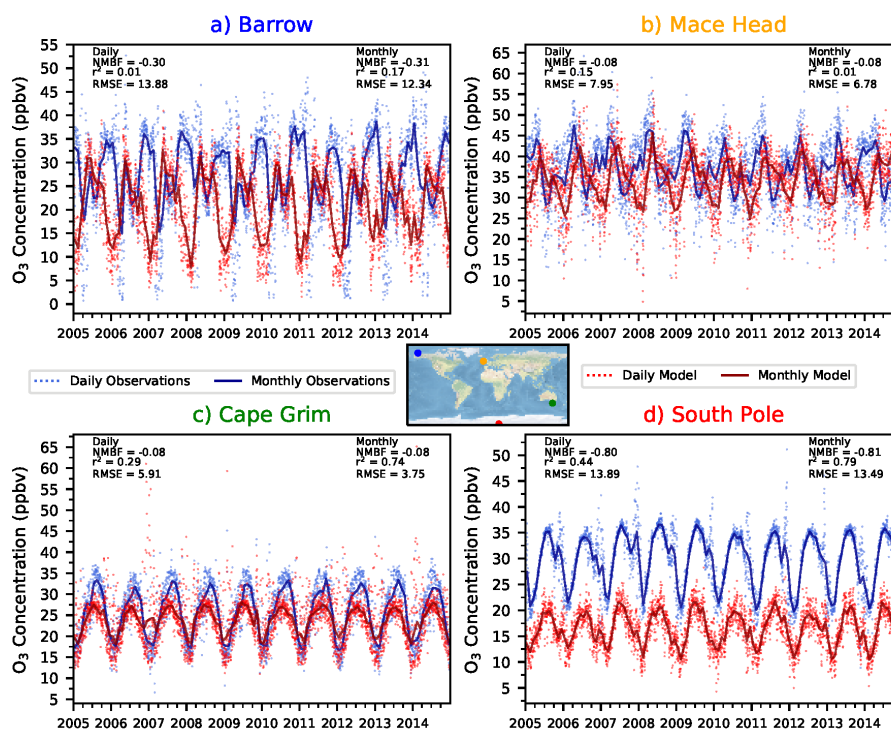
6 Each grid point containing observations has been evaluated against the corresponding model
7 values by calculating a normalised mean bias factor (NMBF, Yu et al., 2006). Figure 8 shows
8 the distribution of NMBFs within a particular region for different seasons. Over northern
9 midlatitudes (Europe, North America and East Asia) the model clearly underrepresents
10 surface O₃ in DJF (by a factor of 1.5 to 2), suggesting excessive O₃ titration by NO_x. The model
11 agrees better with observations in other seasons across these regions, with a slight
12 overprediction in JJA. The limited available observations in other regions (<10 grid points)
13 makes it difficult to draw firm conclusions but suggests that UKCA StratTrop in UKESM1 tends
14 to overpredict surface O₃ across the oceanic and southern hemisphere sites. The model
15 consistently underpredicts observed surface O₃ at sites located in Antarctica, implying a lack
16 of transport and a too low modelled O₃ lifetime in this region, particularly in March-April-May
17 (MAM) and JJA.
18



1
 2
 3
 4
 5
 6
 7
 8
 9
 10
 11
 12
 13
 14
 15
 16
 17
 18
 19
 20
 21
 22
 23

Figure 8. Normalised mean bias factors (NMBF) calculated for annual and seasonal means by comparing modelled concentrations of surface O₃ in UKESM1 to gridded observations from the TOAR database across each region over the 2005-2014 period. The solid line shows the median value for the region, the boxes show the 25th and 75th percentile values with the error bars showing the maximum and minimum values and the crosses representing outliers (values >1.5 x interquartile range). The total number of sites used for each region is shown in parenthesis. Comparisons on annual (grey), DJF (blue), MAM (green), JJA (red) and SON (orange) timescales are shown.

Simulated daily and monthly mean surface O₃ concentrations over the period 2005-2014 from UKESM1 have been interpolated and compared to four individual observation locations from the TOAR database (Figure 9). UKESM1 is able to reproduce the seasonal cycle of surface O₃ observed at Cape Grimm ($r^2 = 0.74$, NMBF = -0.08) and South Pole ($r^2 = 0.79$, NMBF = -0.81), although it underestimates the magnitude in JJA at Cape Grimm and in all seasons at the South Pole (Figure 9). There is reasonably good model observational agreement in JJA at the two northern hemisphere sites (Barrow and Mace Head) (albeit with some disagreement in the phase), although in DJF the model underpredicts surface O₃ at both sites. The surface model evaluation of UKESM1 at selected individual measurement locations exhibits a similar performance to that of HadGEM2-ES in O'Connor et al. (2014).



1
2 **Figure 9.** Simulated and observed daily and monthly mean surface O₃ over the period 2005-2014 at
3 four individual monitoring locations of a) Barrow, b) Mace Head, c) Cape Grimm and d) South Pole
4

5 **4.2 Dry deposition of ozone – comparison with HTAP models and observations**

6 Roughly 1000 Tg(O₃), around 20 % to 25 % of the gross chemical ozone production in the
7 troposphere, is removed from the atmosphere at present every year through dry deposition at
8 the surface (Stevenson et al., 2006; Wild, 2007; Young et al., 2013; Hardacre et al., 2015).
9 Uptake by terrestrial vegetation plays a crucial role, however, Hardacre et al. (2015)
10 demonstrated that the oceans represent a very important sink, too. Much uncertainty still
11 remains about the exact magnitude and many of the processes around ozone removal at the
12 surface (e.g., Hardacre et al. 2015; Luhar et al., 2017). A thorough evaluation and, if
13 necessary, re-calibration of ozone dry deposition models is, thus, critical in developing robust
14 models of atmospheric composition.
15

16 **4.2.1 Comparison with the HTAP multi-model ensemble ozone deposition fluxes**

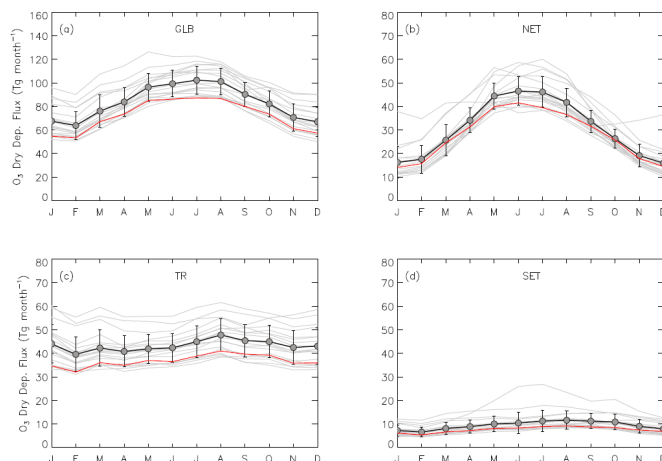
17 Figure 10 shows a comparison of multi-annual average monthly mean ozone deposition
18 modelled by UKCA StratTrop in UKESM1 with a multi-model ensemble of 15 HTAP
19 atmospheric composition models (Hardacre et al., 2015). The StratTrop model data here are
20 taken from the FR simulation. Monthly mean ozone deposition is depicted for the entire global
21 domain (Figure 10 a) and split into the northern extra-tropics, the tropics, and the southern
22 extra-tropics, respectively, each representing a distinctly different deposition regime (Figure
23 10 b-d). The solid black line and filled circles represent ensemble average monthly mean
24 ozone deposition with the error bars indicating $\pm 1\sigma$ in the single model monthly mean
25 ensemble; the solid grey lines represent single model monthly means from the HTAP models



1 indicating the spread in the multi-model ensemble. The multi-annual average (10 years)
2 monthly mean ozone dry deposition flux modeled by UKESM1-UKCA is shown as the red solid
3 line.

4
5 In general, ozone dry deposition from UKCA StratTrop in UKESM1 compares favorably with
6 the HTAP multi-model ensemble falling nearly always within the 1σ -range of the HTAP multi-
7 model average. UKCA StratTrop also correlates well with the multi-model average seasonal
8 cycle for each of the depicted regions; however, a systematic low-bias is evident, particularly
9 in the global and tropical domains (plots a and c in Figure 10). Most of the low bias occurs in
10 the tropical region. Since the tropics are dominated by both a large ocean surface area and
11 the most productive portion of the Earth's terrestrial vegetation in the form of the tropical rain
12 forests of South America, equatorial Africa and the maritime continent, the tropical low bias in
13 the model could be due to an underestimation of O_3 concentration, the stomatal ozone uptake
14 by tropical rain forests or a similar underestimation of O_3 removal at the ocean's air-sea
15 interface. The latter seems less likely in view of the relatively good performance in the southern
16 extratropics which are also dominated by a large ocean surface.

17
18



19

20 **Figure 10.** Multi-annual average monthly mean O_3 dry deposition for the global domain (a) and three
21 latitudinal sections (b-d): northern extra-tropics (NET; 90N-30N; b), tropics (TR; 30N-30S; c), and
22 southern extra-tropics (SET; 30S-90S; d) for 15 models participating in the HTAP model
23 intercomparison. Multi-model ensemble average (solid black line and filled circles) and single model
24 monthly means (grey solid lines) were provided by Hardacre et al. (2015). Error bars indicate $\pm 1\sigma$ in the
25 single model monthly means. Solid red line shows UKCA StratTrop multi-annual average (2005-2014)
26 monthly mean O_3 dry deposition. (Figure based on Hardacre et al. (2015)).

27

28 4.2.2 Comparison with observations of ozone deposition fluxes.

29 Measurements of ozone dry deposition fluxes collected over extended periods of time are still
30 very sparse, however, a number of long-term datasets exist. Hardacre et al. (2015) compiled
31 a comprehensive dataset from available long-term and short-term observations. This
32 comprehensive dataset has been adopted for our evaluation of O_3 dry deposition in UKCA
33 StratTrop in UKESM1. Table 12 summarises the locations of all the measurement sites
34 included in this comparison. A comparison of the dry deposition fluxes of ozone with



1 observations at these 16 sites is presented in Figure 11. Some sites cover the seasonal cycle
 2 over several years (e.g., Castel Porziano, Harvard Forest, or Ulborg) and others only offer
 3 data spanning less than one month (e.g., Klippeneck, Le Dezert, or Viols en Levant).

4
 5 **Table 12.** Ozone surface dry deposition measurement sites (reproduced from Hardacre et al., 2015).

Site Name	Grid reference	Land cover	Sampling height (m)	Sampling Period	Ref.
Long-term sites					
Auchencorth Moss	55°47'N 3°14'E	Moorland	0.3-3.0	Oct 1995–Dec 2000	1
Blodgett Forest	38°53'N 120°37'W	Pine plantation	12.5	Jan 2001–Dec 2007	2
Citrus Orchard	36°21'N 119°5'W	Citrus Orchard	1.0–9.2	Oct 2009–Nov 2010	4
Castel Porziano	41°44'N 12°24'E	Holm Oak	35	Jan–Dec 2013	5
Harvard Forest	42°32'N 72°11'W	Mixed deciduous forest	30	Jan 1992–Dec 2001	7
Hyytiala	61°51'N 24°17'E	Scots Pine forest	23	Jan 2002–Dec 2003	8
Ulborg	56°17'N 8°25'E	Mixed coniferous	18, 36	Oct 1995–Dec 2000	10
Short-term sites					
Borneo OP3	45°8'N 117°51'E	Tropical forest	75	Apr, Jul 2008	1
Burriana	39°55'N 0°03'W	Citrus Orchard	10	16–29 Jul 1995 28 Apr–3 May 1996	3
La Cape Sud	44°24'N 0°38'E	Maize Crop	3.4, 3.7, 6.4	Jul–Oct 2007	6
Klippeneck	48°10'N 8°45'E	Grass	2, 8	1–22 Sep 1992	3
Le Dezert	44°05'N 0°43'E	Pine forest	37	16–18 Apr 1997	3
San Pietro Capofiume	44°39'N 11°37'E	Beet crop	8	15–22 Jun 1993	3
South-western Amazon	3°00'S 60°00'W	Tropical forest	53	May 1999 Sep–Oct 1999	9
Viols en Levant	43°41'N 3°47'E	Mediterranean shrub	37	16–24 Jul 1998	3
Voghera	45°01'N 9°00'E	Onion field	2.5	May–Jul 2003	11

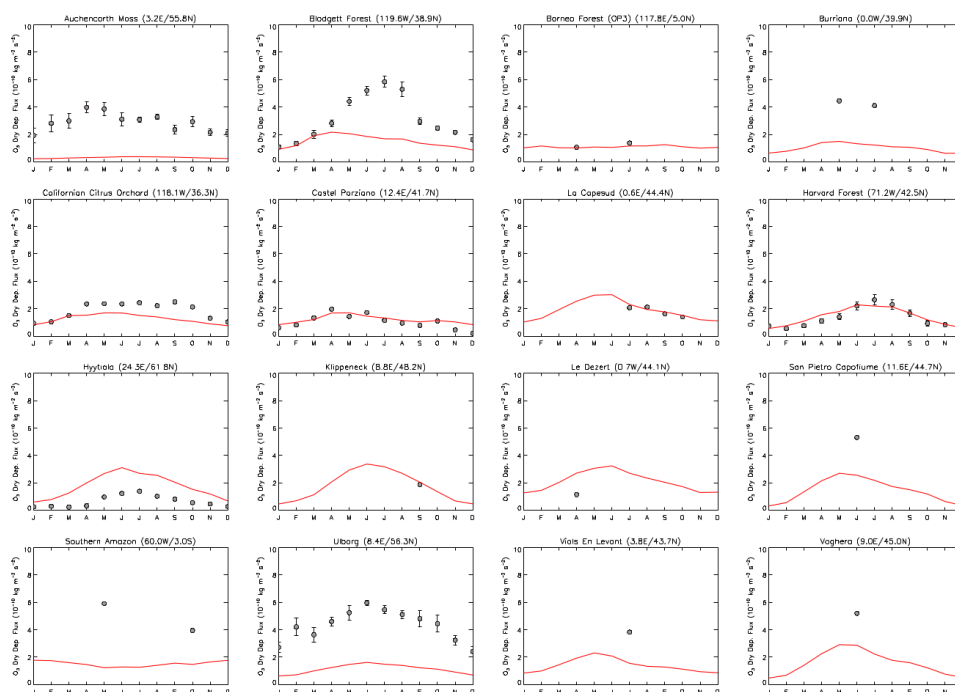
6 References: 1) Fowler et al. (2001); 2) Fares et al. (2010); 3) Cieslik (2004); 4) Fares et al. (2012);
 7 5) Fares et al. (2014); 6) Stella et al. (2011); 7) Munger et al. (1996); 8) Rannik et al. (2012);
 8 9) Fan et al. (1990); 10) Mikkelsen et al. (2004, 2000); 11) Gerosa et al. (2007)
 9

10 Due to its removal via stomatal exchange and relative insolubility in water, O₃ dry deposition
 11 depends strongly on the underlying land surface type. Therefore, a reliable representation of
 12 ozone dry deposition in models requires not only the composition model to perform well. A
 13 robust model of the land surface including dynamic vegetation is also indispensable. The land
 14 surface representation in UKCA StratTrop in UKESM1 relies on JULES (Best et al., 2011;
 15 Clark et al., 2011). Thus, a comparison of ozone dry deposition (or any dry deposition process



1 for that matter) reflects on the broader Earth system framework than just the atmospheric
2 composition component alone.

3
4



5
6 **Figure 11.** Comparison of observed and modelled monthly mean ozone dry deposition fluxes. Grey
7 circles indicate monthly mean ozone deposition fluxes at measurement sites (c.f. Table 12 for site
8 details); error bars denote standard errors. Solid red lines represent modelled multi-annual average
9 monthly mean O_3 deposition fluxes extracted from UKCA StratTrop in UKESM1 at the site locations by
10 interpolation of the nearest grid boxes. Ozone dry deposition fluxes are given in $10^{-10} \text{ kg m}^{-2} \text{ s}^{-1}$,
11 measurement data from Hardacre et al. (2015) and references therein.

12
13 Overall, Figure 11 shows that the UKCA(StratTrop)/JULES/UKESM1 framework shows a
14 reasonably good performance, albeit with some substantial model-to-obs deviations evident
15 from Figure 11. At the Castel Porziano, La Cape Sud, and Harvard Forest sites the model
16 reproduces well both magnitude and seasonal cycle of ozone dry deposition. To a somewhat
17 lesser degree model performance is also good at the California Citrus Orchard and Hyttiala
18 sites. At both locations the model captures most of the seasonal cycle well but fails to
19 reproduce the magnitude of the flux fully. Interestingly, there is no systematic bias in the
20 model-to-obs deviations with respect to magnitude and land cover type.

21
22 Further locations with good model-to-obs agreement include the densely forested OP3 site in
23 Borneo and Klippeneck site in Germany. However, these sites only provide campaign data for
24 a limited period of time. The model shows very low skill in reproducing either magnitude or
25 seasonal cycle at three sites with long-term observational records; namely Auchencorth Moss
26 (Scotland, UK), Blodgett Forest (California, U.S.A), and Ulborg (Denmark). In all three cases



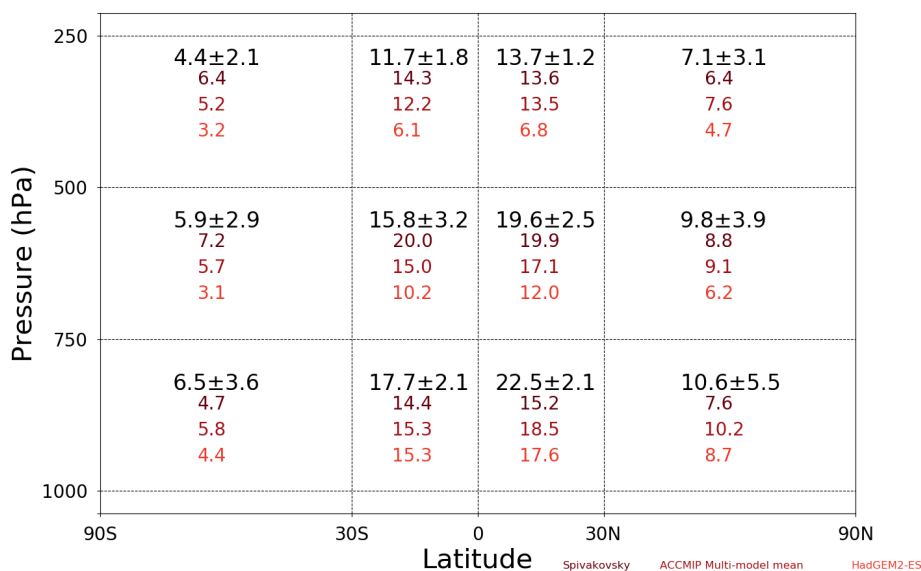
1 the model severely underestimates O₃ dry deposition fluxes. The model also shows a fairly
 2 low skill in reproducing the seasonal cycle at these three sites. Potential reasons for the low
 3 model skill at these long-term observation sites include modelled surface ozone levels,
 4 deposition velocities and the appropriateness of the vegetation type, but more detailed
 5 analysis is required to explore these further. However, by and large, the model performance
 6 appears reasonable when compared to both observations and other models, although with an
 7 overall negative bias.

10 4.3 Model simulated methane and OH

11 Here we discuss the performance of UKCA StratTrop modelled methane and OH distributions
 12 in the troposphere. OH is the primary oxidising agent in the troposphere and is the key
 13 determinant on the burden of methane in the troposphere (Monks et al., 2015).

14
 15 A commonly cited indicator of tropospheric oxidising capacity, the tropospheric lifetime of
 16 methane with respect to OH has been calculated for the FR simulation, averaged over the
 17 entire length of the run. The modelled average tropospheric mean methane lifetime with
 18 respect to OH oxidation is calculated to be 8.5 years (with a standard deviation of 0.1 years).
 19 This value is in good agreement with the ACCMIP ensemble average of 9.7 ± 1.5 years (Naik
 20 et al., 2013) (i.e. falling within one standard deviation of the ACCMIP ensemble). We note that
 21 the methane lifetime for UKESM1 is much shorter than the methane lifetime for HadGEM2ES
 22 and highlight that Figure 4 shows this is largely down to improvement in the treatment of
 23 photolysis since HadGEM2ES (Telford et al., 2013).

24
 25 We further focus our analysis on comparing the climatological distribution of OH as a function
 26 of latitude and altitude (Figure 12).



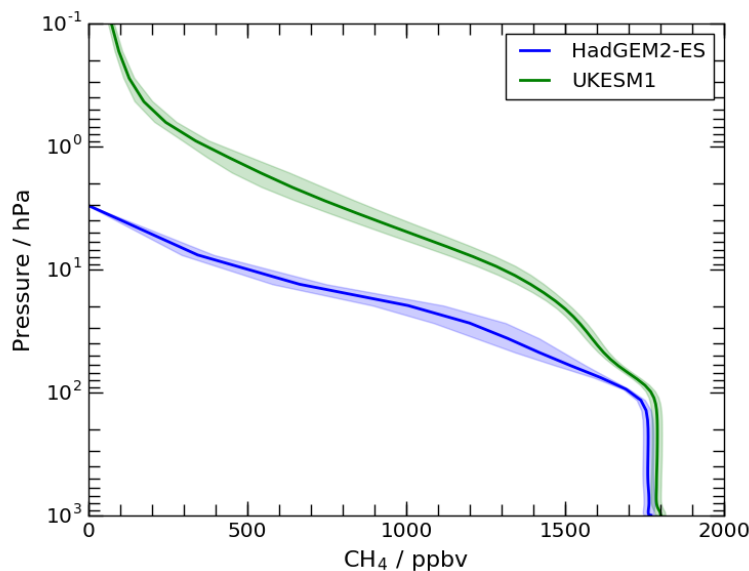


1 **Figure 12.** Evaluation of the UKCA StratTrop zonal distribution of tropospheric [OH] ($\times 10^5$ molecules
2 cm^{-3}). Values plotted in black refer to the UKCA StratTrop multi-annual mean [OH] in each region of
3 latitude and pressure range, with the values following being ± 1 standard deviation around the mean.
4

5 The UKCA StratTrop simulations result in a global mean tropospheric [OH] of 1.22×10^6
6 molecules cm^{-3} , averaged over the period 2005-2014 in the FR simulation. As with the
7 methane lifetime, this value is slightly higher than the ACCMIP ensemble mean ($11.1 \pm 1.6 \times$
8 10^5 molecules cm^{-3}) but sits within the standard deviation of the ACCMIP ensemble mean
9 (Naik et al., 2013). Figure 12 shows how the distribution of [OH] varies throughout the
10 troposphere relative to the ACCMIP multi model mean, the HadGEM2-ES model and the data
11 from Spivakovsky et al. (2000) who pioneered the development of [OH] climatologies in the
12 troposphere. Compared against these data, UKCA StratTrop in UKESM1 performs well: The
13 global tropospheric mean [OH] is within 10 % of the ACCMIP ensemble mean. The model
14 captures the latitudinal and vertical profiles found in the other data sets and agrees on the
15 magnitude of [OH] in 10 of the 12 regions analysed (when considering the model uncertainty).
16

17 The [OH] is higher in UKCA StratTrop than in HadGEM2-ES, partly because of different
18 emissions used in the HadGEM2-ES study, but also in part owing to the change in photolysis
19 scheme (as discussed previously). UKCA StratTrop agrees better with the ACCMIP multi
20 model mean than Spivakovsky or HadGEM2-ES, but the tropics from 1000-750 hPa are
21 regions where the model consistently disagrees with the other datasets, simulating higher
22 levels of OH in these regions. These regions of the troposphere are the regions where most
23 CH_4 is oxidised and so high biases in the model here will tend to lead to lower CH_4 lifetimes in
24 the model than in observation-derived estimates.
25

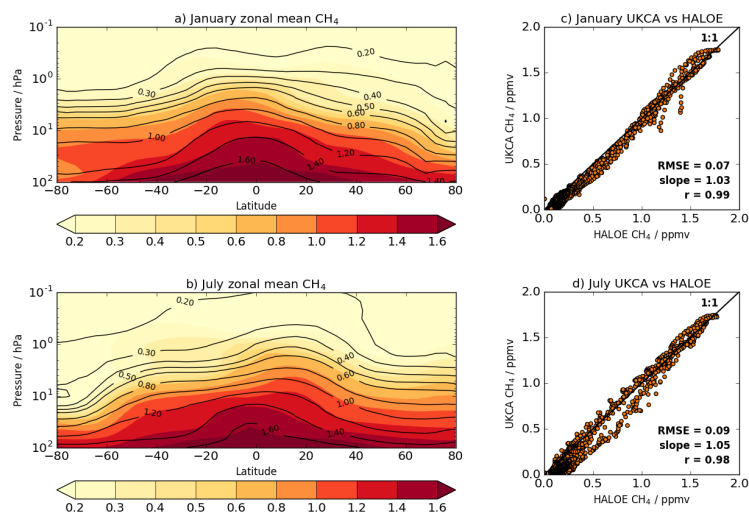
26 In the previous configurations of UKCA (MO09 and OC14), methane concentrations fell off too
27 quickly with height above the tropopause; this was attributed to the stratospheric transport
28 timescale being too long in the respective physical model. Comparisons of methane columns
29 from the HadGEM2-UKCA coupled model with SCIAMACHY, for example, were too low and
30 required modelled methane above 300 hPa to be overwritten with Halogen Occultation
31 Experiment (HALOE, Russell et al., 1993) and Atmospheric Chemistry Experiment (ACE,
32 Bernath et al., 2005) assimilated output from TOMCAT (Hayman et al., 2014). Figure 13 shows
33 that the fall-off of methane with height in UKESM1 is less rapid than in HadGEM2 and is
34 consistent with the age of air in the model being comparable to that inferred from observations
35 (Section 4.6.2). As comparisons with surface observations and SCIAMACHY (with its strong
36 sensitivity to surface concentrations) are not appropriate here, because surface methane
37 concentrations are relaxed to LBCs (Section 2.6), only comparisons with stratospheric
38 observations are shown here.



1
2
3
4
5
6
7
8
9
10
11
12
13
14
15
16

Figure 13. Vertical profiles of the mean tropical ($\pm 10^\circ\text{N}$) modelled methane from multi-annual annual mean output from atmosphere-only simulations of HadGEM2-ES (OC14) and UKCA StratTrop in UKESM1 (this study).

Figure 14 shows multi-annual zonal mean comparisons for January and July of modelled methane against the HALOE/Cryogenic Limb Array Etalon Spectrometer (CLAES) climatology (Kumer et al., 1993). It indicates that UKCA StratTrop in UKESM1 is capable of simulating the absolute concentrations as well as the morphology of the observed distribution. The only exception to this is the tongue of methane-depleted air descending from the mesosphere over the SH high latitudes in July, which was also evident in MO09. Nevertheless, UKESM1 is able to capture the observed vertical fall-off with height. There is an excellent 1:1 correspondence between the model and observations: the slope of the least squares fits for January and July are within 0.05 of unity, the correlation coefficients are greater than 0.98 and the root mean square errors between UKESM1 and the HALOE/CLAES climatology are less than 0.1 ppm.



1
2 **Figure 14.** Multi-annual monthly zonal mean methane in ppm in a) January and b) July, with scatter
3 plots of modelled versus observed concentrations for January and July in panels c) and d), respectively.
4 The coloured contours in a) and b) are from UKCA and the black contours are the HALOE/CLAES
5 climatology. The scatter plots also include a 1:1 line and metrics such as root mean square error
6 (RMSE), the slope of a least squares linear fit, and the correlation coefficient (r).
7

8 **4.4 Comparison of model simulated and observed distribution of H_2O_2 .**

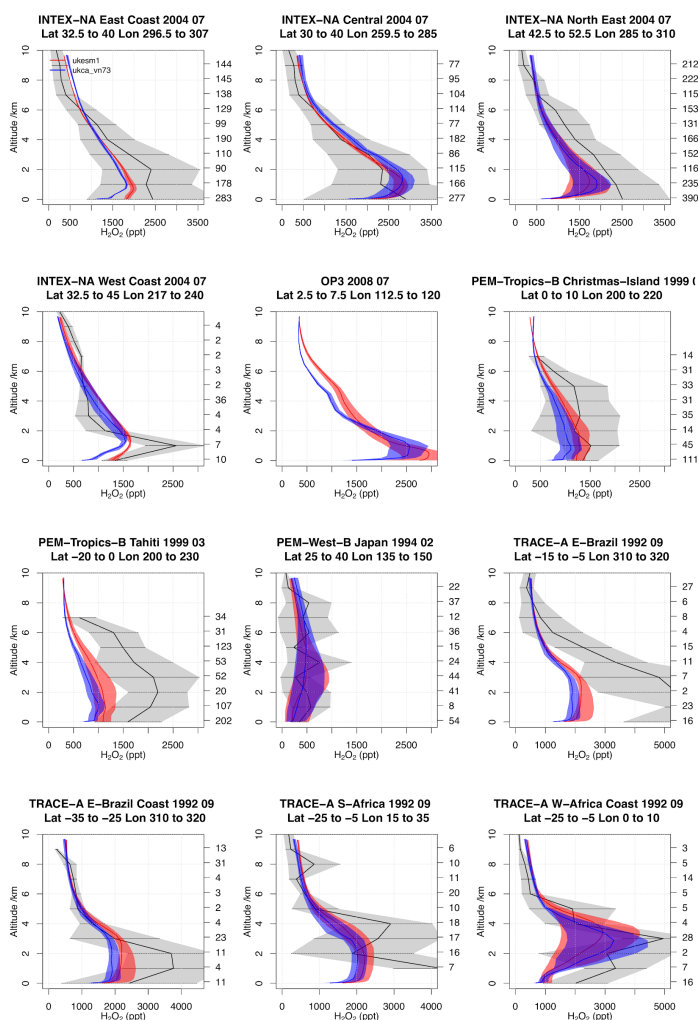
9 Whilst not as important an oxidant as OH or O_3 in the gas phase, H_2O_2 is important for the
10 oxidation of SO_2 in the aqueous phase. Indeed, in our UKCA StratTrop simulations roughly
11 30% of SO_2 is oxidised by H_2O_2 in the aqueous phase and as such it is important to evaluate
12 the performance of our simulation of H_2O_2 . Unlike O_3 , there are no satellite products available
13 to give global coverage, or indirect measures of its abundance as in the case for OH with
14 regards to the lifetime of CH_4 . As such we rely on in situ observations to make an assessment
15 of model performance.
16

17 Figure 15 compares the vertical profiles of the decadal average H_2O_2 mixing ratios from the
18 FR simulation described above in red and in blue one of the older UKCA StratTrop simulations
19 described in Section 2.8 (i.e. Figure 4 blue dots) with observations from a range of aircraft
20 measurement campaigns in grey. This analysis builds on the work of Emmons et al. (2000)
21 and the secondary y axis on each plot (right hand side) indicates the number of observations
22 that make up the observed mean and standard deviation. Each panel in Figure 15 shows the
23 vertical profile of H_2O_2 sampled at different times (monthly averages for the model and periods
24 indicated on the top of the panels for the observations).
25

26 The general feature of Figure 15 is that the UKCA StratTrop in UKESM1 simulations tend to
27 result in higher levels of H_2O_2 than in the previous version of UKCA. There is generally good
28 agreement with the observed vertical profile in most locations. The model simulations tend to
29 underestimate the variability shown in the observations. Nevertheless, caution should be
30 applied when assessing the spread of the observations as many of the campaigns had specific



1 foci to target chemical or meteorological events while here they are compared to monthly
2 mean H_2O_2 in the model.
3
4



5
6 **Figure 15.** Comparison of modelled (red and blue) H_2O_2 vertical profiles against observations from
7 aircraft campaigns (grey). The red profiles indicate the results from the free running UKCA StratTrop in
8 UKESM1 simulation described here and blue for results from an older UKCA StratTrop simulation
9 running in MetUM vn7.3, (Experiment G, see Supplement for details). All plots show the mean as the
10 solid line and the envelope being ± 1 standard deviation.
11
12

13 4.5 Comparisons with satellite retrievals of tropospheric columns of O_3 , CO and NO_2

14 Here we compare the results from the UKCA StratTrop runs against satellite data with a focus
15 on assessing performance in the troposphere. In all cases, the runs analysed are the nudged



1 dynamics runs (ND) discussed in Section 3. Nudging enables a more robust comparison
2 against the satellite observations as it reduces biases caused by circulation errors in the free
3 running model, although we note that it does not completely remove these biases (Orbe et al.,
4 2018). As well as nudging, the model output is sampled instantaneously every three hours to
5 allow for time and space sampling to the satellite data locations. The comparison between the
6 model and the observations is made using OMI-MLS for the tropospheric column of O₃,
7 MOPITT for the tropospheric column of CO and OMI for tropospheric column of NO₂.

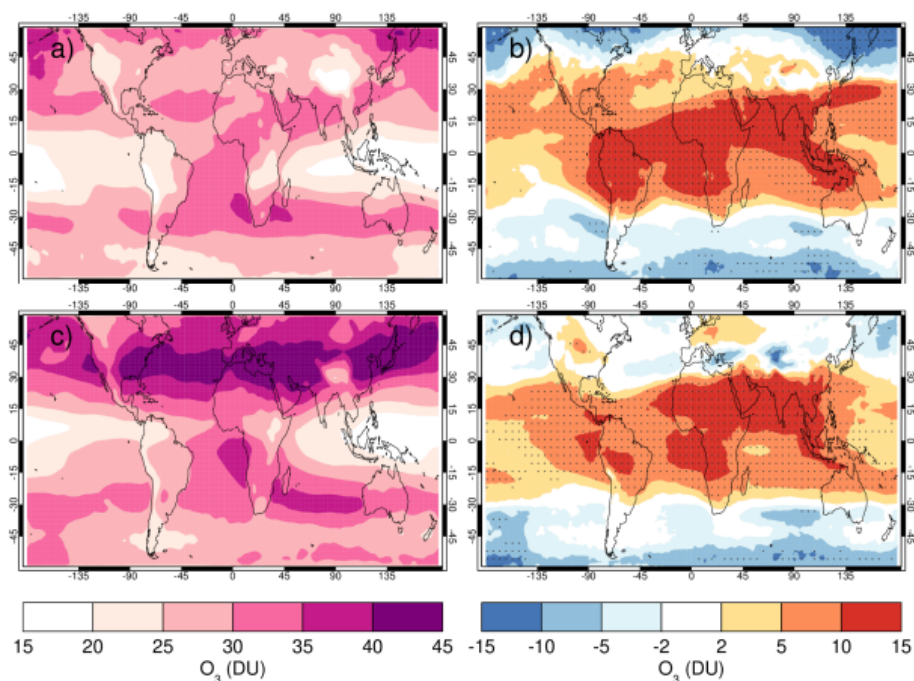
8
9 In the following analysis, the stratosphere has been removed by screening out regions where
10 the monthly mean ozone exceeded 125 ppb, the ozonopause; columns are calculated by
11 summing variables from the surface to the height at which the ozonopause starts. The model
12 ozone data presented here has not been corrected to account for optically thick clouds in the
13 troposphere which may affect retrieved ozone profiles (Ziemke et al. 2006) since averaging
14 kernel (AK) information is not available for the OMI-MLS dataset. Since satellite measurement
15 errors were not available, we have used 2 × standard deviation of the retrievals to estimate
16 when the differences between modelled and observed ozone are significant. This implies that
17 the stippling area in the plots, corresponding to grid cells where |model bias| > satellite error,
18 could be reduced (i.e. better agreement with the observations) if the satellite error is added to
19 the 2 × stdev. The plots therefore show a ‘worst case scenario’.

20
21 The model fields have been co-located in time and space with the observations to reduce
22 representation errors. For each satellite retrieval, the nearest model grid box is sub-sampled
23 within 3 hours of the observation and the model profile interpolated onto the satellite pressure
24 grid. The satellite AKs (where available) are then applied to the model profile, to account for
25 the vertical sensitivity of the instrument. Then the model sub-columns are calculated and
26 summed between the surface and the tropopause to determine the co-located model
27 tropospheric column. The equations used to apply the OMI NO₂ and MOPITT CO AKs to the
28 model profiles are:

29
30 $y = A \cdot x$ and $y = 10^{(A(\log_{10}(x) - \log_{10}(xa)) + \log_{10}(xa))}$

31
32 where x is the co-located model profile interpolated onto the satellite pressure grid, A is the
33 satellite averaging kernel, xa is the satellite a priori and y is the modified model profile. Here x
34 for NO₂ is in sub-columns with units of (10¹⁵ molecules cm⁻²), while x for CO has units of vmr
35 before conversion into sub-columns/tropospheric column. Tropopause height information was
36 provided by the OMI NO₂ files, but for MOPITT derived tropospheric column CO we use the
37 climatological tropopause, described by Monks et al. (2017).

38
39



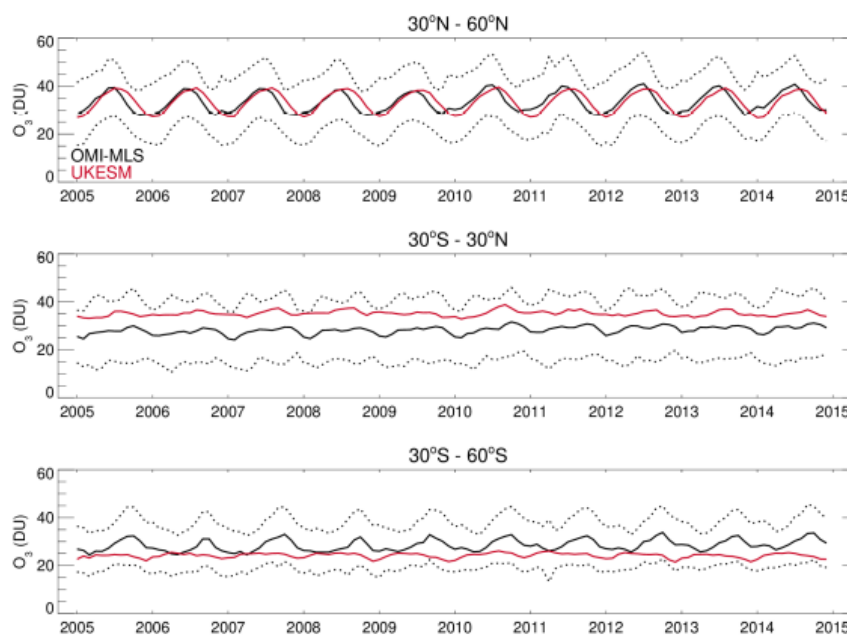
1
2 **Figure 16.** Comparison of observed and modelled tropospheric ozone columns (DU) from the ND
3 simulations. Plots show seasonal means and differences for the period 2005-2014.
4 a) OMI-MLS tropospheric column (DJF); b) difference between the model *nudged* simulations and
5 OMI-MLS tropospheric column (DJF); c) OMI-MLS (JJA) tropospheric column; d) difference between
6 model and OMI-MLS tropospheric column (JJA). Stippling indicates gridpoints where $|\text{bias}| > 2 \times \text{stdev}$
7 of obs.

8
9 The modelled tropospheric ozone column (TC_O3) is evaluated against the OMI-MLS
10 tropospheric ozone column (Ziemke et al., 2006). The general agreement between UKCA
11 StratTrop and OMI-MLS is good and in line with many other CCMs (Young et al., 2013). A
12 general feature of the model is a small underestimation in the tropospheric ozone column in
13 the southern hemisphere extratropics, generally good agreement in the northern hemisphere
14 extratropics but significant positive biases in the tropics. The underestimation in tropospheric
15 ozone in the Southern mid-latitudes is worse in the late summer and early autumn when OMI-
16 MLS shows a seasonal maximum in the Southern Hemisphere that the model fails to
17 reproduce (Figure 17 bottom panel).

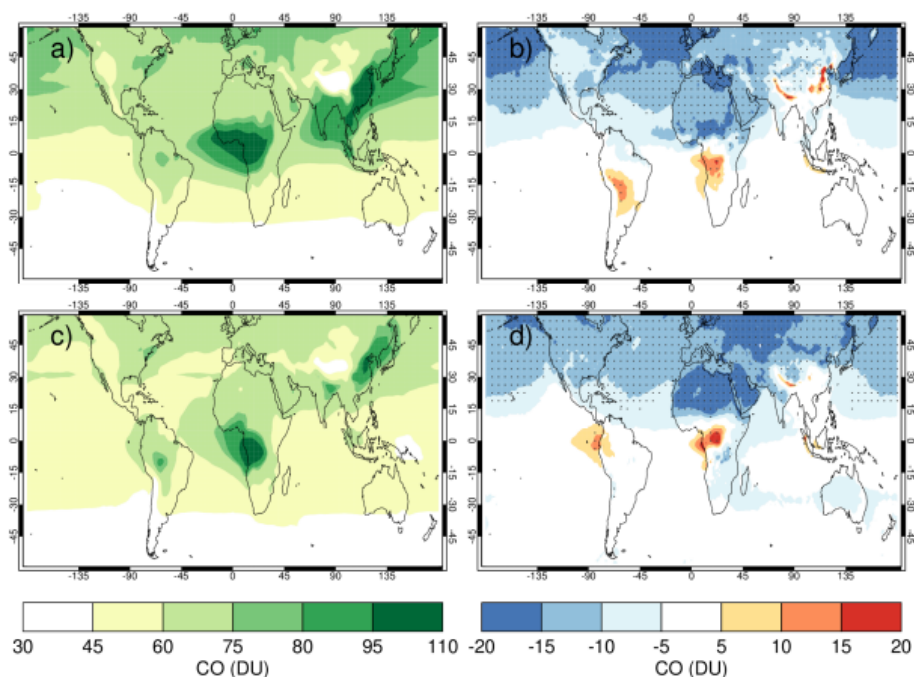
18
19 For the Northern mid latitudes, Figure 16 panel b, shows that in DJF the model overestimates
20 tropospheric ozone over large parts of the North Atlantic Ocean while underestimating it over
21 Northern Russia and large parts of the North Pacific Ocean. These two biases counteract each
22 other in the timeseries plot (Figure 17, top panel) to give good net agreement overall. It is
23 worth noting that the timeseries plots show that there are very small, if any, trends in
24 tropospheric column ozone when averaging across these large domains. Fig 16 panel d and
25 Figure 17 top panel show that in JJA the model biases in the Northern mid latitudes are
26 generally very small and the amplitude and phase of the modelled seasonal cycle is in good



1 agreement with the OMI-MLS data. In the Tropics the differences shown in Fig 16 panel b and
2 d are around 25-50%. There are potentially several causes for this including (a) the
3 representation of chemistry in this region, (b) the underlying emission inventories (c) the
4 deposition rates (which are on the low end of compared with other models) and (d) the
5 emissions of ozone precursors. The pattern of the bias strongly resembles patterns in the
6 emissions of NO_x from lightning. It has been noted before that the modelled tropospheric
7 ozone is extremely sensitive to the average global NO_x emitted by lightning, which is mainly
8 centred around the tropics. The model bias in the tropics might be a result of the simplified
9 parameterisation of lightning NO_x emissions and further work will focus on reducing this bias.



10
11 **Figure 17.** Tropospheric column O_3 (DU) zonal time-series (30-60°N - top panel, 30°N-30°S - middle
12 panel, 30-60°S - bottom panel) for model (red) and OMI-MLS (black). Dashed lines represent the
13 satellite uncertainty range ($\pm 2 \times \text{stdev}$).
14



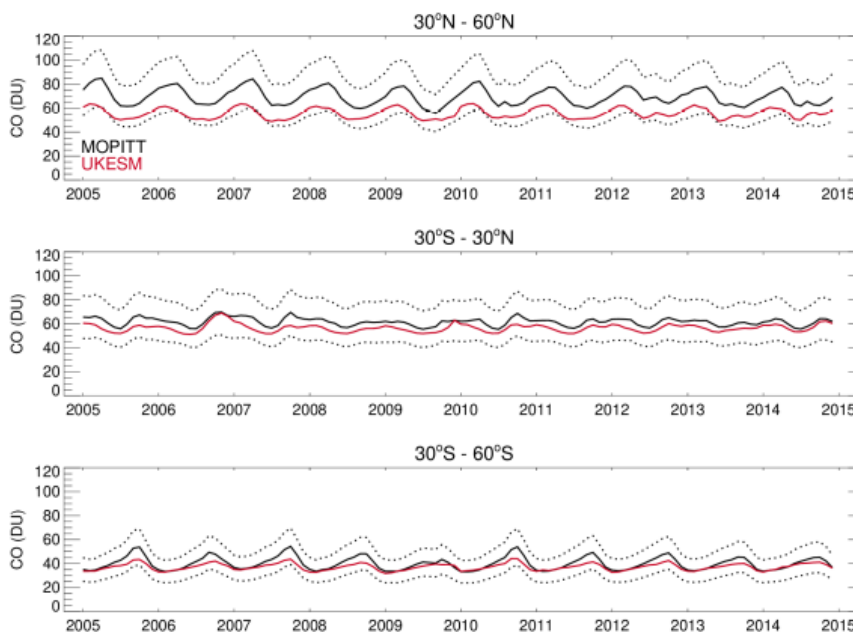
1
2 **Figure 18.** Comparison of observed and modelled tropospheric CO columns (DU) from the ND
3 simulations. Plots show seasonal means and differences for the period 2005-2014.
4 a) MOPITT tropospheric column (DJF); b) difference between model and MOPITT tropospheric
5 column (DJF); c) MOPITT (JJA) tropospheric column; d) difference between model and MOPITT
6 tropospheric column (JJA). Stippling indicates gridpoints where $|\text{bias}| > \text{satellite error}$.
7

8 Figure 18 shows a comparison of tropospheric column of CO in the UKCA StratTrop nudged
9 dynamics runs with retrievals from the MOPITT instrument on board (Terra, Emmons et al.,
10 2004). The MOPITT data reveal that the tropospheric column CO (TC_CO) is highest over
11 anthropogenic and biomass burning emission regions, and lowest over the remote oceans.
12 There is a strong north south gradient which is set up from the short lifetime of CO (~ 30 days)
13 and the time scales for interhemispheric mixing. (NB Figure 18 c highlights strong emissions
14 of CO in DJF in the Northern midlatitudes). The general feature evident from Figure 18 is that
15 the model significantly underestimates TC_CO in the northern hemisphere (NH), in both winter
16 and summer seasons. The negative bias in TC_CO is especially large at high northern
17 latitudes, consistent with surface CO biases in this region (e.g. Shindell et al., 2006). Whilst
18 the NH shows a negative bias, there is a strong positive bias in CO in regions associated with
19 agricultural (Indo gangetic plains) and forest burning (central Africa and northern South
20 America).
21

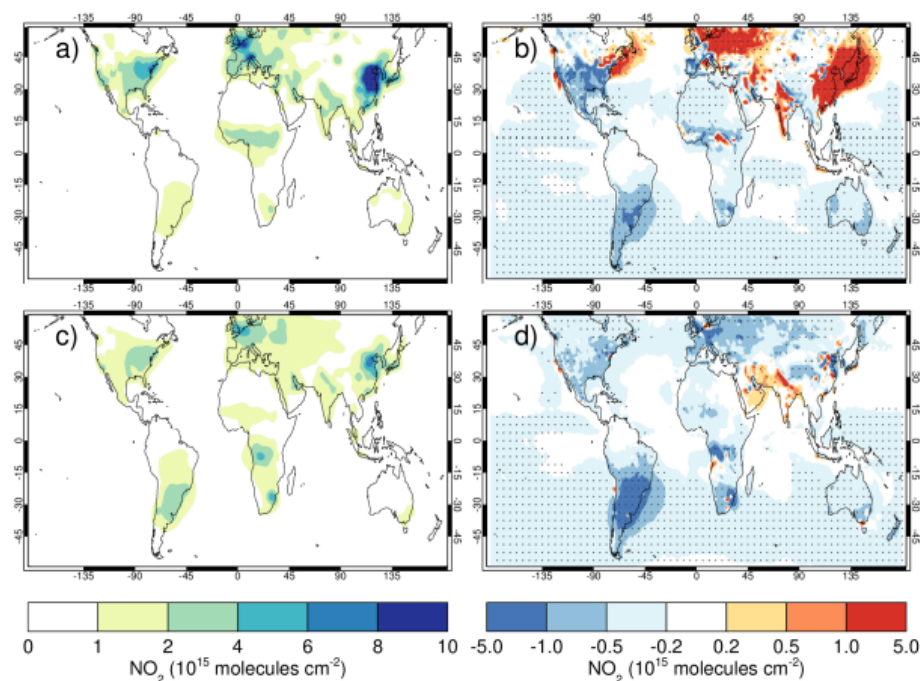
22 There are a number of reasons for the model-satellite biases in TC_CO, including 1)
23 insufficient secondary production of CO from non-methane VOC oxidation (e.g. Grant et al.,
24 2010), 2) excess biomass burning emissions in the southern hemisphere (SH) during DJF
25 (potentially the same cause in central Africa in JJA), 3) strong loss through OH in the NH in



- 1 both seasons. We note that these types of biases are not unique to UKCA StratTrop and that
- 2 further work is required to ameliorate them (Shindell et al., 2006).
- 3



- 4
- 5 **Figure 19.** Tropospheric column CO (DU) zonal time-series (30-60°N - top panel, 30°N-30°S - middle
- 6 panel, 30-60°S - bottom panel) for model (red) and MOPITT (black). Dashed lines represent the
- 7 satellite uncertainty range.
- 8
- 9 As shown in Figure 19, there is no clear trend in modelled and observed TC_CO over time.
- 10 However, both data sets show seasonal cycles in TC_CO in the NH and SH with a very muted
- 11 seasonal cycle in the tropics. The model simulations again underestimate (~10-20 DU)
- 12 TC_CO in the NH mid-latitudes but successfully capture the amplitude and phase of the
- 13 seasonal cycle (albeit with a slightly smaller amplitude) and the magnitude of interannual
- 14 variability well. In the Southern Hemisphere, the model is doing very well capturing absolute
- 15 concentration, seasonal cycle and interannual variability, although it underestimates the peaks
- 16 during the Austral winter. There is also an underestimation of CO in the tropics despite the
- 17 positive bias over biomass burning areas.
- 18
- 19



1
2 **Figure 20.** Comparison of observed and modelled UKCA StratTrop in UKESM1 tropospheric NO₂
3 columns (molecules cm⁻²). Plots show seasonal means and differences for the period 2005-2014. a)
4 OMI tropospheric column (DJF); b) difference between model and OMI tropospheric column (DJF); c)
5 OMI (JJA) tropospheric column; d) difference between model and OMI tropospheric column (JJA).
6 Stippling indicates gridpoints where |bias| > satellite error.

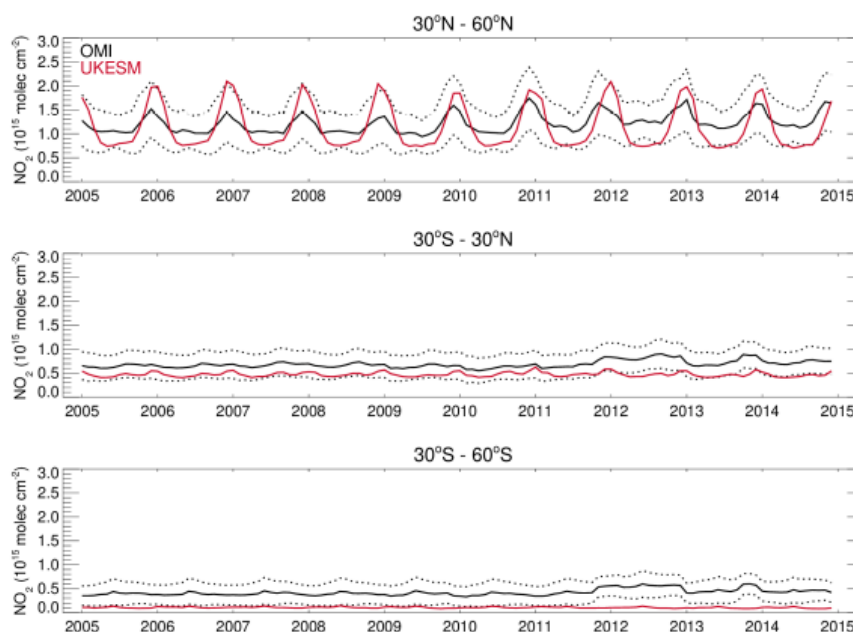
7
8 Finally we focus on the comparison of modelled and observed tropospheric NO₂ columns. The
9 observed tropospheric NO₂ column (TC_NO2) data come from the OMI instrument on board
10 AURA (Boersma et al., 2007).

11
12 The observed NO₂ column is highly heterogeneous and localised to the major industrialised
13 regions, where anthropogenic emissions are highest, and major biomass burning zones
14 (Figure 20). The figure highlights strong seasonal differences in the observations, with
15 TC_NO2 being larger in winter (panel a) than in summer, most likely as a result of higher
16 emissions and longer NO₂ lifetime than in the summer. Averaged across the whole
17 troposphere, the model compares well with OMI TC_NO2 spatially (Figure 20). However, there
18 are very significant positive biases over the main anthropogenic emission regions (i.e. South
19 Asia, Eastern Europe, East Asia and outflow from the US eastern seaboard), particularly in
20 local winter. These biases in TC_NO2 are only weakly correlated with the biases in TC_O3 in
21 these regions, suggesting different causes and they are dominant in different regions of the
22 atmosphere (boundary layer vs free troposphere). A high bias in TC_NO2 extends out from
23 the North China plains region, across the sea of Japan and into the Pacific ocean suggesting
24 either errors in the underlying emission inventory or in the modelled NO₂ lifetime.

25



1 Over biomass burning regions, there is evidence for low biases over central Africa and South
2 America (mainly in JJA). This may well be a vertical sensitivity issue in the comparison of the
3 data sets. As OMI has peak sensitivity in the mid-upper troposphere, OMI detects enhanced
4 NO₂ values over biomass burning regions due to the buoyant fire plumes. In UKEMS, the
5 anthropogenic emissions are injected on the surface level, so most of the NO_x will be trapped
6 in the boundary layer where OMI is less sensitive. Therefore, the satellite AKs will give this
7 sub-column less weighting and a negative bias occurs.
8



9
10 **Figure 21.** Tropospheric column NO₂ (10¹⁵ molecules cm⁻²) zonal time-series (30-60°N - top panel,
11 30°N-30°S - middle panel, 30-60°S - bottom panel) for model (red) and MOPITT (black). Dashed lines
12 represent the satellite uncertainty range.

13
14 Figure 21 highlights that in both the model simulations and satellite data, the average Southern
15 Hemisphere extra tropical TC_NO2 is lower than in the Northern Hemisphere, due to fewer
16 emission sources. However, in the model there is a significant low bias in this region, ~ 50%.
17 This bias is largest over the oceans and may be connected with biases in the representation
18 of NO_y species (i.e. PAN) which are large contributors to NO_x in this region.
19 In the Northern extratropics, the model simulated TC_NO2 is within the observational
20 uncertainty but with too large a seasonal cycle, the simulated mean annual minima/maxima
21 being much lower/higher than the observed mean annual minima/maxima.

22 23 **4.6 Evaluation of zonal mean stratospheric composition**

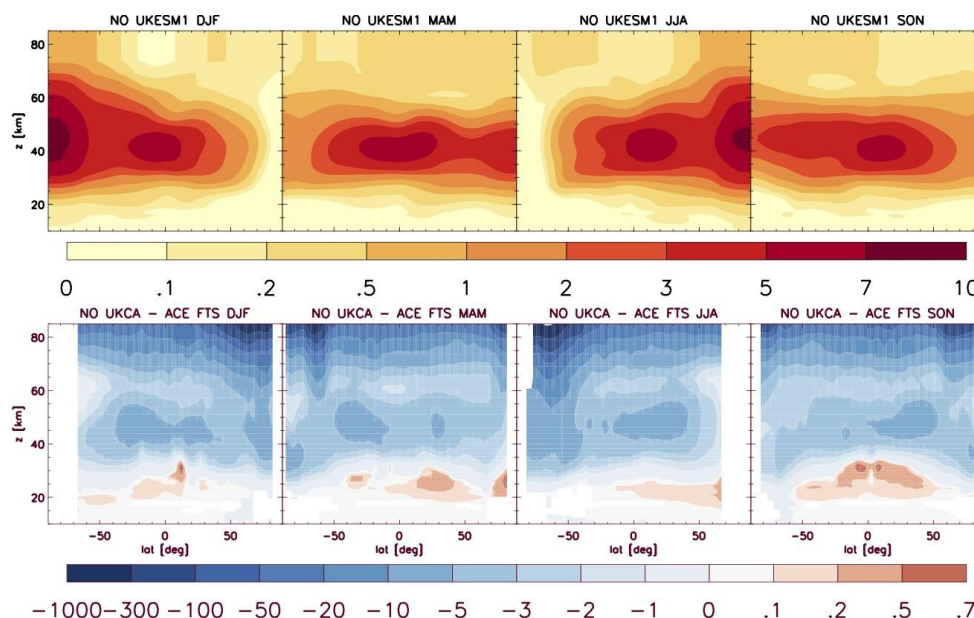
24 Sellar et al. (2019a) provide an overview of the simulation of total-column ozone. They show
25 that UKESM1 produces relatively realistic ozone fields albeit with some remaining issues.
26 Amongst these is a tendency for the Antarctic ozone hole to be too persistent, insufficiently



1 variable, and on average too deep. This is linked to a stratospheric cold bias noted before
2 (Dennison et al., 2019).

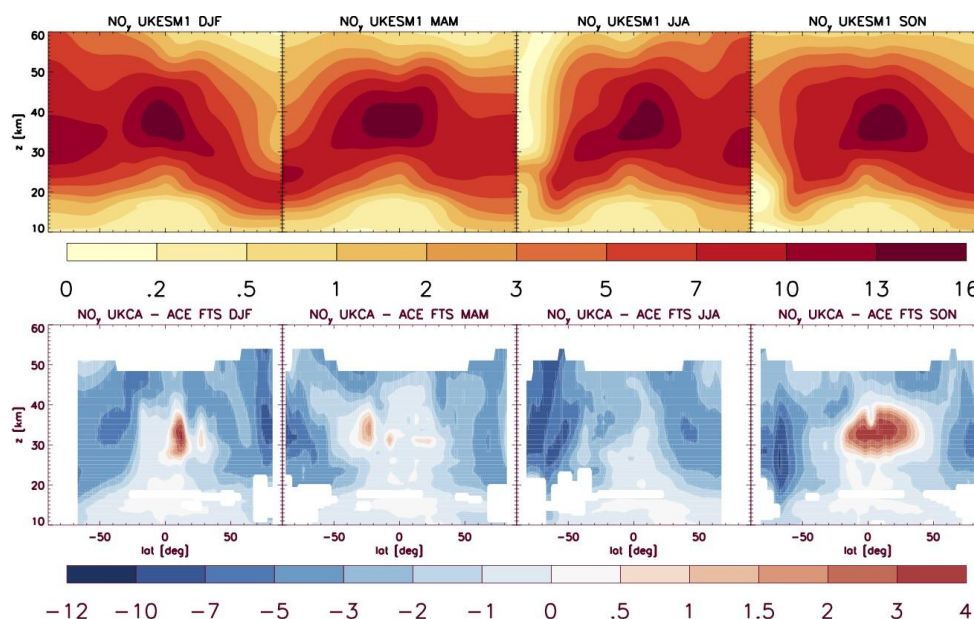
3
4 In the analyses below, UKCA StratTrop seasonal- and zonal-mean composition fields from
5 the FR simulation are compared to the Atmospheric Chemistry Experiment -- Fourier
6 Transform Spectrometer (ACE-FTS) climatology. ACE-FTS is a recent satellite mission
7 sponsored by the Canadian Space Agency; it covers a substantial number of species with a
8 coverage extending in some cases into the mesosphere. The climatology covers the period of
9 February 2004 to February 2013 (http://www.ace.uwaterloo.ca/climatology_3.5.php.) Here we
10 focus on NO, NO_y (defined here as NO + NO₂ + HNO₃), CO, H₂O, and O₃.

11
12



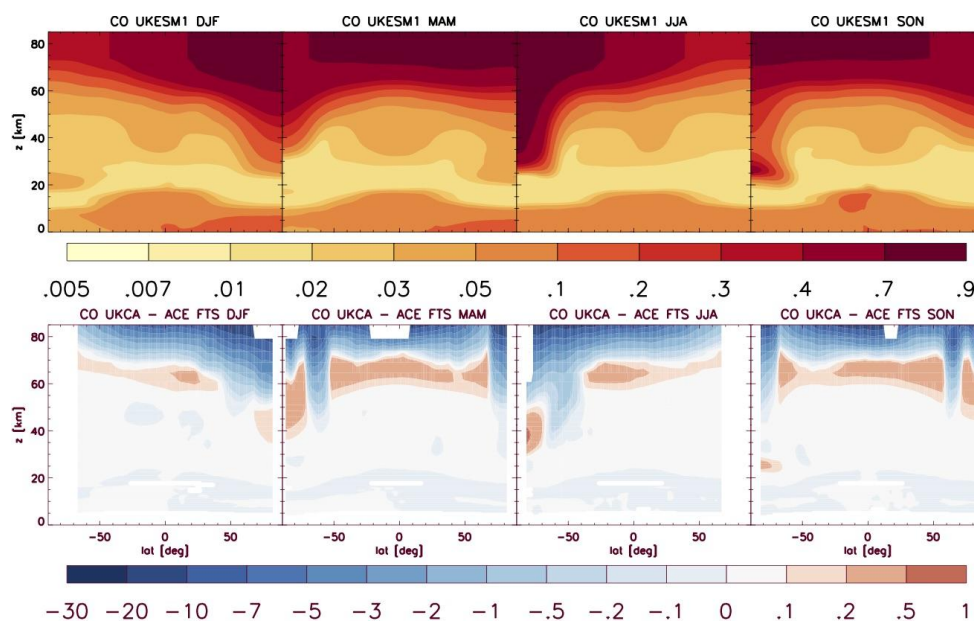
13 -1000 -300 -100 -50 -20 -10 -5 -3 -2 -1 0 .1 .2 .5 .7
14 **Figure 22.** Zonal-, seasonal-, and multiannual mean nitrogen oxide (NO) volume mixing ratio, in ppb.
15 Top: UKCA StratTrop, February 2004 to February 2013. Bottom: Bias versus the ACE-FTS
16 climatology, same units and period. The climatology represents the average of AM (sunrise) and PM
17 (sunset) measurements.

18
19
20
21

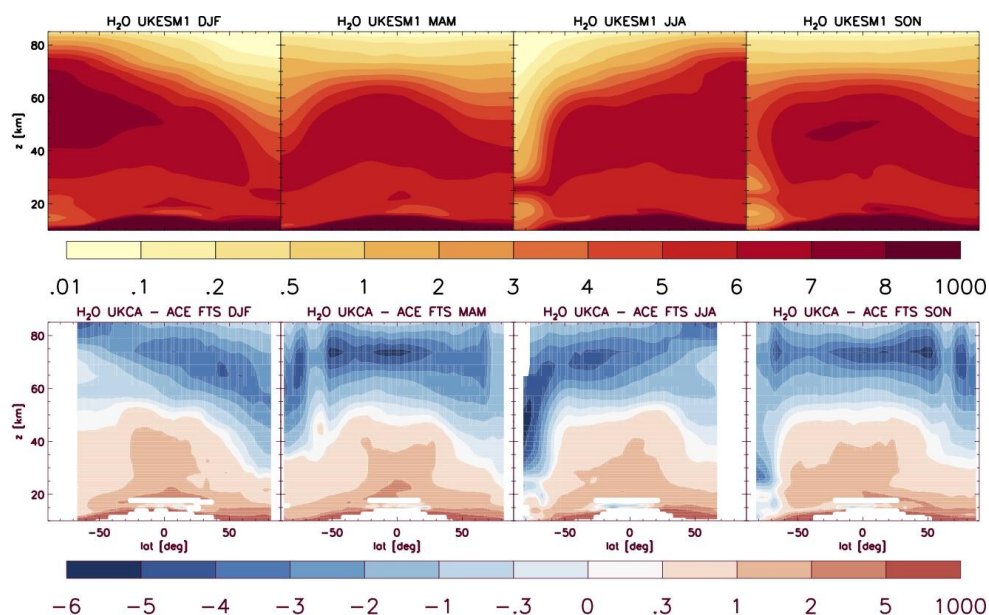


1 -12 -10 -7 -5 -3 -2 -1 0 .5 1 1.5 2 3 4
2 **Figure 23.** Same as Figure 22 but for odd nitrogen (NO_y), defined here as $\text{NO}_y = \text{NO} + \text{NO}_2 + \text{HNO}_3$,
3 in ppb. For ACE-FTS, NO and NO_2 fields are the average of AM and PM measurements.

4
5
6 NO is underestimated throughout the model domain (Figure 22). Away from the polar vortices,
7 this underestimation might be associated with a sampling bias, but in the polar vortices of both
8 hemispheres, the disagreement is so large that a sampling problem alone cannot explain the
9 discrepancy, particularly near the model top where NO is relatively long-lived and the bias
10 reaches 1 ppm. To overcome potential issues with sampling, we compare NO_y (Figure 23).
11 This diagnostic reveals tongues of nitrogen-depleted air descending in the polar vortices of
12 both hemispheres which in the ACE-FTS measurements are however relatively nitrogen-rich.
13 This discrepancy lasts into southern spring when NO_y is underestimated by up to 12 ppb at
14 around 70S. The depletion of HNO_3 due to denitrification in the lower Antarctic polar vortex
15 appears to be well reproduced in winter but is perhaps overestimated in spring, in line with the
16 generally excessively long lifetime of the polar vortex in the model (Sellar et al., 2019a; not
17 shown).
18

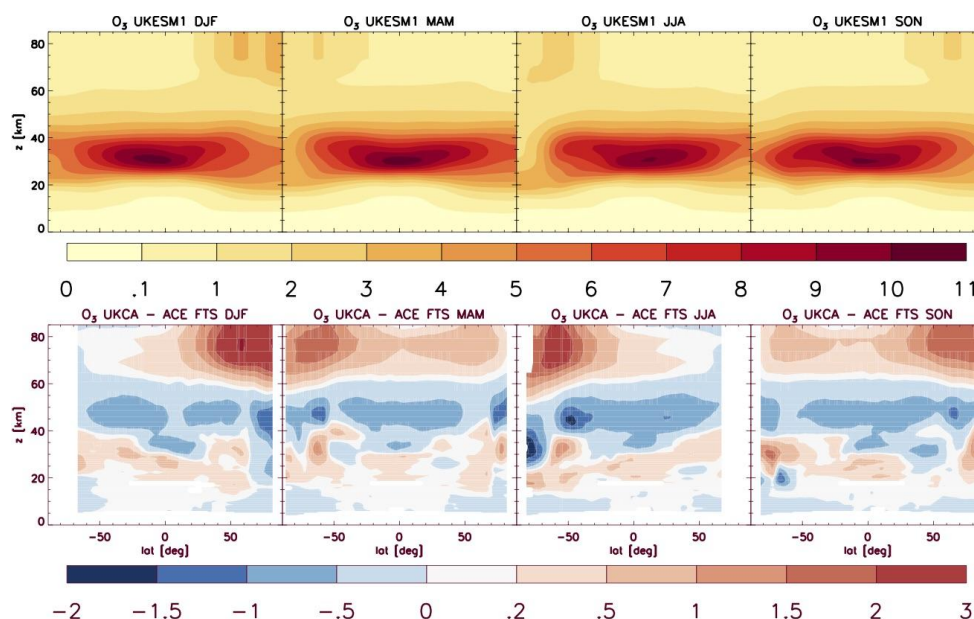


1 -30 -20 -10 -7 -5 -3 -2 -1 -0.5 -0.2 -0.1 0 .1 .2 .5 1
2 **Figure 24.** Same as Figure 22 but for carbon monoxide (CO), in ppm.
3
4 As for non-nitrogen compounds, the model gets the shape of the distribution of CO about right,
5 but substantially underestimates the amount of CO in the mesosphere (Figure 24). A variant
6 simulation with a modified top-boundary condition (TBC), whereby the top two levels are not
7 overwritten with the third-highest level, reveals that with this variant TBC CO would now be
8 overestimated. Essentially, CO production is due to CO₂ photolysis which is extremely height
9 sensitive. The simulation shows that mesospheric air reaches the lower polar vortex in
10 Antarctic spring; this process is relatively well simulated in the model.
11



1 -6 -5 -4 -3 -2 -1 -0.3 0 .3 1 2 5 1000
2 **Figure 25.** Same as Figure 22 but for water vapour (H₂O).

3
4 In much of the stratosphere, H₂O is overestimated by 0.3 to 2 ppm, suggesting that perhaps
5 the tropical-tropopause cold point is still slightly too warm (Figure 25). This has been a
6 persistent problem in the MetUM coupled to UKCA (Morgenstern et al., 2009) and a significant
7 amount of work identified remedies to this issue in earlier versions of UKCA StratTrop
8 (Hardiman et al., 2015). One cause highlighted by Hardiman et al. (2015) was the role of ozone
9 in the upper troposphere / lower stratosphere (UTLS) region region. Biases in ozone here are
10 important to this issue of stratospheric moistening. In addition a new development in UKCA
11 StratTrop has been the interactive simulation of H₂O from CH₄ oxidation in the stratosphere
12 and so biases in CH₄ or the transport of CH₄ into the stratosphere may also play a role. Further
13 work will focus on understanding the causes of this H₂O bias. In the mesosphere and in the
14 polar vortices, however, H₂O is underestimated by several ppm in many locations. Unlike all
15 other gas phase chemical species, H₂O is not subject to the overwriting of the top two levels.
16 It photolyses at similarly short wavelengths as CO₂ (see above); an overestimation of its
17 photolysis explains the mesospheric bias.
18



1
2 **Figure 26.** Same as Figure 22 but for ozone (O₃), in ppm.

3
4 Figure 26 highlights a good simulation of stratospheric ozone in UKCA StratTrop. In the lower
5 stratosphere, ozone is mostly overestimated (by around 0.2 to 1 ppm), whereas in the upper
6 stratosphere it is underestimated by similar amounts. Larger underestimations exist in
7 Antarctic winter. In the mesosphere, ozone is generally overestimated.

8
9 Taken together, these disagreements indicate some progress with the simulation of odd
10 nitrogen compounds albeit with substantial remaining problems. HNO₃ is now in better
11 agreement with observations than documented by Morgenstern et al. (2009); however this
12 appears to be mostly the case because ACE-FTS finds considerably more HNO₃ in the
13 stratosphere than the older data used there. The substantial deficit of NO in the mesosphere
14 is the result of missing model physics: Energetic particle precipitation (EPP) is well
15 documented to cause the break-up of nitrogen molecules and the formation of NO_x (for a
16 review see e.g. Sinnhuber et al., 2012), but this process is not represented in UKCA StratTrop.
17 This model deficiency results in a misrepresentation of odd nitrogen descending in the polar
18 vortices towards the ozone layer. This might explain the NO_y deficit in winter/spring over both
19 poles, although further studies are needed to confirm this. This problem is receiving much
20 more attention here than e.g. in the earlier investigation by Morgenstern et al. (2009) because
21 the newer ACE-FTS satellite data offer much better coverage of high latitudes and altitudes
22 than the observational references used by Morgenstern et al. (2009).

23
24 Morgenstern et al. (2009) had to artificially reduce water vapour at the tropical tropopause; the
25 reasonable agreement found here is achieved without such an intervention. H₂O loss and CO
26 production are both the result of photolysis of molecules (CO₂, H₂O) that photolyse in the
27 mesosphere where the photolysis rate increases sharply with height and may be sensitive to
28 assumptions about the residual ozone column above the model top. In combination, these
29 findings suggest that this residual ozone column (which is a parameter in the photolysis



1 scheme) may be too small, or that making this a simple universal constant in the model may
2 be inadequate.

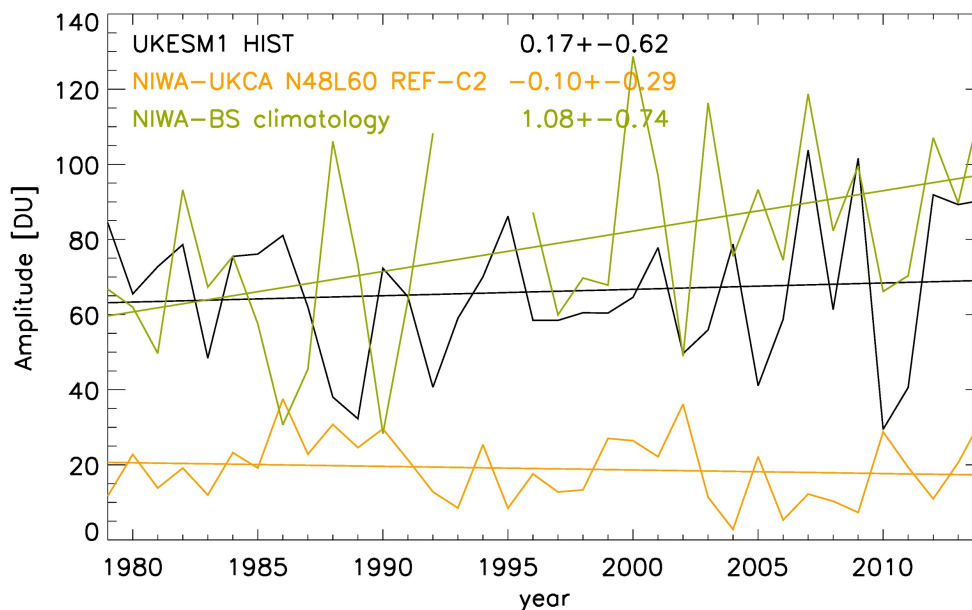
4.7 Analysis of zonal asymmetry of ozone

3
4
5 Stratospheric ozone is often validated against zonal-mean satellite data (e.g. see above). As
6 the simulation of ozone improves in models, attention turns to higher-order diagnostics. A
7 recent analysis by Dennison et al. (2017) revealed that zonal asymmetries of the stratospheric
8 polar vortex, in simulations by a model closely related to UKESM1, were very underestimated;
9 the vortex was generally too circular and its centre too close to the South Pole, when in reality
10 the Southern polar vortex is often distorted and displaced towards the Indian–Ocean sector.
11 Dennison et al. found a westward progression of this displacement, which their model failed
12 to reproduce. The climate impacts of ozone depletion are also often thought of in zonal-mean
13 terms (e.g. Kang et al., 2011); any effort to attribute regional climate change beyond the zonal-
14 mean to ozone depletion might well be impeded by such model behaviour. Hence here we
15 briefly assess how UKCA StratTrop handles zonal asymmetries of the Antarctic polar vortex.
16 Here we focus on the Historic UKESM1 simulations (Sellar et al., 2019a), which use the same
17 version of UKCA StratTrop documented here, rather than the experiments discussed in
18 Section 3.

19
20 The analysis consists of expanding TCO in a Fourier series:

$$21 \text{O}_3 = \text{ZMO}_3 + A \cos(\lambda + b) + \text{higher order terms (ignored here)} \quad \text{Eq 6.}$$

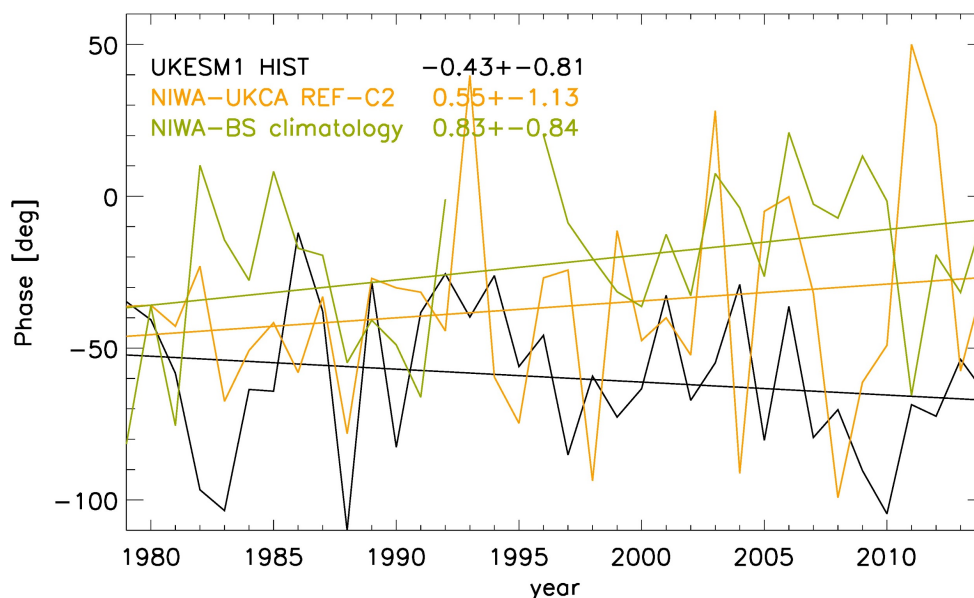
22
23 Here O_3 is monthly-mean total-column ozone, meridionally averaged over 60S to 70S, ZMO_3
24 is its zonal mean, $A \geq 0$ is the amplitude of the zonal asymmetry, λ is longitude, and b is the
25 phase shift. $b=0$ would correspond to an ozone maximum occurring at the Greenwich Meridian
26 and a minimum occurring at the Date Line. Positive values for b correspond to a westward
27 displacement of these features.
28



29



1 **Figure 27.** Amplitude A [DU] of the zonal asymmetry in total-column ozone at 60-70S in October.
2 Green: NIWA-Bodeker Scientific total-column ozone climatology, vn. 3.4. Orange: The model used by
3 Dennison et al. (2017), NIWA-UKCA. The data represent the average of 5 CCMI REF-C2 simulations
4 by their model. Black: UKESM1. The data represent the average of two CMIP6 “historical” simulations
5 (Sellar et al., 2019a). Straight lines are linear regression fits. The numbers represent mean trends and
6 associated 95% confidence intervals in DU/year.
7
8



9
10 **Figure 28.** Same as Figure 27 but for the phase b , in degrees.
11

12 Figure 27 displays A for the months of October (when the ozone hole typically is deepest).
13 The NIWA-Bodeker Scientific total-column ozone climatology
14 (<http://www.bodekerscientific.com/data/total-column-ozone>, green colour) indicates that the
15 zonal asymmetry is typically about 40 to 120 DU in size, and on average there is a positive
16 trend, with the ozone asymmetry increasing significantly by nearly 40 DU between 1979 and
17 2014. UKESM1 (black) reproduces the magnitude and variability of the ozone asymmetry, a
18 big advance over the model used by Dennison et al. (2017) (orange). The difference in the
19 trend is not statistically significant at the 95% confidence level. For the phase b (Figure 28) we
20 find that the model produces an ozone peak usually around 60-70E (i.e. in the Indian Ocean
21 sector) whereas in the NIWA-Bodeker Scientific climatology this maximum occurs further west,
22 on average around 20-30E. The mean eastward trend simulated by UKESM1 is outside the
23 range of possibilities for the observations (which indicate a westward trend), but the
24 uncertainty intervals overlap.
25
26

27 4.8 Evaluation of transport and long-lived tracer-tracer correlation

28 Our final aspect of model evaluation focuses on the comparison of the large-scale transport
29 in the modelled middle atmosphere, analysed through comparison of the modelled age of air
30 profiles against age of air determined using observations of SF_6 made by the MIPAS



1 instrument (Stiller et al., 2008) and through comparison of observed (ACE-FTS) and modelled
2 tracer-tracer correlations. The model data analysed here are from the FR simulation.

3
4 A simple but powerful way to test the representation of stratospheric chemistry in a model is
5 to analyse the correlations between long-lived trace gases (e.g. Chapter 6, SPARC2006).
6 Long-lived tracers are known to exhibit compact correlations with each other (Plumb and Ko,
7 1992) and comparison of modelled and observed correlations can test aspects of the model
8 chemistry independent of dynamics. This is particularly useful when comparing complex 3-D
9 climate models such as UKESM1 with observations made by a range of platforms at different
10 spatial resolution and coverage, and under different meteorological conditions.

11
12 Figure 29 shows the correlations of CH₄ vs N₂O, CH₄ vs H₂O and NO_y vs N₂O from a present
13 day UKESM1 simulation (2005-2010) as well as from ACE and MIPAS satellite data. The ACE
14 V4 (2004-2018) data was obtained from <http://www.ace.uwaterloo.ca/data.php> and monthly
15 mean zonal mean values at 5° latitude bins were created by averaging all profiles with retrieval
16 errors less than 100%. The Michelson Interferometer for Passive Atmospheric Sounding
17 (MIPAS) V1.4 data used here is an update of that used in CCMVal-2010 report (SPARC2010)
18 (see <http://eodg.atm.ox.ac.uk/MIPAS/>). Co-located profiles of H₂O, CH₄, N₂O, NO₂, and HNO₃
19 are retrieved simultaneously for both day and night time profiles and are available for the
20 mission period (2002-2012). MIPAS data was obtained via [ftp://ftp.ceda.ac.uk/neodc/mipas-](ftp://ftp.ceda.ac.uk/neodc/mipas-oxford/data/)
21 [oxford/data/](ftp://ftp.ceda.ac.uk/neodc/mipas-oxford/data/).

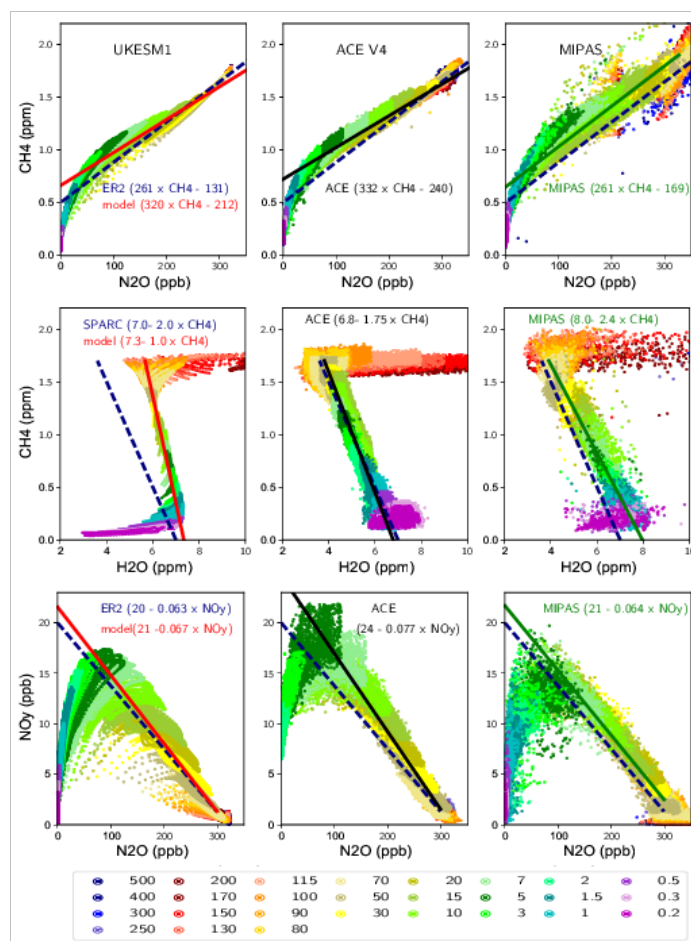
22
23 CH₄ and N₂O are two chemically independent, but long-lived, tracers with significant
24 stratospheric sinks. Accordingly, they are expected to show compact correlations in the
25 stratosphere (Plumb and Ko, 1992). Overall, UKESM1 seems to show very good agreement
26 with the recent satellite-observed relationships, suggesting that the relative loss of CH₄ and
27 N₂O in the stratosphere is well represented. However, the model and the satellite observations
28 differ slightly from the older ER-2 in-situ lower stratospheric observations, possibly due to
29 different relative changes in CH₄ and N₂O in recent years. Note also that the model simulation
30 covers the period 2000-2004 while ACE data covers 2004-2018, hence even after applying
31 the quality flag ACE CH₄ and N₂O values in the troposphere are larger than model values.

32
33 More noticeable model-observation differences are found the CH₄:H₂O correlation. These two
34 long-lived tracers are chemically linked in the stratosphere: CH₄ oxidation leads to the
35 production of nearly 2 molecules of H₂O (with a small yield of H₂). As the maximum observed
36 upper stratosphere H₂O mixing ratio is typically around 7 ppm, and CH₄ is the primary source
37 of stratospheric H₂O, the H₂O vs CH₄ relationship is expected to be close to H₂O + 2×CH₄=7
38 ppmv, which is included in the plots as a reference. The ACE observations show a slightly
39 weaker relationship (H₂O + 1.75×CH₄ = 6.8) while MIPAS data shows a stronger slope, which
40 is larger than 2 (H₂O + 2.4×CH₄ = 8.0). There will be some uncertainty in the satellite data but
41 it is clear that UKESM1 has a significantly different relationship. The upper stratospheric H₂O
42 values are reasonable but the lower stratosphere seems to be much wetter compared to
43 observations. For example, near 90 hPa most of the ACE profiles show H₂O values close to 3
44 ppm, whereas modelled values hardly go below 5 ppm, suggesting water vapour entry mixing
45 ratios near the tropical tropopause layer are not well constrained in the model. However, in
46 UKESM1 CH₄ oxidation appears to yield only 1 H₂O per CH₄ oxidised, which allows the model
47 to achieve realistic upper stratospheric H₂O values. Further detailed studies are required to
48 verify the cause of this model discrepancy. We have noted that there is a missing H₂O product
49 in the reaction HO₂ + MeOO (listed in Table 2). However, we calculate that this reaction only
50 accounts for 2.3% of the fate of MeOO in the stratosphere (which is dominated by reaction
51 with NO), so it appears unlikely that this is the source of the bias.

52



1 Finally, we compare the the NO_y vs N₂O tracers, which are also chemically linked. N₂O is main
 2 source of stratospheric NO_y with a yield of about 6% via reaction of O(¹D) (see equation 6.2b
 3 in SPARC, 2010). ACE NO_y values are calculated simply by adding the observations of HNO₃,
 4 NO, NO₂, 2N₂O₅ and ClONO₂. For MIPAS, zonal mean (5° latitude bin) monthly mean profiles
 5 were calculated by averaging all the measurements with standard errors less than 100%. For
 6 NO_y:N₂O plots, only nighttime profiles are selected (SZA >95) and NO_y is calculated as
 7 HNO₃+ NO₂+ 2N₂O₅ + ClONO₂. For large values of N₂O, the UKESM1 correlation is less
 8 compact than the observations, although the modelled slope indicates a realistic 6.7% yield of
 9 NO_y. The model also produces a reasonable peak NO_y mixing ratio of around 17 ppbv,
 10 although this is slightly smaller than observations, in particular from ACE. The model also
 11 tends to simulate larger occurrences of low NO_y values for a given N₂O, which may be an
 12 indication of strong polar denitrification.
 13
 14



15 **Figure 29:** Correlations between selected long-lived chemical species (monthly mean zonal mean
 16 values for 60°S-60°N) from UKESM1 (left column), ACE V4 data (centre) and MIPAS data (right). The
 17 coloured legend shows the corresponding pressure level of the data points. The linear regression fits
 18 to the model, ACE and MIPAS data are shown in the respective panels along with the equations of
 19 the lines. The MIPAS data is the same as that used in Figures 6.12, 6.13 and 6.14 in the CCMVal-2
 20



1 report (SPARC 2010). ACE NO_y values are calculated as $NO_y = NO + NO_2 + HNO_3 + 2N_2O_5 +$
2 $ClONO_2$. (Top row): CH₄ vs N₂O. The linear fit is calculated for N₂O values ranging from 100 to 300
3 ppb. The dashed line shows estimated fit from ER-2 data (N_2O (ppb) = $261.8 \times CH_4$ (ppm) - 131, see
4 Kawa et al., 1993). (Middle row): CH₄ vs H₂O. The linear fit is calculated for CH₄ values ranging from
5 0.5 to 1.5 ppm. The dashed line represents $H_2O + 2CH_4 = 7$ ppm. (Bottom row): NO_y vs N₂O. The
6 linear fit is calculated for N₂O values ranging from 100 to 300 ppb and the dashed line shows the
7 equation NO_y (ppb) = $20.0 - 0.0625 \times N_2O$ (ppb), based on mid-latitude balloon profiles and ER-2 data
8 (see Kondo et al 1996).

9

10 Figure 30 compares the modelled multi annual mean age of air profile in the stratosphere
11 against observations of SF₆ from 2002-2010 used to calculate the age of air from the MIPAS
12 instrument (Stiller et al., 2008). The model includes a diagnostic to quantify the age of air. This
13 is a effectively a “species” in the model that is emitted at the model surface continually and
14 undergoes full tracer advection and diffusion. Whilst below the modelled tropopause (based
15 on a merger of the 380 K and 2 PVU surfaces) the tracer is set to have an age of zero; above
16 the tropopause the tracer has its age increased every model time step that it stays above the
17 tropopause.

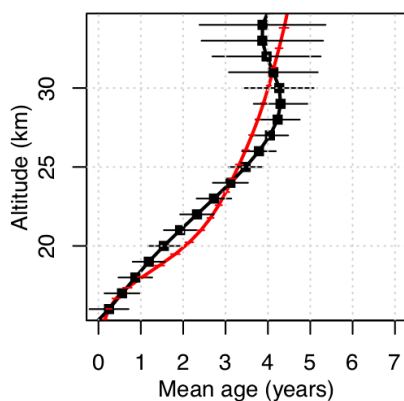
18

19 Figure 30 panel (a) shows the modelled mean tropical ($\pm 10^\circ$) age profile as a function of
20 altitude and that there is very good agreement between the model and the observations, with
21 an increase in the age of air as both profiles increase in altitude and a maximum age of around
22 5 years. The modelled northern hemisphere midlatitude ($35^\circ - 45^\circ N$) age profile (panel b)
23 agrees very well with the observations from 16 km to about 24 km, but the model tends to
24 simulate an age of air which is younger than the observations above 24 km (up to a year
25 difference younger). Panel (c) shows the difference between the tropical and mid-latitude
26 profiles and further emphasises good agreement of the model with the observations below 23
27 km but divergence above this altitude. However, the zonal cross section at 23 km (~ 50 hPa)
28 (panel c) shows that the model generally falls within the observational uncertainty (1 standard
29 deviation of the multi annual observations) at all latitudes.

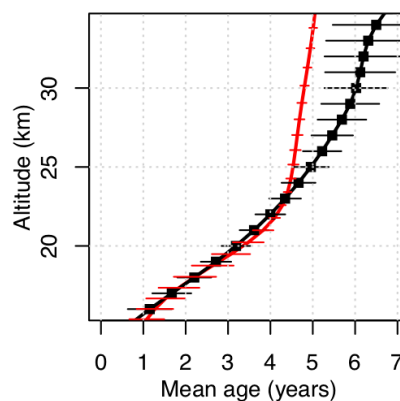
30



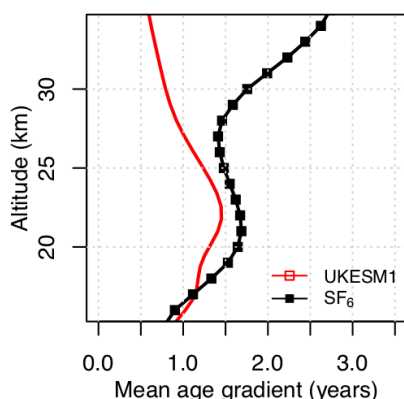
Tropical Mean Age Profile



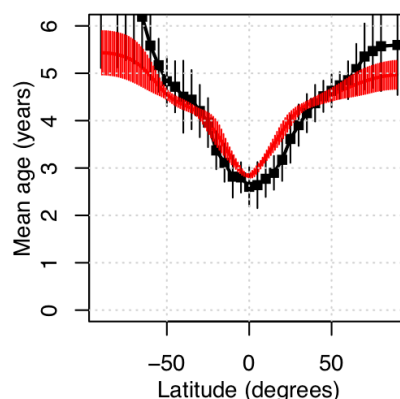
Midlatitude Mean Age Profile



Trop–Midlat Mean Age Gradient Prof



Mean Age, 23km (~50hPa)



1
2 **Figure 30.** Comparison of multi-annual mean modelled (red) age of air with observations (black) from
3 the MIPAS SF₆ record (Stiller et al., 2008).
4
5

6 **5.0 Discussion and Conclusions**

7 In this paper we have documented the species and reactions that make up the UKCA
8 StratTrop mechanism for the first time and performed an evaluation of the model output for
9 the recent past. UKCA is the key module for simulating chemical and aerosol processes in the
10 UKESM1 Earth System model (Sellar et al., 2019a) and UKCA StratTrop enables a holistic
11 representation of gas phase chemistry in the troposphere and stratosphere; important for
12 understanding short lived climate forcers.
13

14 Our focus here has been to document the performance of the chemical fields simulated by
15 UKCA StratTrop as it is implemented in UKESM1; the aerosol schemes, processes and
16 performance are discussed in detail in Mulchay et al. (2019). Further studies are planned



1 which will assess the role of composition-climate Earth system couplings in the UKESM1
2 framework. Hence, we present simulations which have enabled a more focused assessment
3 of key performance indicators of the UCKA StratTrop scheme. We have analysed data from
4 two model runs; the first was a *free-running* (FR) simulation where the meteorology was
5 allowed to evolve independently based on the influence of the prescribed forcing agents
6 (SSTs, GHGs and sea ice) and the second was a *Nudged* (ND) simulation where the
7 meteorology was relaxed toward ERA-Interim reanalysis.

8
9 In general, and focusing on the gas phase as we have here, we find that the performance of
10 UKCA StratTrop in UKESM1 is in line with the range of models that are applied to simulating
11 the coupled chemistry-climate system (Young et al., 2013; 2018).

12
13 Our key performance indicators have included:

14 • An assessment of the magnitude and spatial distribution of lightning NO_x:
15 We note here that whilst the model simulates a global annual total lightning NO_x emissions
16 magnitude that is in the middle of the range quoted in the literature based on observational
17 constraints (~ 6 Tg/yr), and the spatial distribution in lightning flash frequency matches well
18 with observations from satellites, the variability in lightning flash frequency is not in good
19 agreement with the observations (Figure 2). The UKESM1 model predicts too much lightning
20 activity in the tropics at an expense of the extra tropics, something which could be resolved
21 by moving to an ice-flux based scheme (Finney et al., 2018). Moreover, the vertical profile of
22 lightning NO_x may have a significant impact on modelled O₃. Hakim et al. (2019) have shown
23 that across India the vertical profile in lightning NO_x is very model dependent. We suggest
24 further work is performed to better understand the impacts of both the spatial distribution of
25 lightning NO_x and the impacts of lightning NO_x on the tropospheric column biases in O₃ in the
26 model.

27
28 • Surface ozone correlations and mean bias against TOAR observations:
29 TOAR (Shultz et al., 2018) provides the chemistry modelling community with an
30 unprecedented dataset to evaluate surface O₃. In our analysis of the FR and ND runs
31 presented here, we show that the annual mean bias is very low, but this masks out biases in
32 summer and wintertime (Young et al., 2018). However, we suggest that further work be
33 performed to understand the cause of the low and high biases in surface O₃, especially with
34 regards to how these may impact studies that use UKESM1 surface O₃ in health assessment
35 studies.

36
37 • The tropospheric oxidising capacity:
38 A key component to determine the lifetime of emitted reactive gases in the troposphere is the
39 oxidising capacity. Whilst this has to be inferred from observations (i.e. through the inferred
40 lifetime of methane) it is an important metric to evaluate the model against. In this study we
41 found that the methane lifetime in the troposphere with respect to OH was 8.5 years, within
42 the ACCMIP multi model range but slightly low compared to observational analyses (Naik et
43 al., 2013). When compared against other model estimates of the zonal distribution of OH, the
44 model performs well in 10 out of 12 regions analysed; with a significantly high bias in the
45 tropical boundary layer. This is a region where the majority of methane oxidation takes place
46 and may explain the slightly low modelled methane lifetime. With the recent development of
47 aircraft OH datasets appropriate for global model evaluation (Prather et al., 2017) we hope to



1 extend this analysis further and interrogate the model with these data to confirm if the bias is
2 indeed large compared with direct observations.

3
4 • Tropospheric columns of reactive gases (CO, NO₂ and O₃):
5 The analysis of the model ND runs highlighted some success and failure in the models
6 representation of tropospheric columns of CO, NO₂ and O₃. The best performance was found
7 for O₃ (Figures 16-17), although we note that there is a significant bias in the tropics (which
8 has been shown to have an effect on modelled tropospheric photolysis rates (Hall et al.,
9 2018)). In part we believe this bias is connected with the vertical profile and magnitude of
10 lightning NO_x and further work will focus specifically on this area. The modelled tropospheric
11 column of CO shows significant biases in the northern hemisphere (Figure 18). In part this is
12 believed to relate to biases in the representation of higher hydrocarbons that could contribute
13 significantly to secondary CO production (Grant et al., 2010) but high OH could also be a
14 contributing factor. The performance of modelled NO₂ tropospheric columns was found to be
15 generally acceptable in Northern midlatitudes (Figure 21) but there are large biases in regions
16 of high emissions (such as the North China plains (Figure 20)). One hypothesis is that the
17 model simulates too little OH in the regions of high NO₂ emissions, owing to lack of reactive
18 VOC emissions and titration of O₃, which extends the lifetime of NO₂ in these regions. Further
19 studies are required to evaluate the modelled NO₂ lifetime and its response to changes in
20 emissions of NO_x.

21
22 • Biases in stratospheric composition
23 By examining extensive climatologies of observations from satellite (Figures 22-26) we've
24 been able to show here that the simulation of stratospheric composition has improved
25 significantly in StratTrop compared with the older "stratosphere" focused scheme of MO09. In
26 part this is largely thanks to improvements in the dynamical model (MetUM) and improvements
27 in biases in modelled water vapour (Hardiman et al., 2017). Key questions remain about the
28 fidelity of the upper stratospheric/mesospheric photolysis rates and the upper boundary
29 conditions. Given the generally poorer performance of NO and NO_y it would be useful to
30 investigate the implementation of parametrised EPP to see if this ameliorates the problems.
31 Further work is also required to understand the cause of the disagreement between the
32 CH₄:H₂O correlation in the stratosphere, which suggests that too little H₂O is produced from
33 methane oxidation in the model.

34
35 • Middle atmosphere age of air:
36 The modelled middle atmosphere circulation has been evaluated against observations of SF₆
37 and through the use of tracer-tracer correlations. The tracer-tracer correlations further
38 motivate the need for a more detailed investigation of the modelled stratospheric NO_y and its
39 budget (production and loss). The comparison of the age of air in the model generally looks
40 acceptable in the middle stratosphere but tends to deviate at higher altitudes. In part there is
41 more uncertainty in observations at higher altitudes (owing to loss process of SF₆) but further
42 studies are required to understand if these biases are dependent on the resolution of the
43 model. To understand this a high top, > 120 km, version of the model is in preparation as are
44 simulations of UKESM1 at much higher horizontal resolution (~ 25 km).

45
46 In summary, UKCA StratTrop represents a substantial step forward compared to previous
47 versions of UKCA. We have shown here that it is fully suited to the challenges of representing
48 interactions in a coupled Earth System Model (key for CMIP6 and beyond) and we have



1 identified key areas and components for future development that will make it even better in
2 the future.

3 4 **Acknowledgements**

5 The authors would like to acknowledge the international community of UKCA users for all their
6 efforts in developing and applying the model. In particular we would like to acknowledge Prof.
7 John A. Pyle who pioneered the development of the UKCA project. We would especially like
8 to thank the atmospheric chemistry observational community who have developed numerous
9 datasets used in this paper to help evaluate the model. This work used JASMIN, the UK
10 collaborative data analysis facility.

11 12 **Data and Model Code Availability**

13 Due to intellectual property rights restrictions, we cannot provide either the source code or
14 documentation papers for the UM (including UKCA) or JULES.

15 *Obtaining the UM (including UKCA).* The Met Office Unified Model (MetUM) is available for
16 use under licence. A number of research organisations and national meteorological services
17 use the UM in collaboration with the Met Office to undertake basic atmospheric process
18 research, produce forecasts, develop the UM code, and build and evaluate Earth system
19 models. For further information on how to apply for a licence, see
20 <http://www.metoffice.gov.uk/research/modelling-systems/unified-model> (last access: 14
21 August 2019).

22 *Obtaining JULES.* JULES is available under licence, free of charge. For further information on
23 how to gain permission to use JULES for research purposes see [http://jules-](http://jules-lsm.github.io/access_req/JULES_access.html)
24 [lsm.github.io/access_req/JULES_access.html](http://jules-lsm.github.io/access_req/JULES_access.html) (last access: 14 August 2019).

25 *Details of the simulations performed.* UM and JULES simulations are compiled and run in
26 suites developed using the Rose suite engine
27 (<http://metomi.github.io/rose/doc/html/index.html>, last access: 14 August 2019) and scheduled
28 using the Cylc workflow engine (<https://cylc.github.io/cylc/>, last access: 14 August 2019). Both
29 Rose and Cylc are available under version 3 of the GNU General Public License (GPL). In this
30 framework, the suite contains the information required to extract and build the code as well as
31 configure and run the simulations. Each suite is labelled with a unique identifier and is held in
32 the same revision-controlled repository service in which we hold and develop the model's
33 code. This means that these suites are available to any licensed user of both the UM and
34 JULES.

35 All code related to the offline emissions is freely available on Github: [https://github.com/acsis-](https://github.com/acsis-project/emissions)
36 [project/emissions](https://github.com/acsis-project/emissions) and the data for biogenic emissions are available for free download
37 from <http://eccad.sedoo.fr/>. The model-satellite evaluation codes are available on request.
38 We acknowledge the use of the TEMIS OMI NO₂ (DOMINO vn 2.0;
39 <http://www.temis.nl/airpollution/no2.html>) data and NASA's MOPITT CO (vn7.0;
40 <https://search.earthdata.nasa.gov/>) data. The observations used to evaluate age of air were
41 the IMK/IAA generated MIPAS-ENVISAT datasets developed at KIT and available from:
42 <http://www.imk-asf.kit.edu/english/308.php>.

43
44
45 **Author contributions.** ATA and NLA lead the initial development of StratTrop and ATA and
46 FOC lead the writing of the manuscript. NLA, FO'C, JPM, AJH, GAF, MD, ST, contributed
47 during model development, data analysis and paper preparation. Simulation design, setup,
48 and execution was performed by FO'C and MD. CH and OW provided the ozone data for the



1 O₃ dry deposition evaluation. All co-authors contributed to writing sections of the manuscript,
2 performing evaluation and reviewing drafts of the manuscript.

3
4 **Competing interests.** The authors declare that they have no conflict of interest.

5
6 **Financial support.**

7 MD, GAF, AJH, JPM, and FO'C were supported by the Joint UK BEIS/Defra Met Office Hadley
8 Centre Climate Programme (GA01101). GF and FO'C also acknowledge additional funding
9 received from the Horizon 2020 European Union's Framework Programme for Research and
10 Innovation "Coordinated Research in Earth Systems and Climate: Experiments, Knowledge,
11 Dissemination and Outreach (CRESCENDO)" project under grant agreement no. 641816. ST
12 was supported by the UK-China Research and Innovation Partnership Fund through the Met
13 Office Climate Science for Service Partnership (CSSP) China as part of the Newton Fund.
14 JMK received funding from the European Community's Seventh Frame-work Programme
15 (FP7/2007-2013) under grant agreement no. 603557 (StratoClim). The development of UKCA
16 for inclusion in UKESM1 has also been facilitated by the use of the Monsoon2/NEXCS system,
17 a collaborative facility supplied under the Joint Weather and Climate Research Programme, a
18 strategic partnership between the Met Office and the Natural Environment Research Council.
19 OW and CH thank the Natural Environment Research Council for support under grant
20 NE/K001272/1. RJP was supported by the UK Natural Environment Research Council (NERC)
21 by providing funding for the National Centre for Earth Observation (NCEO). CO acknowledges
22 funding from grant RYC-2014-15036. GZ and OM acknowledge support by the New Zealand
23 Government under its Strategic Science Investment Fund, and under the Deep South National
24 Science Challenge.

25
26

27 **References**

28 <http://tntcat.iiasa.ac.at/RcpDb/> for GHG concentrations for the lower boundary conditions.

29

30 Acosta Navarro, J. C., Smolander, S., Struthers, H., Zorita, E., Ekman, A. M. L., Kaplan, J. O.,
31 Guenther, A., Arneth, A., and Riipinen, I.: Global emissions of terpenoid VOCs from
32 terrestrial vegetation in the last millennium, *Journal of Geophysical Research: Atmospheres*,
33 119, 6867–6885, doi:10.1002/2013JD021238, <http://dx.doi.org/10.1002/2013JD021238>,
34 2014.

35

36 Arakawa, A. and Lamb, V. R.: Computational design of the basic dynamic processes of the
37 UCLA general circulation model, *Methods Comput. Phys.*, 17, 173–265, 1977.

38

39 Archibald, A. T., et al. "Impacts of HO_x regeneration and recycling in the oxidation of isoprene:
40 Consequences for the composition of past, present and future atmospheres." *Geophysical
41 Research Letters* 38.5 (2011).

42

43 Arneth, A., Niinemets, U., Pressley, S., Bäck, J., Hari, P., Karl, T., Noe, S., Prentice, I. C.,
44 Serça, D., Hickler, T., Wolf, A., and Smith, B.: Process-based estimates of terrestrial
45 ecosystem isoprene emissions: incorporating the effects of a direct CO₂ -
46 isoprene interaction, *Atmospheric Chemistry and Physics*, 7, 31–53, doi:10.5194/acp-7-31-
47 2007, <https://www.atmos-chem-phys.net/7/31/2007/>, 2007.

48



- 1 Arneth, A., Monson, R. K., Schurgers, G., Niinemets, U., and Palmer, P. I.: Why are estimates
2 of global terrestrial isoprene emissions so similar (and why is this not so for monoterpenes)?,
3 Atmospheric Chemistry and Physics, 8, 4605–4620, doi:10.5194/acp-8-4605-2008,
4 https://www.atmos-chem-phys.net/8/4605/2008/, 2008.
5
- 6 Arneth, A., Schurgers, G., Lathiere, J., Duhal, T., Beerling, D. J., Hewitt, C. N., Martin, M., and
7 Guenther, A.: Global terrestrial isoprene emission models: sensitivity to variability in climate
8 and vegetation, Atmospheric Chemistry and Physics, 11, 8037–8052,
9 doi:10.5194/acp-11-8037-2011, https://www.atmos-chem-phys.net/11/8037/2011/, 2011.
10
- 11 Ashmore, M.: Assessing the future global impacts of ozone on vegetation, Plant Cell Environ.,
12 28, 949–964, 2005.
13
- 14 Aumont, B., Szopa, S., and Madronich, S.: Modelling the evolution of organic carbon during
15 its gas-phase tropospheric oxidation: development of an explicit model based on a self
16 generating approach, Atmos. Chem. Phys., 5, 2497–2517, https://doi.org/10.5194/acp-5-2497-
17 2005, 2005.
18
- 19 Banerjee, A., Archibald, A. T., Maycock, A. C., Telford, P., Abraham, N. L., Yang, X.,
20 Braesicke, P., and Pyle, J. A.: Lightning NO_x, a key chemistry–climate interaction: impacts of
21 future climate change and consequences for tropospheric oxidising capacity, Atmos. Chem.
22 Phys., 14, 9871–9881, https://doi.org/10.5194/acp-14-9871-2014, 2014.
23
- 24 Bauwens, M., Stavrou, T., Müller, J.-F., De Smedt, I., Van Roozendaal, M., van der Werf,
25 G. R., Wiedinmyer, C., Kaiser, J. W., Sindelarova, K., and Guenther, A.: Nine years of global
26 hydrocarbon emissions based on source inversion of OMI formaldehyde observations,
27 Atmospheric Chemistry and Physics, 16, 10 133–10 158, doi:10.5194/acp-16-10133-2016,
28 https://www.atmos-chem-phys.net/16/10133/2016/, 2016.
29
- 30 Bernath, P. F., McElroy, C. T., Abrams, M. C., Boone, C. D., Butler, M., Camy-Peyret, C.,
31 Carleer, M., Clerbaux, C., Coheur, P. F., Colin, R., DeCola, P., DeMazière, M., Drummond, J.
32 R., Dufour, D., Evans, W. F. J., Fast, H., Fussen, D., Gilbert, K., Jennings, D. E., Llewellyn, E.
33 J., Lowe, R. P., Mahieu, E., McConnell, J. C., McHugh, M., McLeod, S. D., Michaud, R.,
34 Midwinter, C., Nassar, R., Nichitiu, F., Nowlan, C., Rinsland, C. P., Rochon, Y. J., Rowlands,
35 N., Semeniuk, K., Simon, P., Skelton, R., Sloan, J. J., Soucy, M.-A., Strong, K., Tremblay, P.,
36 Turnbull, D., Walker, K. A., Walkty, I., Wardle, D. A., Wehrle, V., Zander, R., and Zou, J.:
37 Atmospheric Chemistry Experiment (ACE): mission overview, Geophys. Res. Lett., 32,
38 L15S01, doi:10.1029/2005GL022386, 2005.
39
- 40 Bertram, T. H., and J. A. Thornton: Toward a general parameterization of N₂O₅ reactivity on
41 aqueous particles: the competing effects of particle liquid water, nitrate and chloride,
42 Atmos. Chem. Phys., 9, 8351–8363, 2009.
43
- 44 Best, M. J., Pryor, M., Clark, D. B., Rooney, G. G., Essery, R. L. H., Ménard, C. B., Edwards,
45 J. M., Hendry, M. A., Porson, A., Gedney, N., Mercado, L. M., Sitch, S., Blyth, E., Boucher,
46 O., Cox, P. M., Grimmond, C. S. B., and Harding, R. J. (2011), The Joint UK Land Environment
47 Simulator (JULES), model description Part 1: Energy and water fluxes, Geoscientific Model
48 Development, 4, 677–699, doi:10.5194/gmd-4-677-2011.



- 1
2 Boersma, K.F., Eskes, H.J., Dirksen, R.J., Veefkind, J.P., Stammes, P., Huijnen, V., Kleipool,
3 Q.L., Sneep, M., Claas, J., Leitão, J. and Richter, A., 2011. An improved tropospheric NO₂
4 column retrieval algorithm for the Ozone Monitoring Instrument. *Atmospheric Measurement*
5 *Techniques*, 4(9), pp.1905-1928.
6
7 Bouwman, A. F., Lee, D. S., Asman, W. A. H., Dentener, F. J., Van Der Hoek, K. W., and
8 Olivier, J. G. J. (1997), A global high-resolution emission inventory for ammonia, *Global*
9 *Biogeochem. Cycles*, 11(4), 561– 587, doi:10.1029/97GB02266.
10
11 Brown, A. R., Beare, R. J., Edwards, J. M., Lock, A. P., Keogh, S. J., Milton, S. F., and Walters,
12 D. N.: Upgrades to the boundary-layer scheme in the Met Office numerical
13 weather prediction model, *Bound.-Lay. Meteorol.*, 128, 117–132,
14 <https://doi.org/10.1007/s10546-008-9275-0>, 2008.
15
16 Brown, A., Milton, S., Cullen, M., Golding, B., Mitchell, J., and Shelly, A.: Unified modeling and
17 prediction of weather and climate: a 25 year journey, *B. Am. Meteorol. Soc.*, 93, 1865–1877,
18 <https://doi.org/10.1175/BAMS-D-12-00018.1>, 2012.
19
20 Butkovskaya, N.I., Kukui, A., Pouvesle, N., and Le Bras, G.: *J. Phys. Chem. A*, 109, 6509,
21 2005.
22
23 Butkovskaya, N., Kukui, A., and Le Bras, G.: *J. Phys. Chem. A*, 111, 9047, 2007.
24
25 Butkovskaya, N., Rayez, M.-T., Rayez, J.-C., Kukui, A., and Le Bras, G.: *J. Phys. Chem. A*,
26 113, 11327, 2009.
27
28 Cariolle, D., Evans, M. J., Chipperfield, M. P., Butkovskaya, N., Kukui, A., and Le Bras, G.:
29 Impact of the new HNO₃-forming channel of the HO₂+NO reaction on tropospheric HNO₃,
30 NO_x, HO_x and ozone, *Atmos. Chem. Phys.*, 8, 4061-4068, [https://doi.org/10.5194/acp-8-](https://doi.org/10.5194/acp-8-4061-2008)
31 [4061-2008](https://doi.org/10.5194/acp-8-4061-2008), 2008.
32
33 Charney, J. G. and Phillips, N. A.: Numerical integration of the quasi-geostrophic equations
34 for barotropic and simple baroclinic flows, *J. Meteorol.*, 10, 71–99,
35 [https://doi.org/10.1175/1520-0469\(1953\)010<0071:NIOTQG>2.0.CO;2](https://doi.org/10.1175/1520-0469(1953)010<0071:NIOTQG>2.0.CO;2), 1953.
36
37 Cieslik, S. A.: Ozone uptake by various surface types: a comparison between dose and
38 exposure, *Atmos. Environ.*, 38, 2409–2420, doi:10.1016/j.atmosenv.2003.10.063, 2004.
39
40 Clark, D. B., Mercado, L. M., Sitch, S., Jones, C. D., Gedney, N., Best, M. J., Pryor, M, Rooney,
41 G. G., Essery, R. L. H., Blyth, E., Boucher, O., Harding, R. J., Huntingford, C., and Cox, P. M.
42 (2011), The Joint UK Land Environment Simulator (JULES), model description part 2: Carbon
43 fluxes and vegetation dynamics, *Geoscientific Model Development*, 4, 701-722,
44 doi:10.5194/gmd-4-701-2011.
45
46 Collins, W. J., Bellouin, N., Doutriaux-Boucher, M., Gedney, N., Halloran, P., Hinton, T.,
47 Hughes, J., Jones, C. D., Joshi, M., Liddicoat, S., Martin, G., O'Connor, F., Rae, J., Senior,
48 C., Sitch, S., Totterdell, I., Wiltshire, A., and Woodward, S.: Development and evaluation of an



- 1 Earth-System model – HadGEM2, *Geosci. Model Dev.*, 4, 1051–1075, doi:10.5194/gmd-4-
2 1051-2011, 2011.
- 3
- 4 Cox, P. M. (2001). Description of the “TRIFFID” Dynamic Global Vegetation Model. Hadley
5 Centre technical note.
- 6
- 7 Dee, D. P., Uppala, S. M., Simmons, A. J., Berrisford, P., Poli, P., Kobayashi, S., Andrae,
8 U., Balmaseda, M. A., Balsamo, G., Bauer, P., Bechtold, P., Beljaars, A. C., van de Berg, L.
9 , Bidlot, J., Bormann, N., Delsol, C., Dragani, R., Fuentes, M., Geer, A. J., Haimberger, L.
10 , Healy, S. B., Hersbach, H., Hólm, E. V., Isaksen, L., Kållberg, P., Köhler, M., Matricardi,
11 M., McNally, A. P., Monge-Sanz, B. M., Morcrette, J., Park, B., Peubey, C., de Rosnay, P.
12 , Tavolato, C., Thépaut, J. and Vitart, F. (2011), The ERA-Interim reanalysis: configuration
13 and performance of the data assimilation system. *Q.J.R. Meteorol. Soc.*, 137: 553-597.
14 doi:10.1002/qj.828
- 15
- 16 Durack, Paul J.; Taylor, Karl E. (2016). PCMDI AMIP SST and sea-ice boundary conditions
17 version 1.1.0. Version 20160906. Earth System Grid Federation.
18 <https://doi.org/10.22033/ESGF/input4MIPs.1120>
- 19
- 20 Emmons, L. K., Hauglustaine, D. A., Müller, J.-F., Carroll, M. A., Brasseur, G. P., Brunner, D.,
21 Staehelin, J., Thouret, V., and Marenco, A. (2000), Data composites of airborne observations
22 of tropospheric ozone and its precursors, *J. Geophys. Res.*, 105(D16), 20497– 20538,
23 doi:10.1029/2000JD900232.
- 24
- 25 Emmons, L. K., et al. (2004), Validation of Measurements of Pollution in the Troposphere
26 (MOPITT) CO retrievals with aircraft in situ profiles, *J. Geophys. Res.*, 109, D03309,
27 doi:10.1029/2003JD004101.
- 28
- 29 Eyring, V., Bony, S., Meehl, G. A., Senior, C., Stevens, B., and Stouffer, R. J. Taylor, K. E.:
30 Overview of the Coupled Model Intercomparison Project Phase 6 (CMIP6) experimental
31 design and organisation, *Geosci. Model Dev.*, 9, 1937-1958, [https://doi.org/10.5194/gmd-9-](https://doi.org/10.5194/gmd-9-1937-2016)
32 1937-2016, 2016.
- 33
- 34 Fan, S. M., Wofsy, S. C., Bakwin, P. S., Jacob, D. J., and Fitzjarrald, D. R.: Atmosphere-
35 biosphere Exchange of CO₂ and O₃ In the Central-amazon-forest, *J. Geophys. Res.-Atmos.*,
36 95, 16851–16864, doi:10.1029/JD095iD10p16851, 1990.
- 37
- 38 Fares, S., Park, J.-H., Ormeno, E., Gentner, D. R., McKay, M., Loreto, F., Karlik, J., and
39 Goldstein, A. H.: Ozone uptake by citrus trees exposed to a range of ozone concentrations,
40 *Atmos. Environ.*, 44, 3404–3412, doi:10.1016/j.atmosenv.2010.06.010, 2010.
- 41
- 42 Fares, S., Weber, R., Park, J.-H., Gentner, D., Karlik, J., and Goldstein, A. H.: Ozone
43 deposition to an orange orchard: Partitioning between stomatal and non-stomatal sinks,
44 *Environ. Pollut.*, 169, 258–266, doi:10.1016/j.envpol.2012.01.030, 2012.
- 45
- 46 Fares, S., Savi, F., Muller, J., Matteucci, G., and Paoletti, E.: Simultaneous measurements of
47 above and below canopy ozone fluxes help partitioning ozone deposition between its various
48 sinks in a Mediterranean Oak Forest, *Agr. Forest Meteorol.*, 198–199, 181–191, 2014.



- 1
2 Folberth, G. A., Hauglustaine, D. A., Lathièrè, J., and Brocheton, F.: Interactive chemistry in
3 the Laboratoire de Météorologie Dynamique general circulation model: model description and
4 impact analysis of biogenic hydrocarbons on tropospheric chemistry, *Atmospheric Chemistry
5 and Physics*, 6, 2273–2319, doi:10.5194/acp-6-2273-2006, <https://www.atmos-chem-phys.net/6/2273/2006/>, 2006.
6
7
8 Fowler, D., Flechard, C., Cape, J. N., Storeton-West, R. L., and Coyle, M.: Measurements of
9 ozone deposition to vegetation quantifying the flux, the stomatal and nonstomatal
10 components, *Water Air Soil Poll.*, 130, 63–74, doi:10.1023/A:1012243317471, 2001.
11
12 Gerosa, G., Dergbi, F., and Cieslik, S.: Comparison of different algorithms for stomatal ozone
13 flux determination from micrometeorological measurements, *Water Air Soil Poll.*, 179, 309–
14 321, doi:10.1007/s11270-006-9234-7, 2007.
15
16 Giannakopoulos, C. (1998), Three dimensional modelling of the concentration and deposition
17 of tropospheric trace gases. Ph.D. thesis, University of Cambridge, UK.
18
19 Giannakopoulos, C., Chipperfield, T., Law, K., and Pyle, J. (1999), Validation and
20 intercomparison of wet and dry deposition schemes using Pb-210 in a global three-
21 dimensional off-line chemical transport model, *J. Geophys. Res.*, 104, 23,761-23784.
22
23 Granier, C., J.F. Lamarque, A. Mieville, J.F. Muller, J. Olivier, J. Orlando, J. Peters, G.
24 Petron, G. Tyndall, S. Wallens, POET, a database of surface emissions of ozone
25 precursors, available on internet at <http://www.aero.jussieu.fr/projet/ACCENT/POET.php>
26 2005.
27
28 Grant, A; Archibald, A. T.; Cooke, MC; Shallcross, DE; Modelling the oxidation of
29 seventeen volatile organic compounds to track yields of CO and CO₂. *Atmospheric
30 Environment*, 44, 3797–3804, [doi:10.1016/j.atmosenv.2010.06.049], 2010
31
32 Gregory, D. and Allen, S.: The effect of convective downdraughts upon NWP and climate
33 simulations, in: Ninth conference on numerical weather prediction, Denver, Colorado, 122–
34 123, 1991.
35
36 Gregory, D. and Rowntree, P. R.: A massflux convection scheme with representation of cloud
37 ensemble characteristics and stability dependent closure, *Mon. Weather Rev.*,
38 118, 1483–1506, [https://doi.org/10.1175/1520-0493\(1990\)118<1483:AMFCSW>2.0.CO;2](https://doi.org/10.1175/1520-0493(1990)118<1483:AMFCSW>2.0.CO;2),
39 1990.
40
41 Gregory, D., Kershaw, R., and Inness, P. M.: Parametrization of momentum transport by
42 convection II: Tests in single-column and general circulation models, *Q. J. Roy. Meteorol.
43 Soc.*, 123, 1153–1183, <https://doi.org/10.1002/qj.49712354103>, 1997.
44
45 Guenther, A., Hewitt, C. N., Erickson, D., Fall, R., Geron, C., Graedel, T., Harley, P., Klinger,
46 L., Lerdau, M., Mckay, W. A., Pierce, T., Scholes, B., Steinbrecher, R., Tallamraju, R., Taylor,



- 1 J., and Zimmermann, P.: A global model of natural volatile organic compound emissions,
2 Journal of Geophysical Research, 100, 8873–8892, 1995.
3
- 4 Guenther, A., Jiang, X., Heald, C. L., Sakulyanontvittaya, T., Duhl, T., Emmons, L. K., & Wang,
5 X. (2012, 11). The Model of Emissions of Gases and Aerosols from Nature version 2.1
6 (MEGAN2.1): an extended and updated framework for modeling biogenic emissions.
7 Geoscientific Model Development, 5 (6), 1471–1492. Retrieved from [https://www.geosci-](https://www.geosci-model-dev.net/5/1471/2012/doi:10.5194/gmd-5-1471-2012)
8 [model-dev.net/5/1471/2012/doi: 10.5194/gmd-5-1471-2012](https://www.geosci-model-dev.net/5/1471/2012/doi:10.5194/gmd-5-1471-2012).
9
- 10 Hakim, Z. Q., Archer-Nicholls, S., Beig, G., Folberth, G. A., Sudo, K., Abraham, N. L., Ghude,
11 S., Henze, D. K., and Archibald, A. T.: Evaluation of tropospheric ozone and ozone precursors
12 in simulations from the HTAPII and CCMI model intercomparisons – a focus on the Indian
13 subcontinent, Atmos. Chem. Phys., 19, 6437–6458, [https://doi.org/10.5194/acp-19-6437-](https://doi.org/10.5194/acp-19-6437-2019)
14 [2019](https://doi.org/10.5194/acp-19-6437-2019), 2019.
15
- 16 Hall, S. R., Ullmann, K., Prather, M. J., Flynn, C. M., Murray, L. T., Fiore, A. M., Correa, G.,
17 Strode, S. A., Steenrod, S. D., Lamarque, J.-F., Guth, J., Josse, B., Flemming, J., Huijnen, V.,
18 Abraham, N. L., and Archibald, A. T.: Cloud impacts on photochemistry: building a climatology
19 of photolysis rates from the Atmospheric Tomography mission, Atmos. Chem. Phys., 18,
20 16809–16828, <https://doi.org/10.5194/acp-18-16809-2018>, 2018.
21
- 22 Hardacre, C., Wild, O., and Emberson, L.: An evaluation of ozone dry deposition in global
23 scale chemistry climate models, Atmos. Chem. Phys., 15, 6419–6436,
24 <https://doi.org/10.5194/acp-15-6419-2015>, 2015.
25
- 26 Hardiman, S. C., I. A. Boutle, A. C. Bushell, N. Butchart, M. J. P. Cullen, P. R. Field, K. Furtado,
27 J. C. Manners, S. F. Milton, C. J. Morcrette, F. M. O'Connor, B. J. Shipway, C. Smith, D. N.
28 Walters, K. D. Williams, N. Wood, N. L. Abraham, J. Keeble, A. C. Maycock, J. Thurlburn, and
29 M. T. Woodhouse, Processes controlling tropical tropopause temperature and stratospheric
30 water vapour, J. Climate, 28, 6516–6535, doi: <http://dx.doi.org/10.1175/JCLI-D-15-0075.1>,
31 2015.
32
- 33 Hardiman, S. C., N. Butchart, F. M. O'Connor, and S.T. Rumbold, The Met Office HadGEM3-
34 ES Chemistry-Climate Model: Evaluation of stratospheric dynamics and its impact on ozone,
35 Geosci. Model Dev., 10, 1209–1232, <https://www.geosci-model-dev.net/10/1209/2017/>, 2017.
36
- 37 Harper, A. B., Wiltshire, A. J., Cox, P. M., Friedlingstein, P., Jones, C. D., Mercado, L. M.,
38 Sitch, S., Williams, K., and Duran-Rojas, C.: Vegetation distribution and terrestrial carbon
39 cycle in a carbon cycle configuration of JULES4.6 with new plant functional types, Geosci.
40 Model Dev., 11, 2857–2873, <https://doi.org/10.5194/gmd-11-2857-2018>, 2018.
41
- 42 Hayman, G. D., F. M. O'Connor, M. Dalvi, D. B. Clark, N. Gedney, C. Huntingford, C. Prigent,
43 M. Buchwitz, O. Schneising, J. P. Burrows, C. Wilson, N. Richards, and M. Chipperfield,
44 Comparison of the HadGEM2 climate-chemistry model against in
45 situ and SCIAMACHY atmospheric methane data, Atmos. Chem. Phys., 14, 13257–13280,
46 doi:10.5194/acp-14-13257-2014, 2014.
47



- 1 Hewitt, H. T., Copsey, D., Culverwell, I. D., Harris, C. M., Hill, R. S. R., Keen, A. B., McLaren,
2 A. J., and Hunke, E. C.: Design and implementation of the infrastructure of HadGEM3: the
3 next-generation Met Office climate modelling system, *Geosci. Model Dev.*, 4, 223–253,
4 doi:10.5194/gmd-4-223-2011, 2011.
5
- 6 Hoesly, R. M., Smith, S. J., Feng, L., Klimont, Z., Janssens-Maenhout, G., Pitkanen, T.,
7 Seibert, J. J., Vu, L., Andres, R. J., Bolt, R. M., Bond, T. C., Dawidowski, L., Kholod, N.,
8 Kurokawa, J.-I., Li, M., Liu, L., Lu, Z., Moura, M. C. P., O'Rourke, P. R., and Zhang, Q.:
9 Historical (1750–2014) anthropogenic emissions of reactive gases and aerosols from the
10 Community Emissions Data System (CEDS), *Geosci. Model Dev.*, 11, 369–408,
11 https://doi.org/10.5194/gmd-11-369-2018, 2018.
12
- 13 IUPAC, Task Group on Atmospheric Chemical Kinetic Data Evaluation – Data Sheet I.A3.45
14 NOx15 http://iupac.pole-ether.fr/htdocs/datasheets/pdf/NOx15_HO2_NO.pdf 2017.
15
- 16 Jacob, D. J.: Heterogeneous chemistry and tropospheric ozone, *Atmos. Environ.*, 34, 2131–
17 2159, 2000.
18
- 19 Keeble, J., Braesicke, P., Abraham, N. L., Roscoe, H. K., and Pyle, J. A.: The impact of polar
20 stratospheric ozone loss on Southern Hemisphere stratospheric circulation and climate,
21 *Atmos. Chem. Phys.*, 14, 13705–13717, https://doi.org/10.5194/acp-14-13705-2014, 2014.
22
- 23 Kipling, Z., P. Stier, J. P. Schwarz, A. E. Perrig, J. R. Spackman, G. W. Mann, C. E. Johnson,
24 and P. J. Telford, Constraints on aerosol processes in climate models from vertically-resolved
25 aircraft observations of black carbon, *Atmos. Chem. Phys.*, 13, 5969–5986,
26 https://doi.org/10.5194/acp-13-5969-2013, 2013.
27
- 28 Kumer, J. B., Mergenthaler, J. L., and Roche, A. E.: CLAES CH₄, N₂O and CCl₂F₂ (F12)
29 global data, *Geophys. Res. Lett.*, 20(12), 1239–1242, 1993.
30
- 31 Lary, D. and Pyle, J.: Diffuse-radiation, twilight, and photochemistry, *J. Atmos. Chem.*, 13,
32 393–406, 1991.
33
- 34 Lamarque, J.-F., Shindell, D. T., Josse, B., Young, P. J., Cionni, I., Eyring, V., Bergmann, D.,
35 Cameron-Smith, P., Collins, W. J., Doherty, R., Dalsoren, S., Faluvegi, G., Folberth, G., Ghan,
36 S. J., Horowitz, L. W., Lee, Y. H., MacKenzie, I. A., Nagashima, T., Naik, V., Plummer, D.,
37 Righi, M., Rumbold, S. T., Schulz, M., Skeie, R. B., Stevenson, D. S., Strode, S., Sudo, K.,
38 Szopa, S., Voulgarakis, A., and Zeng, G.: The Atmospheric Chemistry and Climate Model
39 Intercomparison Project (ACCMIP): overview and description of models, simulations and
40 climate diagnostics, *Geosci. Model Dev.*, 6, 179–206, https://doi.org/10.5194/gmd-6-179-
41 2013, 2013.
42
- 43 Lathièrè, J., Hauglustaine, D. A., Friend, A. D., De Noblet Ducoudré, N., Viovy, N., and
44 Folberth, G. A.: Impact of climate variability and land use changes on global biogenic volatile
45 organic compound emissions, *Atmospheric Chemistry and Physics*, 6, 2129–2146,
46 doi:10.5194/acp-6-2129-2006, https://www.atmos-chem-phys.net/6/2129/2006/, 2006.
47



- 1 Lock, A. P., Brown, A. R., Bush, M. R., Martin, G. M., and Smith, R. N. B.: A new boundary
2 layer mixing scheme. Part I: Scheme description and single-column model tests, *Mon.*
3 *Weather Rev.*, 128, 3187–3199, <https://doi.org/10.1175/1520->
4 0493(2000)128<3187:ANBLMS>2.0.CO;2, 2000.
5
6 Lock, A. P.: The numerical representation of entrainment in parametrizations of boundary layer
7 turbulent mixing, *Mon. Weather Rev.*, 129, 1148–1163, <https://doi.org/10.1175/1520->
8 0493(2001)129<1148:TNROEI>2.0.CO;2, 2001.
9
10 Lowe, D., S. Archer-Nicholls, W. Morgan, J. Allan, S. Utembe, B. Ouyang, E. Aruffo, M. Le
11 Breton, R. A. Zaveri, P. Di Carlo, C. Percival, H. Coe, R. Jones, and G. McFiggans:
12 WRF-Chem model predictions of the regional impacts of N₂O₅ heterogeneous processes
13 on night-time chemistry over north-western Europe, *Atmos*
14
15 Luhar, A. K., Galbally, I. E., Woodhouse, M. T., and Thatcher, M.: An improved
16 parameterisation of ozone dry deposition to the ocean and its impact in a global climate–
17 chemistry model, *Atmos. Chem. Phys.*, 17, 3749–3767, <https://doi.org/10.5194/acp-17-3749->
18 2017, 2017.
19
20 Macintyre, H. L. and Evans, M. J.: Sensitivity of a global model to the uptake of N₂O₅ by
21 tropospheric aerosol, *Atmos. Chem. Phys.*, 10, 7409–7414, <https://doi.org/10.5194/acp-10->
22 7409-2010, 2010.
23
24 Mann, G. W., K. S. Carslaw, D. V. Spracklen, D. A. Ridley, P. T. Manktelow, M. P.
25 Chipperfield, S. J. Pickering, and C. E. Johnson, Description and evaluation of GLOMAP-
26 mode: a modal global aerosol microphysics model for the UKCA
27 composition-climate model, *Geosci. Model Dev.*, 3, 519–551, doi: 10.5194/gmd-3-519-2010,
28 2010.
29
30 Meinshausen, M., Vogel, E., Nauels, A., Lorbacher, K., Meinshausen, N., Etheridge, D. M.,
31 Fraser, P. J., Montzka, S. A., Rayner, P. J., Trudinger, C. M., Krummel, P. B., Beyerle, U.,
32 Canadell, J. G., Daniel, J. S., Enting, I. G., Law, R. M., Lunder, C. R., O’Doherty, S., Prinn, R.
33 G., Reimann, S., Rubino, M., Velders, G. J. M., Vollmer, M. K., Wang, R. H. J., and Weiss, R.:
34 Historical greenhouse gas concentrations for climate modelling (CMIP6), *Geosci. Model Dev.*,
35 10, 2057–2116, <https://doi.org/10.5194/gmd-10-2057-2017>, 2017.
36
37 Messina, P., Lathièrè, J., Sindelarova, K., Vuichard, N., Granier, C., Ghattas, J., . . .
38 Hauglustaine, D. A. (2016, 11). Global biogenic volatile organic compound emissions in the
39 ORCHIDEE and MEGAN models and sensitivity to key parameters. *Atmospheric Chemistry*
40 *and Physics*, 16 (22), 14169–14202. Retrieved from [https://www.atmos-chem-](https://www.atmos-chem-phys.net/16/14169/2016/)
41 [phys.net/16/14169/2016/](https://www.atmos-chem-phys.net/16/14169/2016/), doi:10.5194/acp-16-14169-2016.
42
43 Mikkelsen, T. N., Ro-Poulsen, H., Pilegaard, K., Hovmand, M. F., Jensen, N. O., Christensen,
44 C. S., and Hummelshøj, P.: Ozone uptake by an evergreen forest canopy: temporal variation
45 and possible mechanisms, *Environ. Pollut.*, 109, 423–429, doi:10.1016/S0269-
46 7491(00)00045-2, 2000.
47



- 1 Mikkelsen, T. N., Ro-Poulsen, H., Hovmand, M. F., Jensen, N. O., Pilegaard, K., and Egelov,
2 A. H.: Five-year measurements of ozone fluxes to a Danish Norway spruce canopy, *Atmos.*
3 *Environ.*, 38, 2361–2371, doi:10.1016/j.atmosenv.2003.12.036, 2004.
4
5 Monks, P. S., Archibald, A. T., Colette, A., Cooper, O., Coyle, M., Derwent, R., Fowler, D.,
6 Granier, C., Law, K. S., Mills, G. E., Stevenson, D. S., Tarasova, O., Thouret, V., von
7 Schneidmesser, E., Sommariva, R., Wild, O., and Williams, M. L.: Tropospheric ozone and
8 its precursors from the urban to the global scale from air quality to short-lived climate forcer,
9 *Atmos. Chem. Phys.*, 15, 8889–8973, <https://doi.org/10.5194/acp-15-8889-2015>, 2015.
10
11 Monks, S. A., Arnold, S. R., Hollaway, M. J., Pope, R. J., Wilson, C., Feng, W., Emmerson, K.
12 E., Kerridge, B. J., Latter, B. L., Miles, G. M., Siddans, R., and Chipperfield, M. P.: The
13 TOMCAT global chemistry transport model v1.6: description of chemical mechanism and
14 model evaluation, *Geosci. Model Dev.*, 10, 3025–3057, [https://doi.org/10.5194/gmd-10-3025-](https://doi.org/10.5194/gmd-10-3025-2017)
15 [2017](https://doi.org/10.5194/gmd-10-3025-2017), 2017.
16
17 Morgenstern, O., Braesicke, P., O'Connor, F. M., Bushell, A. C., Johnson, C. E., Osprey, S.
18 M., and Pyle, J. A.: Evaluation of the new UKCA climate-composition model – Part 1: The
19 stratosphere, *Geosci. Model Dev.*, 2, 43–57, <https://doi.org/10.5194/gmd-2-43-2009>, 2009.
20
21 Morgenstern, O., M. I. Hegglin, E. Rozanov, F. M. O'Connor, N. L. Abraham, H. Akiyoshi, A.
22 T. Archibald, S. Bekki, N. Butchart, M. P. Chipperfield, M. Deushi, Sandip S. Dhomse, R. R.
23 Garcia, S. C. Hardiman, L. W. Horowitz, P. Jöckel, B. Josse, D. Kinnison, M. Lin, E. Mancini,
24 M. E. Manyin, M. Marchand, V. Marécal, M. Michou, L. D. Oman, Giovanni Pitari, D. A.
25 Plummer, L. E. Revell, D. Saint-Martin, R. Schofield, A. Stenke, K. Stone, K. Sudo, T. Y.
26 Tanaka, S. Tilmes, Y. Yamashita, K. Yoshida, and G. Zeng, Review of the global models used
27 within phase 1 of the Chemistry–Climate Model Initiative (CCMI), *Geosci. Model Dev.*, 10,
28 639–671, <https://doi.org/10.5194/gmd-10-639-2017>, 2017.
29
30 Mulcahy, J. P., Jones, C., Sellar, A., Johnson, B., Boutle, I. A., Jones, A., T. Andrews, S. T.
31 Rumbold, J. Mollard, N. Bellouin, C. E. Johnson, K. D. Williams, D. P. Grosvenor, and D. T.
32 McCoy, Improved aerosol processes and effective radiative forcing in HadGEM3 and
33 UKESM1, *J. Adv. Modeling Earth Sys.*, 10, 2786–2805,
34 <https://doi.org/10.1029/2018MS001464>, 2018.
35
36 Mulcahy, J. P., et al., Description and evaluation of aerosol in UKESM1 and HadGEM-GC3.1
37 CMIP6 historical simulations, *Geosci. Model Dev.*, In preparation (2019).
38
39 Müller, J.-F. F., Stavrakou, T., Wallens, S., De Smedt, I., Van Roozendael, M., Potosnak, M.
40 J., Guenther, A. B., Global isoprene emissions estimated using MEGAN, ECMWF analyses
41 and a detailed canopy environment model, *Atmos. Chem. Phys.*, 8, 1329–1341,
42 <http://www.atmos-chem-phys.net/8/1329/2008/>, doi:10.5194/acp-8-1329-2008, 2008.
43
44 Munger, J. W., Wofsy, S. C., Bakwin, P. S., Fan, S. M., Goulden, M. L., Daube, B. C.,
45 Goldstein, A. H., Moore, K. E., and Fitzjarrald, D. R.: Atmospheric deposition of reactive
46 nitrogen oxides and ozone in a temperate deciduous forest and a subarctic woodland.1.
47 Measurements and mechanisms, *J. Geophys. Res.-Atmos.*, 101, 12639–12657,
doi:10.1029/96JD00230, 1996.



- 1
2 Naik, V., Voulgarakis, A., Fiore, A. M., Horowitz, L. W., Lamarque, J.-F., Lin, M., Prather, M.
3 J., Young, P. J., Bergmann, D., Cameron-Smith, P. J., Cionni, I., Collins, W. J., Dalsøren, S.
4 B., Doherty, R., Eyring, V., Faluvegi, G., Folberth, G. A., Josse, B., Lee, Y. H., MacKenzie, I.
5 A., Nagashima, T., van Noije, T. P. C., Plummer, D. A., Righi, M., Rumbold, S. T., Skeie, R.,
6 Shindell, D. T., Stevenson, D. S., Strode, S., Sudo, K., Szopa, S., and Zeng, G.: Preindustrial
7 to present-day changes in tropospheric hydroxyl radical and methane lifetime from the
8 Atmospheric Chemistry and Climate Model Intercomparison Project (ACCMIP), *Atmos. Chem.*
9 *Phys.*, 13, 5277-5298, <https://doi.org/10.5194/acp-13-5277-2013>, 2013.
- 10
11 O'Connor, F. M., C.E. Johnson, O. Morgenstern, N.L. Abraham, P. Braesicke, M. Dalvi, G.A.
12 Folberth, M.G. Sanderson, P.J. Telford, A. Voulgarakis, P.J. Young, G. Zeng, W.J. Collins,
13 and J.A. Pyle, Evaluation of the new UKCA climate-composition model. Part II. The
14 troposphere, *Geosci. Model Dev.*, 7, 41-91, <https://doi.org/10.5194/gmd-7-41-2014>, 2014.
- 15
16 O'Connor, F.M., et al., Pre-industrial to present-day anthropogenic and natural effective
17 radiative forcings from UKESM1, In preparation, 2019.
- 18
19 Oliver, R. J., Mercado, L. M., Sitch, S., Simpson, D., Medlyn, B. E., Lin, Y.-S., and Folberth,
20 G. A.: Large but decreasing effect of ozone on the European carbon sink, *Biogeosciences*,
21 15, 4245-4269, <https://doi.org/10.5194/bg-15-4245-2018>, 2018.
- 22
23 Orbe, C., Yang, H., Waugh, D. W., Zeng, G., Morgenstern, O., Kinnison, D. E., Lamarque, J.-
24 F., Tilmes, S., Plummer, D. A., Scinocca, J. F., Josse, B., Marecal, V., Jöckel, P., Oman, L.
25 D., Strahan, S. E., Deushi, M., Tanaka, T. Y., Yoshida, K., Akiyoshi, H., Yamashita, Y., Stenke,
26 A., Revell, L., Sukhodolov, T., Rozanov, E., Pitari, G., Visioni, D., Stone, K. A., Schofield, R.,
27 and Banerjee, A.: Large-scale tropospheric transport in the Chemistry–Climate Model Initiative
28 (CCMI) simulations, *Atmos. Chem. Phys.*, 18, 7217-7235, [https://doi.org/10.5194/acp-18-](https://doi.org/10.5194/acp-18-7217-2018)
29 [7217-2018](https://doi.org/10.5194/acp-18-7217-2018), 2018.
- 30
31 Pacifico, F., Harrison, S. P., Jones, C. D., Arneth, A., Sitch, S., Weedon, G. P., Barkley, M. P.,
32 Palmer, P. I., Serca, D., Potosnak, M., Fu, T.-M., Goldstein, A., Bai, J., and Schurgers, G.
33 (2011), Evaluation of a photosynthesis-based biogenic isoprene emissions scheme in JULES
34 and simulation of isoprene emissions under present-day climate conditions, *Atmos. Chem.*
35 *Phys.*, 11, 4271-4389, doi:10.5194/acp-11-4371-2011.
- 36
37 Penner, J., Atherton, C., Dignon, J., Ghan, S., Walton, J., and Hameed, S. (1991),
38 Tropospheric nitrogen - a 3-dimensional study of sources, distributions, and deposition, *J.*
39 *Geophys. Res.*, 96, 959-990, doi:10.1029/90JD02228.
- 40
41 Prather, M. J., Zhu, X., Flynn, C. M., Strode, S. A., Rodriguez, J. M., Steenrod, S. D., Liu, J.,
42 Lamarque, J.-F., Fiore, A. M., Horowitz, L. W., Mao, J., Murray, L. T., Shindell, D. T., and
43 Wofsy, S. C.: Global atmospheric chemistry – which air matters, *Atmos. Chem. Phys.*, 17,
44 9081–9102, <https://doi.org/10.5194/acp-17-9081-2017>, 2017.
- 45
46 Price, C. and D. Rind, A Simple Lightning Parametrization for Calculating Global Lightning
47 Distributions, *J. Geophys. Res.*, 97, D9, 9919-9933 (1992).
- 48



- 1 Price, C. and D. Rind, What determines the cloud-to-ground lightning fraction in
2 thunderstorms?, *Geophys. Res. Letts.*, 20, 463-466, 1993.
- 3
- 4 Price, C. and D. Rind, Modeling Global Lightning Distributions in a General Circulation Model,
5 *Mon. Weather Rev.*, 122, 1930-1939, 1994.
- 6
- 7 Rabin, S. S., Melton, J. R., Lasslop, G., Bachelet, D., Forrest, M., Hantson, S., Kaplan, J. O.,
8 Li, F., Mangeon, S., Ward, D. S., Yue, C., Arora, V. K., Hickler, T., Kloster, S., Knorr, W.,
9 Nieradzki, L., Spessa, A., Folberth, G. A., Sheehan, T., Voulgarakis, A., Kelley, D. I., Prentice,
10 I. C., Sitch, S., Harrison, S., and Arneth, A.: The Fire Modeling Intercomparison Project
11 (FireMIP), phase 1: experimental and analytical protocols with detailed model descriptions,
12 *Geosci. Model Dev.*, 10, 1175– 1197, doi.org/10.5194/gmd-10-1175-2017, 2017.
- 13
- 14 Rannik, Ü., Altimir, N., Mammarella, I., Bäck, J., Rinne, J., Ruuskanen, T. M., Hari, P., Vesala,
15 T., and Kulmala, M.: Ozone deposition into a boreal forest over a decade of observations:
16 evaluating deposition partitioning and driving variables, *Atmos. Chem. Phys.*, 12, 12165–
17 12182, doi:10.5194/acp-12-12165-2012, 2012.
- 18
- 19 Russell, J. M., Gordley, L. L., Park, J. H., Drayson, S. R., Hesketh, W. D., Cicerone, R. J.,
20 Tuck, A. F., Frederick, J. E., Harries, J. E., and Crutzen, P. J.: The Halogen Occultation
21 Experiment, *J. Geophys. Res.-Atmos.*, 98, 10777–10797, doi:10.1029/93JD00799, 1993.
- 22
- 23 Schultz, M. G., Schröder, S., Lyapina, O., Cooper, O., Galbally, I., Petropavlovskikh, I., Von
24 Schneidmesser, E., Tanimoto, H., Elshorbany, Y., Naja, M., Seguel, R., Dauert, U., Eckhardt,
25 P., Feigenspahn, S., Fiebig, M., Hjellbrekke, A.-G., Hong, Y.-D., Christian Kjeld, P., Koide, H.,
26 Lear, G., Tarasick, D., Ueno, M., Wallasch, M., Baumgardner, D., Chuang, M.-T., Gillett, R.,
27 Lee, M., Molloy, S., Moolia, R., Wang, T., Sharps, K., Adame, J. A., Ancellet, G., Apadula, F.,
28 Artaxo, P., Barlasina, M., Bogucka, M., Bonasoni, P., Chang, L., Colomb, A., Cuevas, E.,
29 Cupeiro, M., Degorska, A., Ding, A., Fröhlich, M., Frolova, M., Gadhavi, H., Gheusi, F., Gilje,
30 S., Gonzalez, M. Y., Gros, V., Hamad, S. H., Helmig, D., Henriques, D., Hermansen, O., Holla,
31 R., Huber, J., Im, U., Jaffe, D. A., Komala, N., Kubistin, D., Lam, K.-S., Laurila, T., Lee, H.,
32 Levy, I., Mazzoleni, C., Mazzoleni, L., McClure-Begley, A., Mohamad, M., Murovic, M.,
33 Navarro-Comas, M., Nicodim, F., Parrish, D., Read, K. A., Reid, N., Ries, L., Saxena, P.,
34 Schwab, J. J., Scorgie, Y., Senik, I., Simmonds, P., Sinha, V., Skorokhod, A., Spain, G.,
35 Spangl, W., Spoor, R., Springston, S. R., Steer, K., Steinbacher, M., Suharguniyawan, E.,
36 Torre, P., Trickl, T., Weili, L., Weller, R., Xu, X., Xue, L. and Zhiqiang, M.: Tropospheric Ozone
37 Assessment Report: Database and Metrics Data of Global Surface Ozone Observations, *Elem
38 Sci Anth*, 5(0), 58, doi:10.1525/elementa.244, 2017.
- 39
- 40 Seinfeld, J. and Pandis, S.: *Atmospheric Chemistry and Physics: From Air Pollution to Climate
41 Change*, John Wiley & Sons, Hoboken, New Jersey, USA, 2nd Edn., 2006.
- 42
- 43 Sellar, A. A., C. G. Jones., J. Mulcahy, Y. Tang, A. Yool, A. Wiltshire, F. M. O'Connor, M.
44 Stringer, R. Hill, J. Palmieri, S. Woodward, L. de Mora, T. Kuhlbrodt, S. Rumbold, D. I. Kelley,
45 R. Ellis, C. E. Johnson, J. Walton, N. L. Abraham, M. B. Andrews, T. Andrews, A. T. Archibald,
46 S. Berthou, E. Burke, E. Blockley, K. Carslaw, M. Dalvi, J. Edwards, G. A. Folberth, N.
47 Gedney, P. T. Griffiths, A. B. Harper, M. A. Hendry, A. J. Hewitt, B. Johnson, A. Jones, C. D.
48 Jones, J. Keeble, S. Liddicoat, O. Morgenstern, R. J. Parker, V. Predoi, E. Robertson, A.



- 1 Siahhaan, R. S. Smith, R. Swaminathan, M. Woodhouse, G. Zeng, and M. Zerroukat, UKESM1:
2 Description and evaluation of the UK Earth System Model, *J. Adv. Modeling Earth Sys.*, Under
3 review, 2019a.
4
5 Sellar, A., Walton, J., Jones, C.G., Abraham, N.L., et al. Implementation of UK Earth system
6 models for CMIP, *J. Adv. Modeling Earth Sys.*, Under review, 2019b.
7
8 Shindell, D. T., et al. (2006), Multimodel simulations of carbon monoxide: Comparison with
9 observations and projected near-future changes, *J. Geophys. Res.*, 111, D19306,
10 doi:10.1029/2006JD007100.
11
12 Sindelarova, K., Granier, C., Bouarar, I., Guenther, A., Tilmes, S., Stavrakou, T., Müller, J.-F.,
13 Kuhn, U., Stefani, P., and Knorr, W.: Global data set of biogenic VOC emissions calculated by
14 the MEGAN model over the last 30 years, *Atmos. Chem. Phys.*, 14, 9317-9341,
15 <https://doi.org/10.5194/acp-14-9317-2014>, 2014.
16 Sinnhuber, M., Nieder, H., and Wieters, N.: Energetic particle precipitation and the chemistry
17 of the mesosphere / lower thermosphere, *Surv. Geophys.*, 33, 6, 1281-1334,
18 <https://doi.org/10.1007/s10712-012-9201-3>, 2012.
19
20 Sitch, S., Cox, P.M., Collins, W.J., and Huntingford, C., Indirect radiative forcing of climate
21 change through ozone effects on the land-carbon sink, *Nature*, 448, 791-4.
22 10.1038/nature06059, 2007.
23
24 Smith, R., Fowler, D., Sutton, M., Flechard, C., and Coyle, M.: Regional estimation of pollutant
25 gas dry deposition in the UK: model description, sensitivity analyses and outputs, *Atmos.*
26 *Environ.*, 34, 3757–3777, 2000.
27
28 SPARC, 2010: SPARC CCMVal Report on the Evaluation of Chemistry-Climate Models. V.
29 Eyring, T. Shepherd and D. Waugh (Eds.), SPARC Report No. 5, WCRP-30/2010, WMO/TD
30 – No. 40, available at www.sparc-climate.org/publications/sparc-reports/
31
32 Spivakovsky, C.M., Logan, J.A., Montzka, S.A., Balkanski, Y.J., Foreman-Fowler, M., Jones,
33 D.B.A., Horowitz, L.W., Fusco, A.C., Brenninkmeijer, C.A.M., Prather, M.J. and Wofsy, S.C.,
34 2000. Three-dimensional climatological distribution of tropospheric OH: Update and
35 evaluation. *Journal of Geophysical Research: Atmospheres*, 105(D7), pp.8931-8980.
36
37 Stavrakou, T., Müller, J.-F., De Smedt, I., Van Roozendaal, M., van der Werf, G. R., Giglio, L.,
38 & Guenther, A. (2009, 2). Evaluating the performance of pyrogenic and biogenic emission
39 inventories against one decade of space-based formaldehyde columns. *Atmospheric*
40 *Chemistry and Physics*, 9 (3), 1037–1060. Retrieved from [http://www.atmos-chem-](http://www.atmos-chem-phys.net/9/1037/2009/)
41 [phys.net/9/1037/2009/](http://www.atmos-chem-phys.net/9/1037/2009/), doi:10.5194/acp-9-1037-2009.
42
43 Stella, P., Personne, E., Loubet, B., Lamaud, E., Ceschia, E., Béziat, P., Bonnefond, J. M.,
44 Irvine, M., Keravec, P., Mascher, N., and Cellier, P.: Predicting and partitioning ozone fluxes
45 to maize crops from sowing to harvest: the Surf atm-O3 model, *Biogeosciences*, 8, 2869–2886,
46 doi:10.5194/bg-8-2869-2011, 2011.
47



- 1 Stevenson, D. S., et al. (2006), Multimodel ensemble simulations of present-day and near-
2 future tropospheric ozone, *J. Geophys. Res.*, 111, D08301, doi:[10.1029/2005JD006338](https://doi.org/10.1029/2005JD006338).
3
- 4 Stiller, G. P., von Clarmann, T., Höpfner, M., Glatthor, N., Grabowski, U., Kellmann, S.,
5 Kleinert, A., Linden, A., Milz, M., Reddmann, T., Steck, T., Fischer, H., Funke, B., López-
6 Puertas, M., and Engel, A.: Global distribution of mean age of stratospheric air from MIPAS
7 SF₆ measurements, *Atmos. Chem. Phys.*, 8, 677-695, [https://doi.org/10.5194/acp-8-677-](https://doi.org/10.5194/acp-8-677-2008)
8 2008, 2008.
9
- 10 Telford, P. J., Braesicke, P., Morgenstern, O., and Pyle, J. A.: Technical Note: Description and
11 assessment of a nudged version of the new dynamics Unified Model, *Atmos. Chem. Phys.*, 8,
12 1701-1712, doi:10.5194/acp-8-1701-2008, 2008
13
- 14 Telford, P., P. Braesicke, O. Morgenstern, and J. Pyle, Reassessment of causes of ozone
15 column variability following the eruption of Mount Pinatubo using a nudged CCM,
16 *Atmos. Chem. Phys.*, 9, 4251-4260, <https://doi.org/10.5194/acp-9-4251-2009>, 2009.
17
- 18 Telford, P. J., Lathièrre, J., Abraham, N. L., Archibald, A. T., Braesicke, P., Johnson, C. E.,
19 Morgenstern, O., O'Connor, F. M., Pike, R. C., Wild, O., Young, P. J., Beerling, D. J., Hewitt,
20 C. N., and Pyle, J.: Effects of climate-induced changes in isoprene emissions after the eruption
21 of Mount Pinatubo, *Atmos. Chem. Phys.*, 10, 7117-7125, doi:10.5194/acp-10-7117-2010,
22 2010.
23
- 24 Thomason, L. W., Ernest, N., Millán, L., Rieger, L., Bourassa, A., Vernier, J.-P., Manney, G.,
25 Luo, B., Arfeuille, F., and Peter, T.: A global space-based stratospheric aerosol climatology:
26 1979–2016, *Earth Syst. Sci. Data*, 10, 469-492, <https://doi.org/10.5194/essd-10-469-2018>,
27 2018.
28
- 29 van Marle, M. J. E., Kloster, S., Magi, B. I., Marlon, J. R., Daniau, A.-L., Field, R. D., Arneth,
30 A., Forrest, M., Hantson, S., Kehrwald, N. M., Knorr, W., Lasslop, G., Li, F., Mangeon, S., Yue,
31 C., Kaiser, J. W., and van der Werf, G. R.: Historic global biomass burning emissions for
32 CMIP6 (BB4CMIP) based on merging satellite observations with proxies and fire models
33 (1750–2015), *Geosci. Model Dev.*, 10, 3329-3357, [https://doi.org/10.5194/gmd-10-3329-](https://doi.org/10.5194/gmd-10-3329-2017)
34 2017, 2017.
35
- 36 Voulgarakis, A., Wild, O., Savage, N. H., Carver, G. D., and Pyle, J. A.: Clouds, photolysis and
37 regional tropospheric ozone budgets, *Atmos. Chem. Phys.*, 9, 8235-8246,
38 <https://doi.org/10.5194/acp-9-8235-2009>, 2009.
39
- 40 Walters, D., A. J. Baran, I. Boutle, M. Brooks, P. Earnshaw, J. Edwards, K. Furtado, P. Hill, A.
41 Lock, J. Manners, C. Morcrette, J. Mulcahy, C. Sanchez, C. Smith, R. Stratton, W. Tennant,
42 L. Tomassini, K. Van Weverberg, S. Vosper, M. Willett, J. Browse, A. Bushell, K. Carslaw, M.
43 Dalvi, R. Essery, N. Gedney, S. Hardiman, B. Johnson, C. Johnson, A. Jones, C. Jones, G.
44 Mann, S. Milton, H. Rumbold, A. Sellar, M. Ujiie, M. Whittall, K. Williams, and M. Zerroukat,
45 The Met Office Unified Model Global Atmosphere 7.0/7.1 and JULES Global Land 7.0
46 configurations, *Geosci. Model Dev.*, 12, 1909–1963, [https://doi.org/10.5194/gmd-12-1909-](https://doi.org/10.5194/gmd-12-1909-2019)
47 2019, 2019.
48



- 1 Walton, J., MacCracken, M., and Ghan, S. (1988), A global-scale lagrangian trace species
2 model of transport, transformation, and removal processes, *J. Geophys. Res.*, 93, 8339-8354,
3 doi:10.1029/JD093iD07p08339.
4
- 5 Wang, W., Shao, M., Hu, M., Zeng, L., and Wu, Y.: The impact of aerosols on photolysis
6 frequencies and ozone production in urban Beijing during the four-year period 2012–2015,
7 *Atmos. Chem. Phys. Discuss.*, <https://doi.org/10.5194/acp-2019-84>, in review, 2019.
8
- 9 Wesely, M.: Parameterization of surface resistances to gaseous dry deposition in regional-
10 scale numerical-models, *Atmos. Environ.*, 23, 1293–1304, 1989.
11
- 12 Wild, O.: Modelling the global tropospheric ozone budget: exploring the variability in current
13 models, *Atmos. Chem. Phys.*, 7, 2643-2660, <https://doi.org/10.5194/acp-7-2643-2007>, 2007.
14
- 15 Wood, N., Staniforth, A., White, A., Allen, T., Diamantakis, M., Gross, M., T. Melvin, C. Smith,
16 S. Vosper, M. Zerroukat, and J. Thuburn, Lagrangian discretization of the deep-atmosphere
17 global non-hydrostatic equations, *Quart. J. Royal Meteorol. Soc.*, 1505–1520. doi:
18 10.1002/qj.2235, 2014.
19
- 20 Xing, J., Wang, J., Mathur, R., Wang, S., Sarwar, G., Pleim, J., Hogrefe, C., Zhang, Y., Jiang,
21 J., Wong, D. C., and Hao, J.: Impacts of aerosol direct effects on tropospheric ozone through
22 changes in atmospheric dynamics and photolysis rates, *Atmos. Chem. Phys.*, 17, 9869-9883,
23 <https://doi.org/10.5194/acp-17-9869-2017>, 2017.
24
- 25 Yienger, J. J., and Levy, H. (1995), Empirical model of global soil-biogenic NO_x emissions, *J.*
26 *Geophys. Res.*, 100(D6), 11447– 11464, doi:10.1029/95JD00370.
27
- 28 Yool, A., Popova, E. E., and Anderson, T. R.: MEDUSA-2.0: an intermediate complexity
29 biogeochemical model of the marine carbon cycle for climate change and ocean acidification
30 studies, *Geosci. Model Dev.*, 6, 1767-1811, <https://doi.org/10.5194/gmd-6-1767-2013>
31
- 32 Young, P. J., Ameth, A., Schurgers, G., Zeng, G., & Pyle, J. A. (2009). The CO₂ inhibition of
33 terrestrial isoprene emission significantly affects future ozone projections. *Atmospheric*
34 *Chemistry and Physics*. doi: 10.5194/acp-9-2793-2009.
35
- 36 Young, P. J., Archibald, A. T., Bowman, K. W., Lamarque, J.-F., Naik, V., Stevenson, D. S.,
37 Tilmes, S., Voulgarakis, A., Wild, O., Bergmann, D., Cameron-Smith, P., Cionni, I., Collins, W.
38 J., Dalsøren, S. B., Doherty, R. M., Eyring, V., Faluvegi, G., Horowitz, L. W., Josse, B., Lee,
39 Y. H., MacKenzie, I. A., Nagashima, T., Plummer, D. A., Righi, M., Rumbold, S. T., Skeie, R.
40 B., Shindell, D. T., Strode, S. A., Sudo, K., Szopa, S., and Zeng, G.: Pre-industrial to end 21st
41 century projections of tropospheric ozone from the Atmospheric Chemistry and Climate Model
42 Intercomparison Project (ACCMIP), *Atmos. Chem. Phys.*, 13, 2063-2090,
43 <https://doi.org/10.5194/acp-13-2063-2013>, 2013.
44
- 45 Young, P. J., Naik, V., Fiore, A. M., Gaudel, A., Guo, J., Lin, M. Y., Neu, J. L., Parrish, D. D.,
46 Rieder, H. E., Schnell, J. L., Tilmes, S., Wild, O., Zhang, L., Ziemke, J. R., Brandt, J., Delcloo,
47 A., Doherty, R. M., Geels, C., Hegglin, M. I., Hu, L., Im, U., Kumar, R., Luhar, A., Murray, L.,
48 Plummer, D., Rodriguez, J., Saiz-Lopez, A., Schultz, M. G., Woodhouse, M. T. and Zeng, G.:



- 1 Tropospheric Ozone Assessment Report: Assessment of global-scale model performance for
- 2 global and regional ozone distributions, variability, and trends, *Elem Sci Anth*, 6(1), 10,
- 3 doi:10.1525/elementa.265, 2018.
- 4
- 5 Yu, S., Eder, B., Dennis, R., Chu, S.-H. and Schwartz, S. E.: New unbiased symmetric metrics
- 6 for evaluation of air quality models, *Atmos. Sci. Lett.*, 7(1), 26–34, doi:10.1002/asl.125, 2006.
- 7
- 8 Zerroukat, M. and Allen, T.: On the monotonic and conservative transport on overset/Yin-Yang
- 9 grids, *J. Comput. Phys.*, 302, 285–299, <https://doi.org/10.1016/j.jcp.2015.09.006>, 2015.